NUMERICAL SIMULATION OF FLOW THROUGH A SPILLWAY AND DIVERSION STRUCTURE

Julian D. Gacek

Department of Civil Engineering and Applied Mechanics

McGill University, Montréal

October 2007

A Thesis submitted to McGill University in partial fulfillment of the requirements of the degree of Master's of Engineering (Thesis).

Abstract

Flow through the Keeyask Generating Station's diversion and spillway (rollway), to be constructed 730km north of Winnipeg, Canada on the Nelson River, is investigated by a comparison of a numerical model and a 1:50 scaled sectional physical model. The physical model was constructed at the LaSalle Consulting Group's laboratory in a permanent flume. A commercially available computational fluid dynamics (CFD) program, Flow3D, was used to model the physical model by using the Reynolds-averaged Navier-Stokes equations in combination with the standard K-ε eddy-viscosity closure model. In order to determine the required mesh size to obtain a mesh independent solution tests were conducted on the diversion structure in 2D for four partial gate openings and in 3D for a fully open gate condition, as 2D did not model the contraction of the physical model adequately. Mesh independence was only obtained for the fully open condition and was nearly obtained for a 6m gate opening while other gate openings diverged with refinement. Further refinement was not realistic due to excessive computing times. The two meshes that adequately modeled the flow were used for all subsequent investigations. Sensitivity tests were performed for the diversion structure for the fully open case in 3D and the 6m gate opening in 2D in order to observe the effects of the numerical model scale (prototype, 1:50 scale) and the effects of two turbulence models (K-ε, RNG). For both tests, similar results were obtained. Finally, numerical modeling was performed in 3D for the fully open gate condition for both the diversion and rollway structures in order to compare discharges/discharge coefficients, water surfaces and pressures to those of the physical model. Modeling of partial gate openings in 3D was not possible due to large calculation times. Results for the fully open case showed that the numerical model and physical model are in reasonably good agreement with one another.

Résumé

L'écoulement des eaux vers l'ouvrage de dérivation et l'évacuateur de crues de la centrale Keeyask, qui sont projetés sur la rivière Nelson, à 730 km au nord de Winnipeg (Canada), est étudié par la comparaison d'un modèle numérique et d'un modèle réduit à l'échelle 1:50, qui a été construit dans le laboratoire du Groupe-Conseil LaSalle. Le logiciel Flow3D a été utilisé pour simuler les conditions étudiées au modèle réduit, en utilisant les équations de Reynolds en combinaison avec la méthode de fermeture K-ε. Pour s'assurer que le maillage du modèle était adéquat pour modéliser l'écoulement, des essais ont été effectués sur l'ouvrage de dérivation en 2D pour des ouvertures partielles des vannes et en 3D pour l'ouverture complète (le 2D n'étant pas en mesure de modéliser la réduction en largeur simulée sur le modèle réduit) afin de déterminer le niveau de raffinement du maillage requis pour obtenir une solution indépendante de ce dernier. L'indépendance du maillage a été atteinte uniquement pour une ouverture complète de la vanne et presque atteinte pour une ouverture de 6m. Pour des raisons inconnues, toutes autres ouvertures partielles des vannes ont conduit à des solutions divergentes. De plus, le raffinement supplémentaire des maillages n'était pas possible, à cause des temps de calcul excessifs. Les maillages utilisés pour l'ouverture complète et l'ouverture de 6m ont donc été utilisés pour toutes les autres simulations. Des essais de sensibilité ont été effectués sur l'ouvrage de dérivation pour ces deux ouvertures, en vue d'observer l'effet du changement de l'échelle du modèle numérique (échelle 1:50 et prototype) et l'effet de deux différentes méthode de fermeture (K-ε et RNG) sur l'écoulement. Pour les deux essais, des solutions semblables ont été obtenues. Finalement, des simulations numériques ont été effectuées en 3D pour une ouverture complète sur l'ouvrage de dérivation et l'évacuateur, afin de comparer avec le modèle réduit les valeurs obtenues pour les débits, les coefficients de débit, les profils des niveaux d'eau et les pressions. La modélisation des ouvertures partielles de vanne en 3D n'était pas possible à cause des durées excessives des temps de calcul nécessaire. La comparaison des deux modèles démontre que les résultats du modèle numérique sont passablement proches de ceux du modèle réduit.

Acknowledgments

I wish to express my deepest gratitude to my supervisor, Professor Susan Gaskin, for her guidance, constant encouragement and advice during the course of this research. In particular, I would like to thank her for her time spent improving my understanding of the topic. I would also like to thank the LaSalle Consulting Group for giving me the opportunity to research this topic and for helping me with the software, especially Graham K. Holder, Marc Villeneuve, Jonathan Nicolle and Tristan Aubel. I would also like to thank Salem Bouhairie and France Suerich-Gulick for their help regarding numerical modeling. Finally, I would like to thank Kristina Bondy, Miguel Nunes, my parents Adam and Joanna, my sister Helena and many others for their words of encouragement along the way.

Table of Contents

List of Figures

List of Tables

List of Symbols

Latin Symbols

b	Net width of spillway crest
d	Symbol used to denote derivatives
g	Gravitational acceleration equal to 9.81m/s^2
k_s	Grain roughness
l	Length scale
p	Pressure of the fluid
q	Discharge per unit width
t	Time component
u_i, u_j	Fluid velocity tensor
x_i, x_j	Directional tensors
y	Flow depth
z_{crest}	Elevation of the crest
z_{HWL-C}	Water elevation at HWL-C
$z_{\max}$	Maximum discritized elevation with non-zero velocities
$z_{\min}$	Minimum discritized elevation with non-zero velocities
A	Area
C	Dimensionless discharge coefficient
C_c	Contraction coefficient
C_d	Discharge coefficient
C_K	Coefficient for the K-ε eddy viscosity turbulence model
C_ε	Coefficient for the K-ε eddy viscosity turbulence model
$C_{\varepsilon 1}$	Coefficient for the K-ε eddy viscosity turbulence model
$C_{\varepsilon 2}$	Coefficient for the K-ε eddy viscosity turbulence model

$C_{\varepsilon 3}$	Coefficient for the K-ε eddy viscosity turbulence model
C_{μ}	Coefficient for the K-ε eddy viscosity turbulence model
D	Denotes the substantive differential operator
Eu	Euler number
$\vec{F}_g$	Gravitational force vector
$\vec{F}_I$	Inertial force vector
$\vec{F}_P$	Force vector due to fluid pressure
$\vec{F}_\mu$	Viscous force vector
$\vec{F}_\sigma$	Force vector due to surface tension
Fr	Froude number
G_o	Size of the gate opening
H_d	Total design head over the crest of an ogee weir
H_s	Total design head over a sharp-crested weir
K	Reynolds averaged kinetic energy of turbulent eddies
$M_1 \sim M_4$	Dimensionless constants
P	Wetted perimeter
Q	Volumetric discharge
Q_{2DP}	Quasi-2D discharge converted to prototype units
Q_{3Deq}	3D equivalent discharge in prototype units
R	Hydraulic radius
Re	Reynolds number
S_{ij}	Strain rate tensor
V	Average velocity of fluid
W_{bay}	Width of the spillway bay
W_{cell}	Width of the quasi-2D mesh cell
We	Weber number
X	Model scale

Greek Symbols

δ_{ij}	Kroenecker delta function
ε	Dissipation rate of turbulent kinetic energy
μ	Molecular viscosity of the fluid
ν	Kinematic molecular viscosity of the fluid
ν_t	Kinematic eddy viscosity of the fluid (Boussinesq)
ρ	Fluid density
σ	Surface tension force per unit length
σ_{ij}	Viscous stress tensor
ς	Filled fraction of a control volume
∂	Symbol used to denote partial derivatives

Subscripts

$-F3D$	Denotes information extracted from Flow3D
$-LaSalle$	Denotes measurements from the physical model
bay	Denotes information related to the operational bay of the model
d	Denotes values taken downstream of the gate
m	Denotes model dimensions
p	Denotes prototype dimensions
u	Denotes values taken upstream of the gate

Chapter 1

Introduction

Due to recent advances in computing technologies, numerical modeling of hydraulic structures is becoming increasingly important in the engineering field, to the point where these models frequently replace the former industry standard of scaled physical modeling. This replacement is due to certain advantages that are associated with numerical modeling. Numerical models are often much less expensive than physical models because they require no laboratory space, no materials or construction and can be easily modified to accommodate design changes. All that is required for simulations is the computer, the software and the engineering know-how to interpret the results. Although many numerical models exist, validation data is often difficult to obtain and therefore, there is always a level of uncertainty associated with results.

Since physical models are considered to be the basis from which all other methods are compared (Savage & Johnson 2001), the purpose of this thesis is to compare the results of a numerical model in Flow3D, a commercially available software package, with the measured results obtained from the LaSalle Consulting Group's 1:50 scale sectional physical model of the Keeyask Generating Station spillway and diversion works for validation purposes. According to the construction plans, initially, the river is to be diverted through the diversion works in order to construct the main dam. Once completed, all seven bays of the control structure will be individually blocked off with stoplogs in order to construct the ogee crest of the spillway. Thus, the diversion and rollway phases of the project use the same approach channel, tailrace and control structure. The project, which at the time of publication had not yet been constructed, is to be located on the Nelson River, 730km north of Winnipeg, Canada.

Previous studies (e.g. Savage & Johnson (2001), Guo et al. (1998), Chatila & Tabbara (2004), etc.) have shown that numerical models are sufficiently advanced so as to compute reasonable results for water surface profiles, pressures and discharges/discharge coefficients over ogee overflow spillways. These studies often used variations of 1D, 2D and 3D equations that govern fluid flow as well as preprogrammed 3D numerical software. However, the cases that were examined were frequently of a simplified and academic nature, with the absence of approach channels, without the presence of piers to obstruct the flow and in the absence of gates.

This study seeks to model a real-life design of an ogee spillway for both ungated and gated cases, for varying water levels while including tailwater when necessary. The first objective is to confirm that numerical models are capable of modeling the ungated cases satisfactorily for more complex real-life designs. The second objective is to ascertain whether, and to what degree, the numerical model can model the partially open gated cases.

The following describes the approach taken to fulfill these objectives. In order to determine the required mesh size to obtain a mesh independent solution, tests were conducted in quasi-2D on the diversion structure for a single upstream water level for a fully open gate condition and four partial gate openings. The fully open condition was later reanalyzed in 3D since 2D did not adequately model the horizontal contraction found on the physical model. The meshes during these tests were used for subsequent simulations. Sensitivity tests were conducted for the same conditions for the fully open case in 3D and a partial gate opening in 2D in order to observe the effects associated with scaling (1:50, prototype) and the effects of two turbulence closure models (K-ε, RNG). Finally, 3D results for the fully open case for the rollway and diversion structures were compared to the results from the physical scale model for three different upstream water levels.

This thesis includes a review of a typical hydropower plant layout, the design and uses of ogee spillways and hydraulic gates and a summary of recent advances in the numerical modeling of spillways (Chapter 2). Chapter 3 describes the background theory of physical modeling as well as a brief overview of numerical modeling including the Navier-Stokes equations, the Reynolds-averaged Navier-Stokes (RANS) method, turbulence closure models and discretization techniques. Chapter 4 describes the methodology involved in the research, including in-depth descriptions of the physical and numerical models. Chapter 5 presents the results of the numerical simulations along with brief discussions concerning trends in results while Chapter 6 attempts to relate these results to previous studies. Finally, the conclusion of Chapter 7 summarizes the ideas and results of the three previous chapters. The appendices contain additional drawings of the physical model and additional experimental data.

Chapter 2

Literature Review

A typical layout of a hydro-electric installation is presented followed by a more detailed review of ogee-type spillways and hydraulic gates. The final section critically examines recent advances in the numerical modeling of spillways in one, two and three-dimensions.

2.1 Hydropower Plant Layout

The design and layout of hydro-electric projects is highly dependant on the characteristics of the site however, structures common to all installations are in most cases present in one form or another. Figure 2.1 provides a view of the typical layout of a hydro-electric installation.

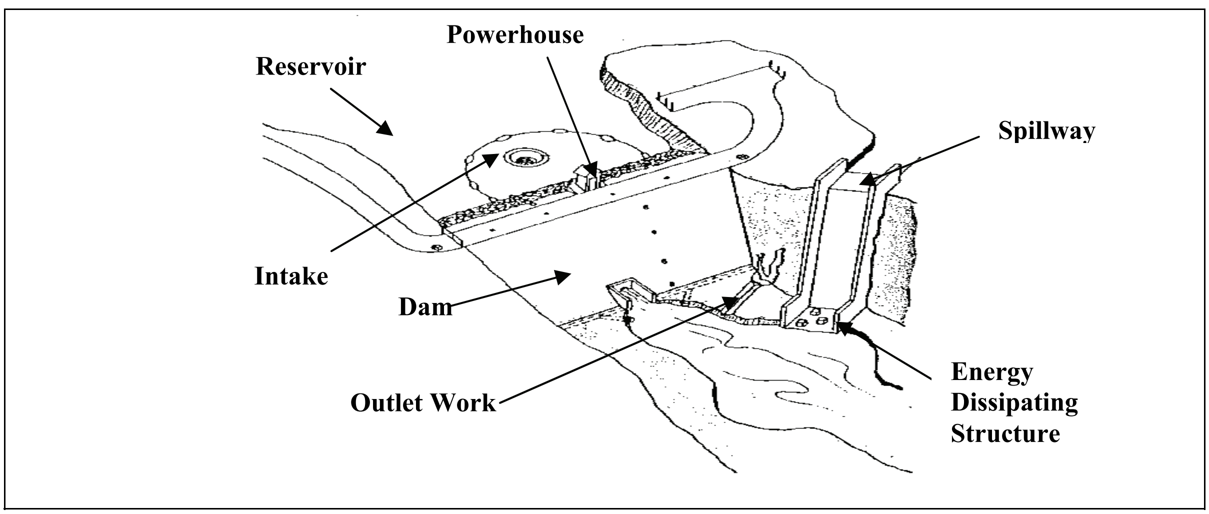

Figure 2.1: Typical Hydro-Electric Project Layout (www.dec.state.ny.us)

The dam, the largest structure in hydro-electric installations, is used predominantly for water retention and storage. The river reach upstream of the structure is allowed to back up, causing water to pool to a desired elevation, thus increasing the potential energy of the flow and creating a quasi lake-like environment called the reservoir. A reservoir is not always required, especially if velocities and discharges are adequate on the existing river. In this case it is called a “run of the river” installation and the smaller dam simply acts as a powerhouse, housing the turbines in order to create electricity using the pre-existing kinetic energy of the river.

The potential energy of the stored water in the reservoir of standard hydropower installations is converted to kinetic energy as the flow is allowed to exit the reservoir through the intake and penstock placed either near the bottom of the dam or at the water surface, which leads to the turbines in the powerhouse. The turbines rotate as the water jet impacts the impellors and, with a shaft connected to a generator, electricity is produced.

In the event that the dam requires maintenance work or a release of water from the reservoir is required for downstream needs, an outlet structure may be included in the project’s design in combination with a suitable energy dissipating structure, if required. The outlet is generally placed near the bottom of the dam in order to release the water at the highest possible rate (Bureau of Reclamation 1974). In some cases, the outlet may even double as the spillway.

The role of the spillway is to discharge excess water in times of floods in such a way that the safety of the dam and other structures is maintained (Smith 1995). The spillway is generally located at or near the design elevation of the reservoir and may be controlled by suitable hydraulic gates. Excess water is simply allowed to discharge downstream while an appropriate structure dissipates the kinetic energy of the flow. In some cases, the energy dissipating structure may be included along the slope of the spillway, therefore reducing the amount of space required to adequately discharge the flow without risk of scouring the downstream river reach or undermining the dam (Bureau of Reclamation 1974). A more detailed review of ogee-type spillways follows.

2.2 Ogee-Type Spillways

Many factors including the design flow, tailwater rating curves, site conditions, economy of design and available space influence the design and layout of the spillway structure. The spillway is generally classified by its most prominent feature and is described as controlled or uncontrolled (gated or ungated) (Bureau of Reclamation 1974). Several types of spillways currently exist; however, only those including an ogee-weir will be reviewed as the others are outside the scope of this thesis.

An ogee-shaped weir is designed so as to take the shape of the lower nappe as it would occur when water is discharging from a sharp-crested weir at the design flow (Smith 1995) as seen in Figure 2.2. The pressure profile along the surface of the weir is therefore essentially atmospheric and prevents the access of air to the underlying material, which could cause cavitation damage. At design conditions, the water flows smoothly over the crest without boundary layer interference and is almost at maximum efficiency (Bureau of Reclamation 1974).

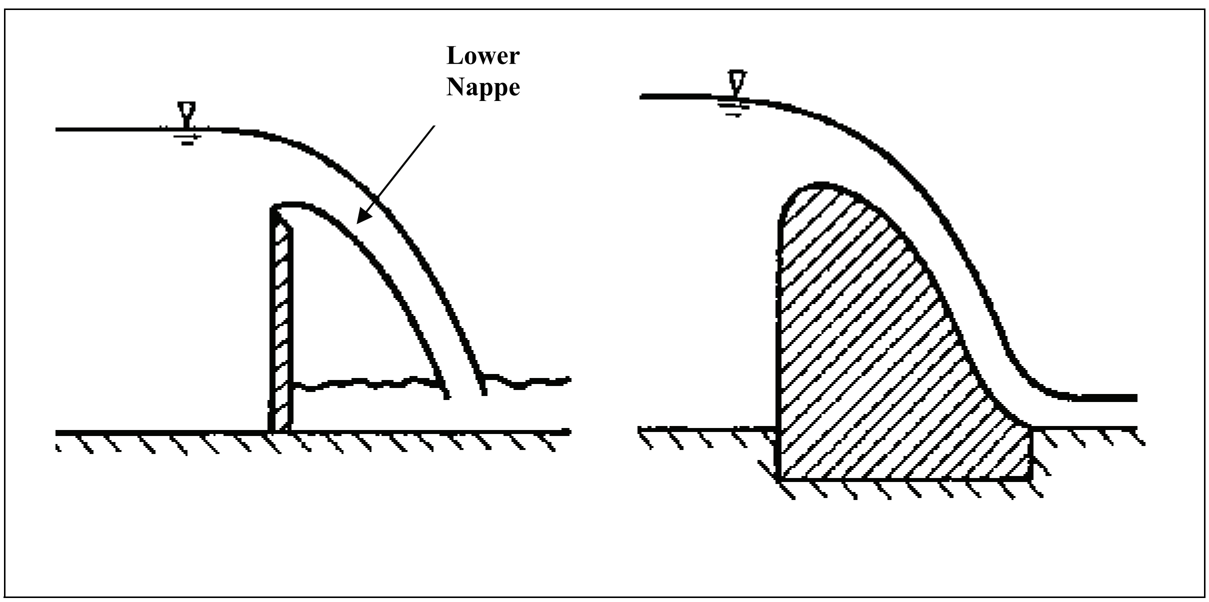

Figure 2.2: Sketch of Sharp-Crested and Ogee Weirs (www.fao.org)

If the weir shape is made broader, the crest will support positive hydrostatic pressures at design conditions. This creates a backwater effect and therefore negatively impacts the discharge efficiency of the structure. Conversely, if the weir shape is made sharper, negative hydrostatic pressures will develop for the same design conditions which would increase the effective head on the crest (Bureau of Reclamation 1974). While the discharge efficiency does increase due to the rise in effective head, the harmful effects of cavitation caused by the negative pressures limit the use of a sharper crest. However, the increase in efficiency is considered to be an advantage because with a properly designed ogee weir, it is possible to slightly exceed the design discharge without any negative consequences. If this situation develops, due to a flood exceeding design conditions, the crest acts as if it were sharper in shape and the discharge efficiency increases allowing the excess water to pass. Although negative pressures do arise, if these remain above negative 2m, no cavitation will occur (Smith 1995).

The discharge Q for an ogee-weir depends on the geometry of the overflow section (i.e. width, height), the gravitational constant g, the total head on the equivalent sharp-crested weir H_s and the dimensionless discharge coefficient C. The value of this coefficient is a function of the geometry, the surface tension and viscosity of the liquid and it is determined experimentally (Smith 1995). Through dimensional analysis and model testing, the general weir equation is given by:

$$Q = \frac{2}{3} C \sqrt{2g} b H_s^{3/2} \tag{2.1}$$

or in it's more common form:

$$Q = C_d b H_d^{3/2} \tag{2.2}$$

where b is the net width, C_d is the discharge coefficient which includes the multiplication of the term $(2/3)\sqrt{2g}$ and ranges from 1.759 to 2.195 for a vertical upstream face depending on the height of the sill and H_d is the total design head over the crest of the ogee weir and is equal to $(1\text{-}0.112)H_s$ (US Army Corp of Engineers 1995).

The spillway containing an ogee-shaped weir can either be an integral part of the dam, or it can be constructed in a remote location along the reservoir such as in the cases of chute or side-channel spillways. The overflow ogee spillway is generally constructed on concrete-gravity dams. The crest of the spillway is located at the approximate operational head of the dam connecting usually to the upstream vertical face although, for design purposes, a small offsetting may be required (Smith 1995). The ogee-shape continues with downstream distance until it reaches the slope of the downstream face. This slope is maintained for the remainder of the spillway until the base of the dam, where the flow enters a suitable energy dissipating structure. A variation of the overflow ogee spillway, the cascade spillway, is a structure on which the generally smooth surface of the ogee spillway is stepped, thus including the energy dissipating structure along its length. For more information on the design of cascade spillways, refer to Christodoulou (1993), Vischer & Hager (1998) and Boes & Hager (2003a).

When a dam is too small to include an overflow type spillway it may be necessary to construct the spillway elsewhere along the reservoir. In the case of the chute spillway, the discharge is conveyed from the reservoir to the downstream portion of the river through an open channel, which is why it is sometimes referred to as an open channel spillway (Smith 1995). The slopes of the approach channel and tailrace are dictated by the topography of the site with the entire section, similarly to the overflow ogee spillway, ending with an energy dissipating structure (Bureau of Reclamation 1974). Towards the center of the channel, one or several ogee weirs separated by piers, are constructed and may be gated or ungated depending on the design.

Conversely, the side channel spillway is used when abutments are too high or too steep to accommodate a chute spillway. It is a separate structure located at the end of the dam in a narrow canyon where the flow must change directions at an angle of approximately

90º (Smith 1995). It is similar in design to the ogee overflow spillway but in some cases, depending on the material in the canyon, it may not require an energy dissipating structure.

2.3 Hydraulic Gates of Spillways

Three different designs for spillway control currently exist and can be classified as: uncontrolled which are characterized by the absence of any type of hydraulic gate, movable crest devices and regulating devices (Smith 1995, Bureau of Reclamation 1974). Uncontrolled crests are generally used on small spillways and weirs when the release of water is only required when the reservoir head exceeds the design level. The advantages of this design include eliminating the need for constant supervision by an operator and the elimination of maintenance and repair costs (Bureau of Reclamation 1974). Movable crest and regulating devices are often employed when there is the presence of a sufficiently long uncontrolled crest or when the spillway crest is located under the normal operating level of the reservoir (Bureau of Reclamation 1974).

Most spillways on major dams are gated since extra head is obtained above a lower crest, which allows the design flow to pass with a narrower and more economical structure (Smith 1995). Since most types of gates are designed for overflow spillways and that all other types of spillways are generally characterized by uncontrolled crests, spillway gates are rectangular in shape and are located between vertical piers, the role of which is to successfully transfer the hydraulic load acting on the gate to the main structure (Smith 1995). The selection of the type and size of the gate is based on the type of spillway present, the discharge characteristics of the individual device, climate, the frequency and magnitude of floods, winter storage requirements, flood control storage, outflow requirements, ice and debris passage, the need for an operator, the availability of electricity, operating mechanisms, economy, adaptability, reliability, efficiency etc. (Bureau of Reclamation 1974). The main devices reviewed are flashboards, stoplogs and drum gates for movable crest devices, and plain sliding/self-closing gates, radial gates and rolling gates for regulating devices.

When the spillway is not needed for releasing flood water, flashboards, stoplogs or drum gates can be used to raise the water-level of the reservoir above the spillway crest. Flashboards usually consist of panels and can be designed to be placed and removed manually, to fail once overtopping begins or to drop out of position once the reservoir has reached a certain water level (Bureau of Reclamation 1974). Stoplogs, in contrast, consist of individual beams that are placed in pre-fabricated grooves constructed in the spillway piers and must always be removed individually using a hoisting mechanism (Bureau of Reclamation 1974). Differing from the two other gate designs, the drum gate's opening fluctuates freely with the water-level of the reservoir through an automated process in which a float within a well dictates the sustained position of the gate, and therefore, the drum gate is not designed to fail or to be removed when a sizable flood occurs. Its design consists of a hollow water tight body that has a triangular cross section with a steel plate placed on its top to match the shape of the crest and generally fits in a large recess constructed in the crest of the spillway (Smith 1995).

The plain sliding gate is the simplest of all spillway regulating devices. For small sizes, the gate is completely cast in steel or consists of a vertical flat plate with reinforcing steel ribs on its downstream side. For larger sizes, a structural steel framework is enclosed within specially cut steel or bronze skin plates which prevent the entry of water (Smith 1995). The gates are placed in grooves that are constructed into the adjoining piers which act as guide members. Sealing is provided by the contact pressure of the gate in conjunction with specially designed rubber seals (Bureau of Reclamation 1974, Smith 1995). While plain sliding gates are allowed to slide freely within the gate slots incorporated into the piers, another variation, termed self-closing gates, include the addition of wheels or caterpillar rollers that are used to reduce frictional forces caused by the full contact of the steel/bronze and rubber seals along the concrete. As their name implies, these gates are capable of closing under their own weight.

When the gate is fully-closed there is contact between the bottom portion of the gate and the spillway surface. As the gate is lifted by the hoisting mechanism (e.g. motor or hydraulic cylinder with screw-type or rack-and-pinion-type hoist), an orifice develops between the crest and the gate and the water is undershot for all gate openings (Bureau of Reclamation 1974). The rate of gate travel associated with the plain sliding gate is usually of the order of 0.05 to 0.1m/min and can obtain speeds of 1m/min for self-closing gates (Smith 1995).

The radial gate consists of a concentric steel plate, reinforced by steel ribs and is supported by a structural steel frame. The arms of the gate are supported by a pinned hinge that acts as the centre of curvature (Lewin 2001). A counter-weight is often installed on the opposite side of the hinge to reduce the effect of the weight of the gate structure and therefore a small hoisting effort is required which makes manual operation practical on small installations (Bureau of Reclamation 1974).

The rolling gate consists of a structural steel frame which is covered by a steel plate in such a way as to form a hollow steel cylinder. The diameter of the pier-supported and horizontally-placed cylinder is selected to be smaller than the required diameter to completely block the flow, forming an orifice below it. An apron is placed below the steel cylinder to effectively make up the difference. The gate is operated on an inclined track similar to a rack-and-pinion in which gear-like teeth placed on the downstream portion of the steel cylinder coincide with teeth on the inclined track (Smith 1995).

2.4 Recent Advances in the Modeling of Overflow Spillways

Presently, hydraulic engineering practice relies heavily on physical models for the design of spillways and indeed, most hydraulic structures. With the advances in numerical methods and computing power, computational models of spillway flows are increasingly being used in industry but still require validation from a physical model to ensure that the virtual modeling of physical processes is accurate. The consequences of the failure of a large hydro-electric dam on downstream sections of a river reach and most importantly, on human life, can be catastrophic (Bureau of Reclamation 1974). Several computational approaches have been developed including modeling in one, two or three-dimensions which use a wide variety of equations and discretization techniques.

The simplest models are one-dimensional and are used to verify river stage and the water surface profile upstream and along the length of the spillway but are incapable of simulating 3D flow patterns (Song & Zhou 1999). These models include that of Steffler & Jin (1993), adapted by Khan & Steffler (1996a and 1996b), where the 2D Reynolds equations were vertically averaged, the moment equations were developed by vertically integrating the Reynolds equations after they had been multiplied by a vertical coordinate and the equations were finally discretized using a Petrov-Galerkin and Bubnov-Galerkin finite element method. Their intentions were to extend the range of applicability of 1D modeling to highly curved, steep flows and finally free overfalls. Results were compared to the experimental data of Montes (1994) and showed that the vertically averaged and moment equations performed satisfactorily for both calculating the location of the water surface and estimating the bed pressure for tests involving a horizontal to steep slope transition, a spillway and flip-bucket case and symmetric and asymmetric bed profiles. Furthermore, excellent results were found for the upstream water surface and trajectory of the jet for the modeling of various free overfalls, however, in general, the results for both studies diverged in circumstances where large flows, steep gradients and large bed and water surface curvature were present. These approaches differ from the previous methods of Hager & Hutter (1984), Hager (1985) and Matthew (1991) in which the Boussinesq equations were applied using various meshing techniques and were found to be geometrically limited to mild slopes.

Gurcio & Magini. (1998) approached the modeling of 1D spillway flow by a different method using an equation for the free surface profile that is based on the momentum equation developed by Yen & Wenzel (1970) and further updated by Yen (1973) based on the St-Venant equations. This equation neglected the turbulent components of the velocity, assumed hydrostatic pressure and assumed a constant spillway width. The problem found in this approach is that it requires an accurate estimation of the momentum correction factor which is dependant on the velocity profile of the flow. In turn, the velocity profile is affected by three-dimensional features of the flow including fluctuating components caused by turbulence which were initially neglected. As a result, the model relies on tests done on the physical model to evaluate this correction factor which represents a disadvantage from an engineering point of view as the ultimate goal of computational modeling is to eventually eliminate the need for a physical model. Since the numerical model was heavily reliant on the physical model, water surface profiles were adequately predicted.

In other cases, such as that of Zarrati et al. (2004), a mathematical model that can be solved both numerically and analytically was used to predict the flow profile on a spillway. Zarrati et al. (2004) used the flow at a corner and free streamline theory methods as a comparison against the results obtained from a physical model. The flow was assumed to be irrotational (i.e. non turbulent) and the effect of gravity forces was assumed to be small within a short distance of a sudden change in slope due to the presence of high velocities creating a high Froude number on the spillway. Results showed that both the pressure profiles and water surface profiles of both numerical modeling techniques were in good agreement with those of the physical model although, free streamline theory tended to be more accurate. Furthermore, it was found in particular that free streamline theory is a powerful tool for the analysis of flow within the vicinity of a sudden change in channel slope. Unfortunately, the results are only valid for high-speed free surface flows therefore requiring a more accurate model upstream of the spillway, where velocities are much smaller. Similar cases were previously studied by Henderson & Tierney (1963), Strelkoff & Moayeri (1970), Wei & De Fazio (1982), etc.

Additional levels of accuracy and detail are found in two-dimensional models which allow perturbations of flow caused by obstructions, supercritical flow, etc., to be modeled (Causon et al. 1999). Many methods have been developed to model curved beds and spillways which are primarily based on the vertically integrated Euler's equations, the shallow water equations and the boundary integral equations.

Berger & Carey (1998) modified the standard shallow water equations by deriving them in their non-conservative form which allowed the inclusion of the effects due to the curvature of the bed. Furthermore, these equations were depth-averaged and by using the

Petrov-Galerkin finite element method, allowed them to be modeled computationally. The model was then compared to the St-Venant equations, standard steep slope shallow water equations and a high-Reynolds number physical model built in a flume. Results indicated that the modified shallow water equations accurately predicted both the capacity of the spillway and bed pressure found on the physical model however, this was not the case for the two other sets of equations which required higher water surface elevations in order to accurately predict the steady-state capacity. As a result, pressures on the two latter models were also over-estimated. The limitation of this approach is that in the cases where hydraulic jumps occur, the additional terms introduced into the equations that take into account the effects of curvature cause an error in the modeling of its location. Furthermore, the results were found to be only adequate for highly 2D flows.

Causon et al. (1999) used the 2D non-linear shallow water equations using a cell-centered Godunov-type finite volume approach to model supercritical flow in spillway channels which included six tests related to shockwaves. Many previous studies such as those of Hager (1989), Berger & Stockstill (1993), Reinauer & Hager (1998), etc., have focused on supercritical flow since this situation, common on spillways, is of importance to hydraulic engineers that wish to know the locations of hydraulic jumps and standing waves, the presence of which could cause depths much larger than the mean. Results of the simulations were compared to the physical model study of Ippen & Dawson (1951) with which satisfactory agreement was found for the maximum rise in water depth due to shock reflection. Nevertheless, the nature of the model assumes hydrostatic pressure and neglects the terms representing vertical acceleration and flow viscosity and is therefore limited in its applicability.

Other works, such as those of Laible & Lillys (1997), Anastasiou & Chan (1997) and Unami et al. (1999) used the vertically-integrated Euler's equations to model two-dimensional flow. In particular, Unami et al. (1999) used both the standard Galerkin finite element scheme to solve the continuity equation and an upwind finite volume method to solve the momentum equation so as to model the flow over an ogee spillway. Results were compared to those obtained by Taruya et al. (1986) on a 1:30 scale model however, the physical model could not predict the increase of free surface level caused by air entrainment. Conversely, the numerical model was able to obtain a physically realistic solution for the transition from subcritical to supercritical flow on the spillway while predicting the increase in water level due to air entrainment by including a depth-averaged empirical formula. Although the results are in good agreement with those found on the physical model, a more accurate analysis of spillway flow would require the solving of 3D equations which include a convection-diffusion equation meant to govern the concentrations of entrained air.

Guo et al. (1998) used analytic functional boundary theory and the substitution of variables to derive the non-singular boundary integral equations in the physical plane to model spillway flow on a partially supported free overfall spillway with initially unknown discharge. A synchronous iterative method was then applied to determine the discharge and profile of the flow. Results for water surface profiles, discharges and pressures along the bed were found to be in good agreement with those measured on the physical model used for comparison, however; the numerical model was found to be only valid for 2D steady potential flows.

For more accurate analyses of spillway flows, it is necessary to solve 3D equations (Unami et al. 1999) which allow the inclusion of turbulence defined as an unsteady, three-dimensional, rotational and random motion in which density, pressure and velocities fluctuate in time and space (Jaw & Chen 1998). The main approaches used are the Reynolds-averaged Navier-Stokes (RANS) equations combined with variations of the K-ε closure model and the large eddy simulation method.

Olsen & Kjellesvig (1998) extended the 2D work of Kjellesvig (1996) and used RANS combined with the K-ε eddy viscosity model of Launder et al. (1972) to predict the coefficient of discharge on an ogee overflow spillway. The equations were discretized using the control volume based finite element method and the power law scheme, a first order upstream method. Furthermore, the SIMPLE method was used for pressure coupling of all cells, and a modified continuity equation was used to track the water surface. All simulations were compared with a physical model. Results of the simulations indicated that the numerical model was in good agreement with the physical model: the value of discharge coefficients deviated by less than 1% and the calculated pressure along the bed of the spillway was adequate. Similarly, Chen et al. (2002) used the same closure and discretization techniques to model the flow over a stepped spillway. However, in this case, the authors opted for the volume of fluid method to track the location of the free surface because of its ability to calculate the fraction of entrained air, the effects of which are extremely important on stepped spillways. Results of the numerical simulations were compared to a stepped spillway physical model constructed in Plexiglas. It was found that the computational model modeled the flow over the stepped spillway adequately. In addition, the volume of fluid method was able to track the free surface adequately despite the large quantities of entrained air, and pressures extracted on each step of the spillway were similar to those of the physical model.

Song & Zhou (1999) used large eddy simulation in combination with an explicit finite volume scheme to determine the free surface flow over an ogee overflow spillway. The location of the free surface was computed using the marker and cell method of Harlow & Welsh (1965) while a free surface steepness limiting approach was used to model the free surface waves. Air entrainment was however neglected since the interest was on the flow at the inlet and transition where entrainment is negligible. Time averaged results of the numerical model were compared to a physical model. The numerical model initially used a 1D model to predict the general location of the free surface along the spillway and used its results as initial conditions for the 3D model so as to decrease the computational load on the computer. The findings of the study show that both the numerical model and the physical model are in good agreement at the entrance, however, the omission of air entrainment effects tend to predict smaller water levels further downstream.

An alternative option to deriving and implementing sets of equations is to purchase commercially available software. Savage & Johnson (2001) used Flow3D to compare its results of ogee spillway flow with those of a physical model. Flow3D uses the volume of fluid method for tracking the water surface, uses fractional area/volume obstacle representation to determine the location of solid objects and uses a finite volume scheme to discretize the domain. The Reynolds-averaged Navier-Stokes equations were used in combination with the renormalized grouping formulation of the K-ε eddy viscosity closure model of Yakhot & Orszag (1986). Data from the physical model indicated that the flow was essentially two-dimensional in nature despite the presence of slightly larger depths along the walls of the flume. Although one simulation was done in 3D, it was later decided that the remainder would be computed in quasi-2D, i.e. simulations were run on a mesh exactly one cell thick, since it was determined that a 2D analysis was sufficient and computationally faster for calculating coefficients of discharge. The study showed that Flow3D is sufficiently advanced for calculating discharge and pressures along uncontrolled ogee spillways.

Chatila & Tabbara (2004) and Tabbara et al. (2005) modeled the flow over an ogee spillway and a stepped spillway respectively by using the ADINA-F computational fluid dynamics software package. Both studies used the software's default K-ε closure model in which the equations are discretized using the finite element method. Results from simulations were compared to physical models that were constructed in long flumes with glass walls. For each study, water surface profiles were calculated by the numerical model and compared with the physical model. For the simple ogee spillway case, water surface profiles were in good agreement with those of the physical model; however, discrepancies in the mid-section were observed, possibly caused by the omission of air entrainment in the numerical model. For the stepped spillway case, predicted water surfaces were both qualitatively consistent with general flow characteristics and quantitatively agreed with measure profiles. Furthermore, the energy dissipation ratios were comparable to the experimental results.

Many approaches for the modeling of spillway flow currently exist, the choice of which depends on the level of detail the researcher wishes to obtain. From a practical view point, 3D modeling is the most important as engineers designing these structures require an increased level of detail so as to ensure the stability and safety of complex structures.

Chapter 3

Background Theory

This chapter presents the scientific theory relevant for the construction and design of physical models for incompressible fluids as well as a review of the theory behind numerical modeling of incompressible fluids. The first section will examine, in particular, hydraulic similitude, similitude laws and the basic assumptions involved in the design of physical models. The second section will review the Navier-Stokes equations and methods of solutions including turbulence models, with particular emphasis on the Reynolds-average Navier-Stokes equations and the K-ε closure models as well as the finite-volume method discretization technique.

3.1 Physical Models for Incompressible Fluids

To aid in the visualization and design of engineering works, physical models are often used to solve problems in fluid mechanics when boundary conditions are complex, when the problem is unsolvable by theory, when there is very little empirical data available etc. (Henderson 1966, Webber 1965). The testing of physical models can be used to observe the effects of different design proposals under conditions that are likely to be found in practice which would be costly and impractical if they were performed at the full scale (Webber 1965). This is often the case with the design of most major hydraulic projects such as dam spillways and outlet works, canal chutes, irrigation distribution systems, diversion works, sediment control works, drop structures etc. (Bureau of Reclamation 1958).

For the results of the physical model to be directly transferable to the prototype, the two flows must be hydraulically similar (Webber 1965). Perfect hydraulic similitude is often unattainable for various reasons and as a result, errors, called *scale effects*, are introduced into the model's results (Webber 1965, Henderson 1966). The most common scale effect in hydraulics is caused by the viscosity of water and its origin will be examined in further detail later in this section.

For perfect hydraulic similarity to exist between two systems, three criteria must be met. The first criterion is geometric similarity. Geometric similarity refers to the similarity of length scales and it follows that the ratio of any section of the model to its prototypical counter-part is the same (Henderson 1966). For complete geometric similarity, the boundary roughness of both the model and prototype must also be similar using the same scalar relationship meaning that at best, the ratio of the grain roughness k_s must be equal to that of any other dimensional ratio (Webber 1965). On occasion, the scale of a physical model is deliberately distorted, namely in cases where the length is large in proportion to the depth (Bureau of Reclamation 1958) however, this topic will not be reviewed as it is outside the scope of this thesis.

The second criterion for obtaining hydraulic similarity is kinematic similarity which refers to the similitude of motion. Kinematic similarity implies that the two flow patterns given by the model and prototype are similar (Henderson 1966). This means that the velocities and accelerations at any given homologous points and times must have the same ratios (Webber 1965). Since the velocity and acceleration of the flow are vector quantities, the directions at each point must also be the same (Webber 1965, Henderson 1966, Bureau of Reclamation 1958). For perfect kinematic similitude of the model and prototype, geometric similarity must also be present as the shape of streamlines is determined by boundary conditions (Webber 1965).

The final criterion is dynamic similarity. For dynamic similarity between the model and prototype to be achieved, the forces at homologous points located on both the model and prototype must have the same ratio and direction (Webber 1965, Henderson 1966). Dynamic similarity implies that kinematic similarity must also exist since the mobility of the fluid is governed by the presence of similar forces. As a result, the implications of dynamic similarity and hydraulic similarity are identical (Webber 1965).

With the main forces acting on incompressible fluids being pressure, gravity, viscosity and surface tension, the following relationship is established:

$$\frac{[\vec{F}_P]_m}{[\vec{F}_P]_p} = \frac{[\vec{F}_g]_m}{[\vec{F}_g]_p} = \frac{[\vec{F}_\mu]_m}{[\vec{F}_\mu]_p} = \frac{[\vec{F}_\sigma]_m}{[\vec{F}_\sigma]_p} \tag{3.1}$$

where $\vec{F}_P$, $\vec{F}_g$, $\vec{F}_\mu$ and $\vec{F}_\sigma$ are the force vectors for pressure, gravity, viscosity and surface tension respectively and the subscripts m and p denote model and prototype values. If the magnitude and direction of these forces are known, the resultant, the inertial force $\vec{F}_I$, can be found by the construction of vector polygon which gives:

$$\vec{F}_P \mapsto \vec{F}_g \mapsto \vec{F}_\mu \mapsto \vec{F}_\sigma = \vec{F}_I \tag{3.2}$$

Dividing Equation 3.2 by $\vec{F}_I$ gives:

$$\frac{\vec{F}_P}{\vec{F}_I} \mapsto \frac{\vec{F}_g}{\vec{F}_I} \mapsto \frac{\vec{F}_\mu}{\vec{F}_I} \mapsto \frac{\vec{F}_\sigma}{\vec{F}_I} = 1 \tag{3.3}$$

and if each force ratio is recognized as the inverse of the relevant dimensionless parameter the result is:

$$\frac{M_1}{Eu} \mapsto \frac{M_2}{Fr} \mapsto \frac{M_3}{\mathrm{Re}} \mapsto \frac{M_4}{We} = 1 \tag{3.4}$$

in which M_1, M_2 , M_3 and M_4 are dimensionless coefficients and Eu, Fr , Re and We are the Euler, Froude, Reynolds and Webber numbers respectively (Webber 1965). These numbers are dimensionless and are also known as similarity laws when their model/prototype values are compared for a given point. In this work the important similarity laws are the Froude, Reynolds and Weber numbers, a description of each of these follows.

The Froude number is defined as being a function of the ratio of the inertial forces and the gravity forces of the fluid and is used in flows that are influenced by gravity: primarily free surface flows (Potter et al. 2002). As a result, most models constructed for civil engineering design purposes are highly dependent on the Froude number similitude (Webber 1965). The standard equation for the Froude number is:

$$Fr = \frac{V}{\sqrt{gl}} \qquad (3.5)$$

where V is the velocity of the fluid and l is a length scale, generally taken as the depth for open channel flow problems.

The Reynolds number is a function of the ratio of the inertial forces and the viscous forces and essentially describes the level of turbulence of the flow. It is generally used in problems involving boundary layer effects, pipe flow, open channels etc. (Potter et al. 2002) and is given by:

$$\mathrm{Re} = \frac{\rho V l}{\mu} \text{ or } \frac{Vl}{\nu} \qquad (3.6)$$

where ρ is the density of the fluid and μ and ν are the viscosity and kinematic viscosity of the fluid respectively. The value of l for open channels is generally taken as R, where R is the hydraulic radius of the channel.

The Weber number describes the effects of surface tension of the fluid. It is the ratio of inertial and surface tension forces of the fluid and is used in flows with interfaces (e.g. air-water interface in open channel flow) (Potter et al. 2002). The general form of the Weber number is given by:

$$We = \frac{\rho V^2 l}{\sigma} \qquad (3.7)$$

where σ is the surface tension force per unit length of the fluid. The value of l for open channel flow problems is generally taken as the depth.

Theoretical perfect hydraulic similarity implies that all three of the above model's dimensionless numbers must be equal to their prototypical counter-parts. By applying the subscripts m and p to define model and prototype parameters respectively and by defining the model scale X as the ratio of l_m and l_p, the following relationship is established:

$$X^{1/2} = \left(\frac{1}{X}\right)\left(\frac{\nu_m}{\nu_p}\right) = \left(\frac{\rho_p}{\rho_m}\right)^{\frac{1}{2}}\left(\frac{\sigma_m}{\sigma_p}\right)^{\frac{1}{2}}\left(\frac{1}{X^{1/2}}\right) \tag{3.8}$$

It can be seen that under these conditions, there is no known fluid in existence with the correct physical properties that can satisfy this expression unless the model scale is unity (Webber 1965). Fortunately in hydraulics, if the depths and widths of the model are made greater than approximately 0.02m (Chanson & Gonzalez 2005) and $We_m \geq 100$ (Boes & Hager 2003b), surface tension is negligible and therefore the Weber number, representing the right-hand side of Equation 3.8 can be eliminated (Webber 1965) which simplifies the equation to:

$$\nu_m = \nu_p X^{3/2} \tag{3.9}$$

This equation, however, still presents an impracticality as the viscosity of the model fluid would have to be unfeasibly smaller than that of the prototype fluid unless the geometric scale is near unity (Potter et al. 2002). Despite this problem, water is frequently used as the model fluid while the scale is maintained reasonably low, which is in direct violation of the concept of dynamic similitude (Henderson 1966). As a result, in open channel hydraulic models, the Froude numbers of the model and prototype are frequently made equal while viscous effects (i.e. Re) are included through other techniques which introduces slight distortions to the model's forces or, *scale effects* (Potter et al. 2002).

To minimize these effects, Re should be made as high as possible in the model with a lower limit of 1400 for clear water flows so as to ensure fully turbulent flow (Webber 1965, Henderson 1966). In cases where air entrainment is significant and causes large scale effects, Kobus (1984) proposed a minimum Re of 10^5 which has been successfully used in other experiments such as for stepped spillways (Chanson & Gonzalez 2005). This ensures that when the flow is fully turbulent with an increasing Re, the contribution of the surface drag component in the total drag is minimized and therefore dynamic similarity is asymptotically obtained (Potter et al. 2002).

3.2 Incompressible Computational Fluid Dynamics

In the pre-computer era, calculations of water surface profiles and depths were obtained by using manual iterative processes of the steady St-Venant equations (1D simplifications of the Navier-Stokes equations), graphical methods (MacDonald et al. 1997) and by the construction and use of physical models. With the exception of physical modeling, hydraulic engineers were freed from tedious calculations and tasks as the computer era began in the 1960's and 1970's (MacDonald et al. 1997) and a specialized branch of fluid mechanics, termed, computational fluid dynamics, developed. Computational fluid dynamics (CFD) is defined as the use of a computer to obtain numerical solutions for fluid flow problems, by use of modified Navier-Stokes equations (Potter et al. 2002) i.e. the equations that summarize the law of conservation of mass of the bulk fluid and Newton's second law of motion which, with the inclusion of the continuity equation, govern fluid motion (Date 2005). Previously, analytical solutions of these partial differential equations (PDEs) were restricted to fully developed or irrotational flow in pipes or when $Re < 1$ due to the linearity or the negligible value of non-linear terms within the PDEs respectively (Potter et al. 2002).

In Cartesian coordinates, assuming constant fluid properties and written in tensor form, the Navier-Stokes equations for a viscous incompressible Newtonian fluid take the form:

$$\frac{\partial u_i}{\partial t} + u_j \frac{\partial u_i}{\partial x_j} = -\frac{1}{\rho}\frac{\partial p}{\partial x_i} + \frac{\partial \sigma_{ij}}{\partial x_j} \tag{3.10}$$

where u_i and u_j are velocity tensors, x_i and x_j are directional tensors, p is the pressure of the fluid and σ_{ij} is the viscous stress tensor given by

$$\sigma_{ij} = 2\nu S_{ij} \tag{3.11}$$

for a Newtonian fluid. The strain rate tensor S_{ij} is defined as

$$S_{ij} = \frac{1}{2}\left(\frac{\partial u_i}{\partial x_j} + \frac{\partial u_j}{\partial x_i}\right) \tag{3.12}$$

The left hand side of Equation 3.10 represents the momentum of the fluid per unit mass while the right hand side includes the pressure drop and strain rate functions (Muralidhar & Biswas 2005). For more details on different forms of the Navier-Stokes equations, refer to Warsi (2006). It should be noted that the normalization of the incompressible Navier-Stokes equations yield Eu, Re , Fr and We as parameters through boundary conditions (Potter et al. 2002) which further validates the use of physical models as described in Section 3.1.

Although the three equations given by Equation 3.10 with the inclusion of the continuity equations ($\partial u_i / \partial x_i = 0$) completely define fluid motion and are relatively easily solved for low-Reynolds number flows, they have not yet been solved for high-Reynolds numbers within a reasonable amount of time (Potter et al. 2002, Drikakis 2003) due to the unsteady and three-dimensional nature of the flow, known as turbulence (Potter et al. 2002). Since direct numerical simulation (DNS) of the Navier-Stokes equations is for the time being beyond foreseeable computing power, other methods such as large eddy simulation (LES), detached eddy simulation (DES) and the Reynolds-averaged Navier-Stokes (RANS) equations were developed.

In large eddy simulation, scales of wavelengths smaller than the grid size of the computational domain are ignored while the larger scales of flow are allowed to be computed by an appropriately chosen low-pass filter, which eliminates the fluctuations at the sub-grid level (Lesieur & Métais 1996). Similarly, detached eddy simulation uses LES to compute the larger scales but differs by either using a RANS model or DNS to compute sub-grid fluctuations (Yan et al. 2005). These topics will not be discussed in more detail as the methods will not be used within the context of this thesis; however, a more detailed explanation of the RANS method is presented.

In the RANS approach, the Navier-Stokes equations are averaged over a time interval or across a grouping of equivalent flows (Drikakis 2003). The goal of this approach is to obtain the mean effect of turbulent quantities while disregarding the instantaneous effects (Jaw et al. 1998) therefore creating a statistically steady flow (Drikakis 2003).

To develop the RANS equations, the flow characteristics are divided into their mean and fluctuating quantities:

$$u_i = \overline{u}_i + u_i' \tag{3.13}$$

and

$$p = \overline{p} + p' \tag{3.14}$$

where the mean is represented by the bar, and the prime represents the fluctuating component. Furthermore the fluctuating quantities are centered giving $\overline{u_i'} = 0$ and $\overline{p'} = 0$ and the average of the product of any two fluctuating quantities a' and b' gives $\overline{a'b'} = \overline{ab} - \overline{a}\,\overline{b}$.

By substituting Equations 3.13 and 3.14 into the Navier-Stokes equations given by Equation 3.10, the RANS equations for a viscous incompressible Newtonian fluid are obtained yielding the following expression:

$$\frac{\partial \overline{u}_i}{\partial t} + \overline{u}_j \frac{\partial \overline{u}_i}{\partial x_j} = -\frac{1}{\rho}\frac{\partial \overline{p}}{\partial x_i} + \frac{\partial \overline{\sigma}_{ij}}{\partial x_j} - \frac{\partial \left(\overline{u_i' u_j'}\right)}{\partial x_j} \tag{3.15}$$

where $\overline{\sigma}_{ij} = 2\nu \overline{S}_{ij}$, $\overline{S}_{ij}$ is the mean strain rate tensor and $\overline{u_i' u_j'}$ is the Reynolds stress tensor (Gatski 2004).

The addition of the Reynolds stress tensor makes the number of unknowns greater than the number of available equations. As a result, the problem must be solved with the addition of closure models that approximate the value of the Reynolds stresses through the use of additional PDEs related to turbulent characteristics (Jaw & Chen 1998). These models are created with the assumptions that the properties concerning the diffusion of turbulent transport by turbulence are proportional to the gradient of transport properties, that small turbulent eddies are considered to be either isotropic or anisotropic, that all turbulent transport quantities are functions of turbulent kinetic energy, Reynolds stresses, rate of dissipation of energy, mean flow variables and thermodynamic variables, that modeled turbulence must be consistent in symmetry, invariance, permutation and physical observations, that either one or multiple turbulence scales must characterize the turbulence phenomenon and that experimental calibration and determination is required for all turbulence model moduli (Jaw & Chen 1998).

Many closure models have been created over the past 30 years, some of them more complex than others however the emphasis on simplicity, computational robustness and speed within an industrial and commercial context disallows the use of advanced models (Drikakis 2003). In industrial applications the most common model is the two-equation model known as the K-ε eddy viscosity model. The K-ε eddy viscosity model, first formulated by Hanjalić (1970), employs the Boussinesq eddy viscosity (ν_t) concepts where the Reynolds stresses are defined by the following equation:

$$-\overline{u_i'u_j'} = \nu_t\left(\frac{\partial \overline{u}_i}{\partial x_j} + \frac{\partial \overline{u}_j}{\partial x_i}\right) - \frac{2}{3}\delta_{ij}K \tag{3.16}$$

where δ_{ij} is the Kroenecker delta function and ν_t is approximated by $C_\mu\left(K^2/\varepsilon\right)$ in which K is the Reynolds-averaged kinetic energy and ε is the dissipation rate of turbulent kinetic energy. Distributions for K and ε are determined from:

$$\frac{DK}{Dt} = \frac{\partial}{\partial x_j}\left(C_K \frac{K^2}{\varepsilon}\frac{\partial K}{\partial x_j} + \nu \frac{\partial K}{\partial x_j}\right) - \overline{u_i'u_j'}\frac{\partial \overline{u}_i}{\partial x_j} - \varepsilon \tag{3.17}$$

and

$$\begin{aligned}\frac{D\varepsilon}{Dt} &= \frac{\partial}{\partial x_j}\left(C_\varepsilon \frac{K^2}{\varepsilon}\frac{\partial \varepsilon}{\partial x_j} + \nu\frac{\partial \varepsilon}{\partial x_j}\right) - C_{\varepsilon 1}\frac{\varepsilon}{K}\overline{u_i'u_j'}\frac{\partial \overline{u}_i}{\partial x_j} \\ &- C_{\varepsilon 2}\frac{\varepsilon^2}{K} - C_{\varepsilon 3}\frac{\varepsilon}{K}\frac{\partial}{\partial x_j}\left(C_K\frac{K^2}{\varepsilon}\frac{\partial K}{\partial x_j}\right)\end{aligned} \tag{3.18}$$

where C_μ, C_K, C_ε, $C_{\varepsilon1}$, $C_{\varepsilon2}$ and $C_{\varepsilon3}$ are model coefficients, the values of which are presented in the following table with their authors:

Table 3.1: Coefficients of K-ε Eddy Viscosity Models (Jaw & Chen. 1998)

Authors	C_μ	C_K	C_ε	$C_{\varepsilon1}$	$C_{\varepsilon2}$	$C_{\varepsilon3}$
Hanjalić (1970)	0.07	0.07	0.064	1.45	2.0	0
Jones & Launder (1972)	0.09	0.09	0.069	1.55	2.0	0
Launder et al. (1972)	0.09	0.09	0.069	1.44	1.92	0
Yakhot & Orszag (1986)	0.084	0.117	0.117	1.063	1.722	0
Jaw & Chen (1991)	0.09	0.103	0.11	1.23	1.92	1.67

The first three were determined through computational optimization and experimentation, the fourth by renormalization analysis (based on theoretical results, not empirical) and the last by statistical analysis. Presently, the Launder et al. (1972) coefficients are used by most researchers, are the best tested and have been successfully used to model a large number of different flows including plane jets, mixing layers, boundary layer flows, etc. (Jaw & Chen 1998). With the given coefficients, predictions of the model yield unsatisfactory results only in exceptional circumstances, namely axisymmetric jets and weak free shear layers where overall turbulence production is small in comparison to dissipation (Jaw & Chen 1998). For more information regarding other two-equation models, refer to Harlow & Nakayama (1967), Launder & Spalding (1974), Lumley (1983), etc. for other K-ε models, Saffman (1970), Rodi & Spalding (1970), Spalding (1982), etc. for K-ω models, and the K-l models of Ng & Spalding (1972) etc.

Given the nature of computer operations, all equations used in CFD must be discretized since computer calculations are limited by four critical constraints. The first constraint is that computers can only perform arithmetic (i.e. $+,-,\times,\div$) and logic (i.e. true or false) operations which means that derivatives (i.e. the PDEs of turbulence models and Navier-Stokes equations) and integrals (i.e. the method of solution for the PDEs) must be represented by them. The second constraint is that computers represent numbers with a finite number of digits which means that round-off errors are produced and these must be controlled. The third is that computers have a limited amount of storage space which means that solutions can only be obtained with a finite number of points in space and time. Finally, computers perform a finite number of operations per unit time which means that solution procedures should attempt to minimize the computer time needed to achieve a computational task (Potter et al. 2002). Over the years, three discretization methods commonly used in CFD (Ferziger & Perić 2002) have been developed; these are the finite difference, finite volume and finite element methods.

Historically the oldest method for the numerical solution of PDEs, the finite difference (FD) method is believed to have been introduced by Euler in the 18th century. Its starting point in CFD is the differential form of the conservation of mass and momentum equations and requires the solution domain to be covered by a grid. At each grid point, PDEs are approximated in terms of the nodal values of the functions, the result of which is one algebraic equation per grid node that contains its variable value along with unknowns from a certain number of neighboring grids (Ferziger & Perić 2002).

Differing from the FD method, the starting point of the finite volume (FV) method is the integral form of the conservation equations which are subdivided into a finite number of control volumes (CV) and solved. This is done by placing a node at the centroid of each CV where the values of variables are to be calculated. Interpolation is then used to calculate the values of variables at the surface of the CV in terms of the nodal values. By approximating surface and volume integrals (i.e. convective and diffusive fluxes) by using suitable quadrature formulae, algebraic expressions for each CV are obtained in which a number of neighboring nodal values appear (Ferziger & Perić 2002). The FV method can accommodate any grid type and is suitable for complex geometries. It is also the simplest to understand and program and is often used by engineers since all terms that need to be approximated have a physical meaning (Ferziger & Perić 2002).

The finite element (FE) method, which has its origins in solid mechanics and structural analysis (Chen et al. 2000), is similar to the FV method since the solution domain is broken into a set of finite volumes or elements. These elements are often unstructured and in 2D are triangles and quadrilaterals while in 3D they are tetrahedral and hexahedral in shape (Ferziger & Perić 2002). The FE method is distinguished from the FV method by the multiplying of equations by a weight function before they are integrated over the entire domain.

A hybrid of the FV and FE methods called the control volume based finite element method (CV-FEM) also exists. In CV-FEM, shape functions are used to describe the variation over an element and CVs are formed around each node joining the centroids of the elements. The conservation equations are applied to the CVs in integral form in much the same way as the FV method however, fluxes through the CV boundaries and source terms are calculated using the FE method through the elements (Ferziger & Perić 2002). For more information on CV-FEM, refer to Petankar (1980).

Using the same methodology for the definition of the grid structure needed by the various methods described above, it becomes possible to define a set of PDEs to be discretized following the specifications of the selected discretization method, in order to solve for the free surface and obstacles (e.g. bridge piers, gates etc.) found in open channel flow problems. Two popular models for these respective purposes are the volume of fluid (VOF) method and the fractional area/volume obstacle representation (FAVOR) method. The VOF method, which was introduced by Hirt & Nicholls (1981), is categorized as an interface-capturing method like the marker-and-cell method of Harlow et al (1965) (Ferziger et al. 2002) and is a powerful tool that allows the simulation of complex free surface flows (Kvincinsky et al.1999). The computation is performed on a grid that represents the solution domain and extends beyond the free surface of the flow. The shape of the free surface is determined by computing which cell is filled or emptied (Kvincinsky et al.1999).

In addition to the Navier-Stokes equations and the continuity equation, the VOF method requires the solution of the filled fraction of each CV, termed ς, where $\varsigma = 1$ represents a filled CV and $\varsigma = 0$ represents an empty CV. The governing equation is based on the continuity equation and is:

$$\frac{\partial \varsigma}{\partial t} + u_i \frac{\partial \varsigma}{\partial x_i} = 0 \tag{3.19}$$

where ς satisfies $0 \leq \varsigma \leq 1$. In the original approach of Hirt & Nicholls (1981), Equation 3.19 is solved for the entire domain to find the location of the free surface with the Navier-Stokes and continuity equations solved for the liquid phase only (Ferzinger & Perić 2002).

The fractional area/volume obstacle representation (FAVOR) method, introduced by Hirt & Sicilian (1985), uses a similar approach to defining obstacles as the VOF method has to defining the free surface: the grid porosity value is zero within obstacles, 1 for cells without obstacles and a fractional value for cells that are partially filled. The method uses a first-order approximation to define the surface of the obstacle which creates a straight line in 2D and a plane in 3D. As a result, a finer grid is required to approximate curved surfaces so that the chords forming the surface in the computational domain are as small as possible so as to ensure the smoothest surface possible.

Chapter 4

Experimental and Numerical Methods

In May 2004, Manitoba Hydro invited companies to propose for consulting services relating to the Stage IV construction of the Keeyask Generating Station, to be located on the Nelson River upstream of Stephens Lake, 730km north of Winnipeg, Canada. The proposed project would have a hydraulic head of 18m, discharging at 4000m^3/s into a powerhouse containing seven generating units equaling a total capacity of 675MW (LaSalle Consulting Group 2005).

The design included a self-closing gated spillway structure containing 7 bays separated by piers (Figure A.1 of Appendix A), located north of the main dam. During construction, the spillway section would be used for the diversion of the river, which is to be blocked by gravel cofferdams to construct the main dam section. Once the dam is completed, the cofferdams are removed and individually, each spillway bay is closed using stoplogs in slots located on both the upstream and downstream of the piers to block the flow, in order to construct an ogee-type weir (rollway) control structure.

The LaSalle Consulting Group was charged with the construction of a sectional model of the spillway structure for both the diversion and rollway phases on which tests were conducted in order to measure the discharge rating curves, pressure profiles and water surface profiles for different gate openings. The purpose of this thesis is to verify the accuracy of Flow3D, a popular commercial CFD software package, in modeling the flow through the spillway structure by comparison to the sectional physical scale model tests. The following sections describe in detail the physical scale model tests run by the LaSalle Consulting Group, which provided the verification data for the computational model, whose methods and constraints are also described.

4.1 Sectional Physical Model

As specified by Manitoba Hydro in their request for proposal, the main control structure for both diversion and spillway cases was built in Plexiglas with a fixed bed made of smooth concrete at an undistorted scale of 1:50 which allowed for good representation of hydraulic conditions and maintained the model boundaries within a reasonable area. With this scale, the relationships between the model and prototype based on the Froude similarity are given in Table 4.1:

Table 4.1: Prototype to Model Relationships for a Undistorted 1:50 Scale Model

Horizontal	X	1/50
Vertical	X	1/50
Pressure	X	1/50
Plan Area	X^2	1/2500
Sectional Area	X^2	1/2500
Volume	X^3	1/125000
Velocity	$X^{1/2}$	1/7.07
Time	$X^{1/2}$	1/7.07
Discharge	$X^{5/2}$	1/17678

The model was designed with one half bay on each side of two central operational bays with an approach of 200m and a tailrace of 175m in the prototype length scale; each having a slope of 0.04 and 0.01 respectively. Unless otherwise specified, the dimensions of the prototype will be used instead of the dimensions of the model since the results obtained on the model are related back to the prototype. A Plexiglas rollway structure was designed so that it could be easily installed and removed depending on the test being performed. The figure on the following page shows the physical scale model, as designed and constructed by the LaSalle Consulting Group in both the plan and elevation views:

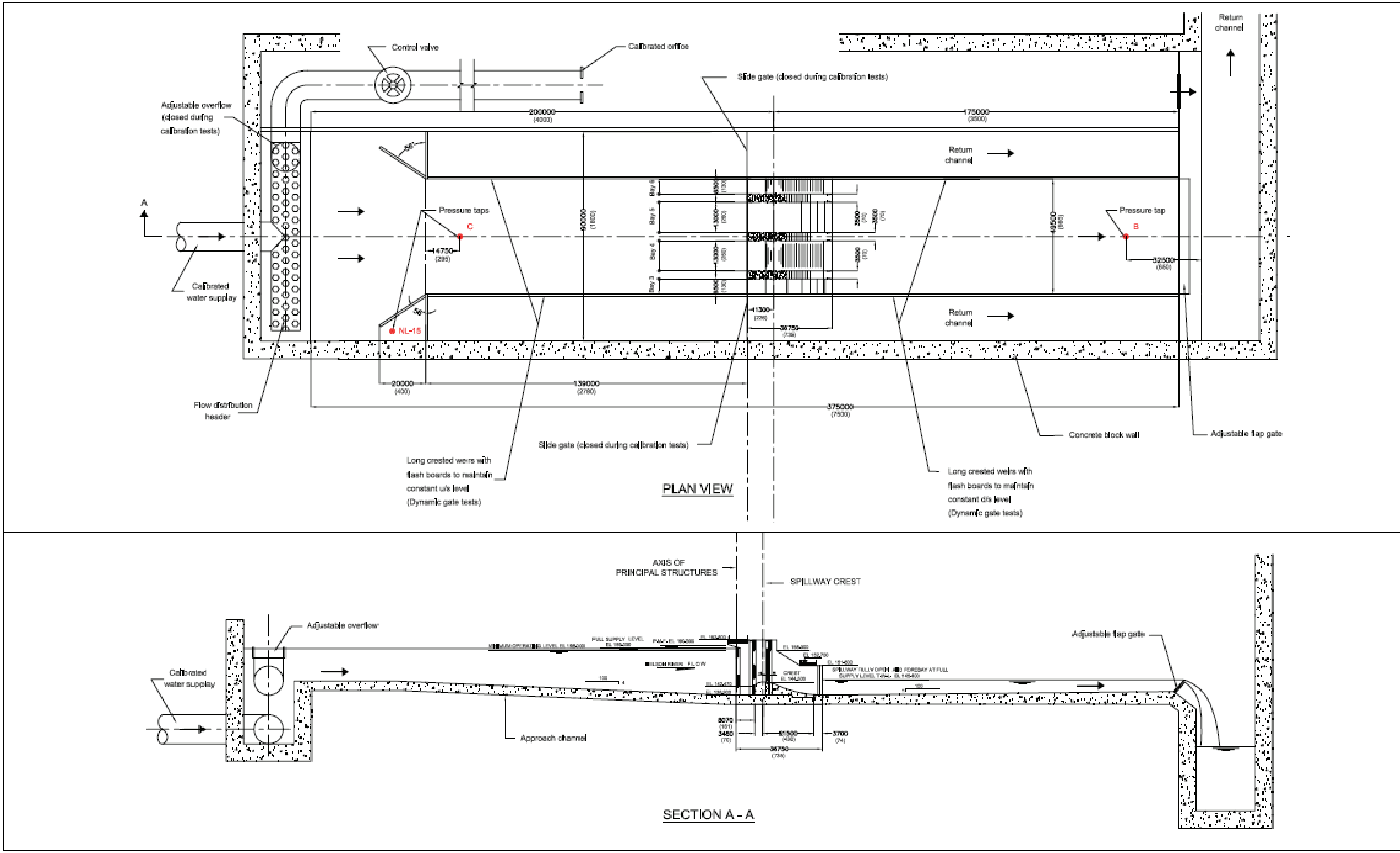

Figure 4.1: Plan and Elevation Views of the Sectional Physical Model (LaSalle Consulting Group 2005)

Pictures of the physical model are shown below:

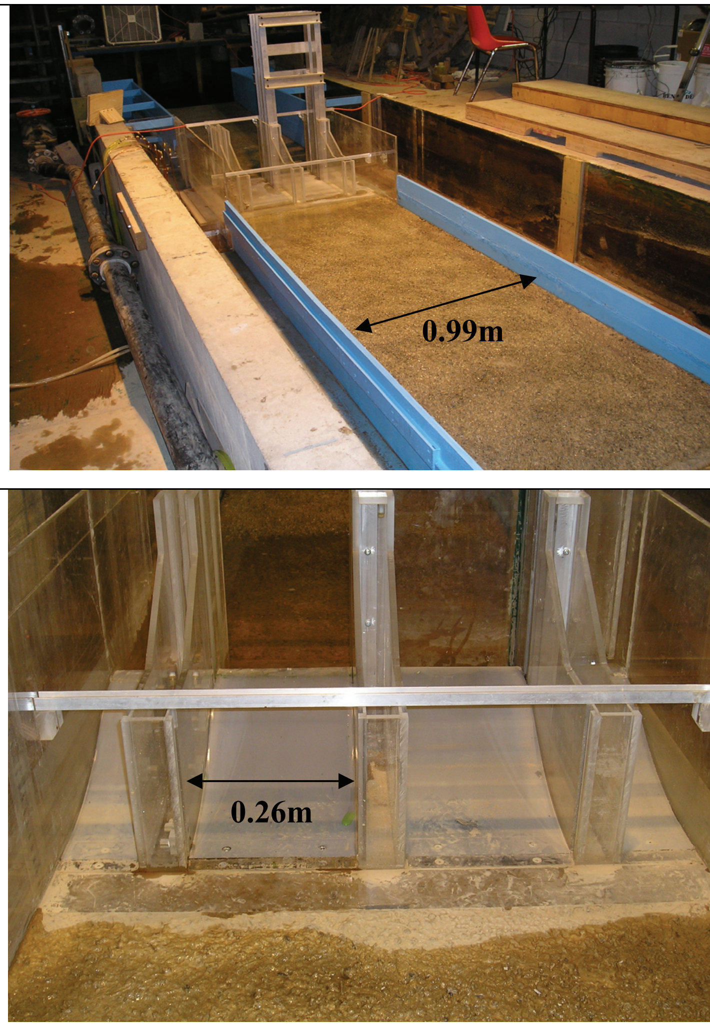

Figure 4.2: Pictures of the Physical Model in Diversion and Rollway Phases (LaSalle Consulting Group 2005)

A gate (Figure A.2), fabricated by the Material Engineering Department of McGill University and constructed in aluminum to preserve the weight of the prototype at the model scale, was placed on an aluminum structure, which was built into the two adjacent piers (seen in Figure 4.2) of one of the operational bays. The gate included a lip at its base, which could be easily removed and replaced with an alternate design, if required. In the upstream stoplog slots, a skeleton gate, attached to the aluminum gate at four different points using rods and turnbuckles, was used to achieve a near frictionless environment by tightening the turnbuckles to the point where the aluminum gate's rollers were just touching the gate slots. The gate was raised and lowered using an electric hoist mechanism equipped with a motor capable of variable speeds while markers on the gate and gate guides were placed to establish when the gate was fully open and fully closed for both the diversion and rollway cases. This assured similar conditions for each test.

For tests performed on the model that are related to this thesis, Plexiglas plates were placed in the gate slots of the two half bays and one of the full bays to effectively block the flow of water therein while the aluminum gate was kept stationary at different openings until the system reached steady-state at which point measurements were taken. Thus, flow was modeled only through one bay. Furthermore, all pressures were measured with pressure taps fitted with copper tubing which was connected to their respective manometers in order to reduce dampening.

4.2 Computational Model in Flow3D

Flow3D is a commercially available CFD package created by Flow Science Inc., which uses both the VOF and FAVOR methods for determining the location of the free surface and the location of obstacles respectively. The computational domain is divided using a structured mesh and all relevant equations are discretized using the FV method. The software includes several turbulence algorithms that allow for the solving of the RANS equations, most importantly, the K-ε and RNG closure models that will be used in this thesis. These closure algorithms are well suited for the modeling of flow over spillways, due their suitability in cases where a large amount of turbulence is created which, in this case, is caused by the flow of the fluid through the control structure.

Just as physical models are constrained by the level of detail required, the minimum scale needed to achieve dynamic similitude and the amount of laboratory space; numerical models are similarly constrained by computing power, the accuracy of results obtained for a certain mesh resolution and the time to run a simulation. These constraints are often interdependant as the increase or decrease in one could have a positive or negative effect on another. For example, a more powerful computer would allow a finer mesh to be created therefore increasing accuracy however this increase in mesh resolution could, possibly, negatively impact the amount of time required to reach steady-state despite the use of the more powerful computer. In addition, decreasing the size of a single mesh cell would require a decrease in time step size in order to keep the Courant number (a function of the ratio of the time step and cell size) at a value which is stable, further increasing the time for each simulation. Conversely, a less powerful computer would limit the fineness of the mesh; however, the simulation time may either decrease or increase due to the combined effects of a slower computer (less calculations/time) and a coarser mesh (fewer calculations to compute, increased time step size). Evidently, in the latter case, there is the possibility that the results are unrealistic which is why it is important to determine the limit at which an increase in mesh refinement does not entail a change in the solution. At this finite limit, the solution is said to be mesh independent.

To ensure that the final solutions were mesh independent and efficiently calculated, quasi-2D simulations (later changed to 3D simulations for the fully open gate condition) in which the lateral dimensions were exactly once cell thick, were performed in order to observe the behavior of the velocity profiles along the channel and beneath the gate during orifice flow, and to compare discharges and water surface profiles, all for varying mesh refinements. It was hypothesized that when velocity profiles, water surface profiles and discharges did not differ significantly with increased refinement, mesh independence had been reached. This is a reasonable assumption since, in a mesh independent solution, information is not missing due to the coarseness of the mesh. Once these tests had been completed and by use of the newly acquired knowledge, comparison tests between both RNG/K-ε closure models and full-sized/1:50 scaled models were performed at the quasi-2D level (3D for fully open case) in order to observe the difference in discharges that such changes would incur. The results of these tests are found in Sections 5.1, 5.2 and 5.3 respectively. The comparison of fully 3D solutions with the physical model results are discussed in Section 5.4.

All simulations were run with a parallel code on a PC containing an Intel Core 2 Duo 2.13 GHz dual processor with 4 Gigabytes of memory running at 667MHz, however, not all simulations made use of the dual processor.

The following sections describe the details of the simulations including the geometry of both the model and the mesh and the initial conditions and boundary conditions.

4.2.1 Model Geometry

The model geometry of the spillway was taken from the engineering design plans found in the LaSalle Consulting Group's report. The geometry was transferred into AutoCAD in prototype dimensions in two sections:

1) the approach channel including either the diversion or rollway structure and the tailrace (Figure 4.1) and
2) the gate (Figure A.2).

The gate height was increased to avoid overtopping and the lip at the bottom of the gate was omitted due to its small size, which the mesh would be unable to define. Once the transfer was completed, the geometry was imported into Flow3D in STL format as seen in Figure 4.3.

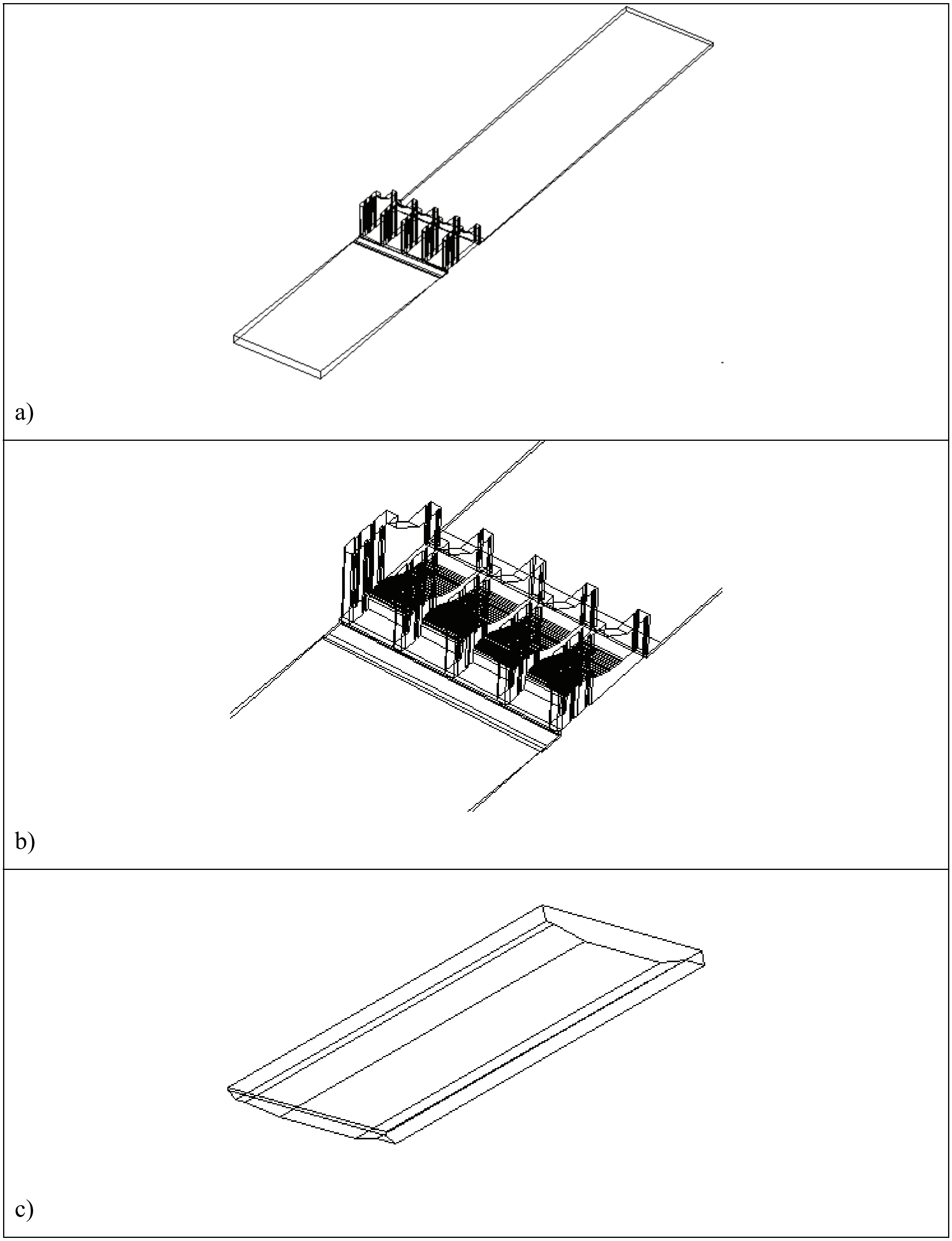

Figure 4.3: Views in AutoCAD of: a) the Sectional Physical Model during the Diversion Phase, b) the Control Structure with Rollways, c) the Modeled Gate

The full design for the Keeyask Generating Station required 7 spillway bays separated by piers, as previously stated (Figure A.1), however, the sectional model was constructed with only 3 spillway bays (2 full bays and 2 half bays). Four bays are present in the AutoCAD STL files due to the fact that it was easier to transfer 4 full bays for the CFD model geometry rather than exactly replicate the physical model. The correction of this discrepancy is discussed in the following section.

Within Flow3D, the two outer bays and one of the middle bays were subsequently blocked using rectangular subcomponents placed in the gate position while the other full bay was equipped with the gate segment, which can be placed to model the desired opening. Hence, just like the tests performed on the physical model, flow was modeled through only one bay.

4.2.2 Mesh Geometry

In this study, the x component represents the lateral direction with respect to the origin, the y component represents the longitudinal direction along the channel and the z direction represents the change in vertical distance. The origin of the domain is positioned at an elevation of 137.9m (1m below the bottom face of both the diversion and rollway structures) in the centre of the middle pier along the same line as the rollway crest as illustrated in Figure 4.4.

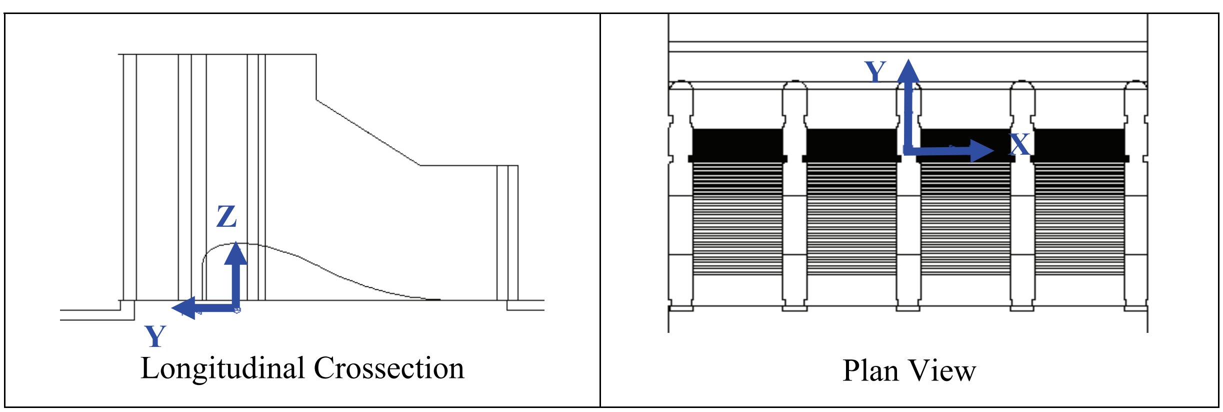

Figure 4.4: Location of the Coordinate Origin of the Numerical Model

As a result, the gate is fully closed at 138.9m during the diversion phase and 145.45m during the rollway phase. The difference is caused by inclusion of the ogee weir or rollway in the latter case. An illustration is provided in Figure 4.5:

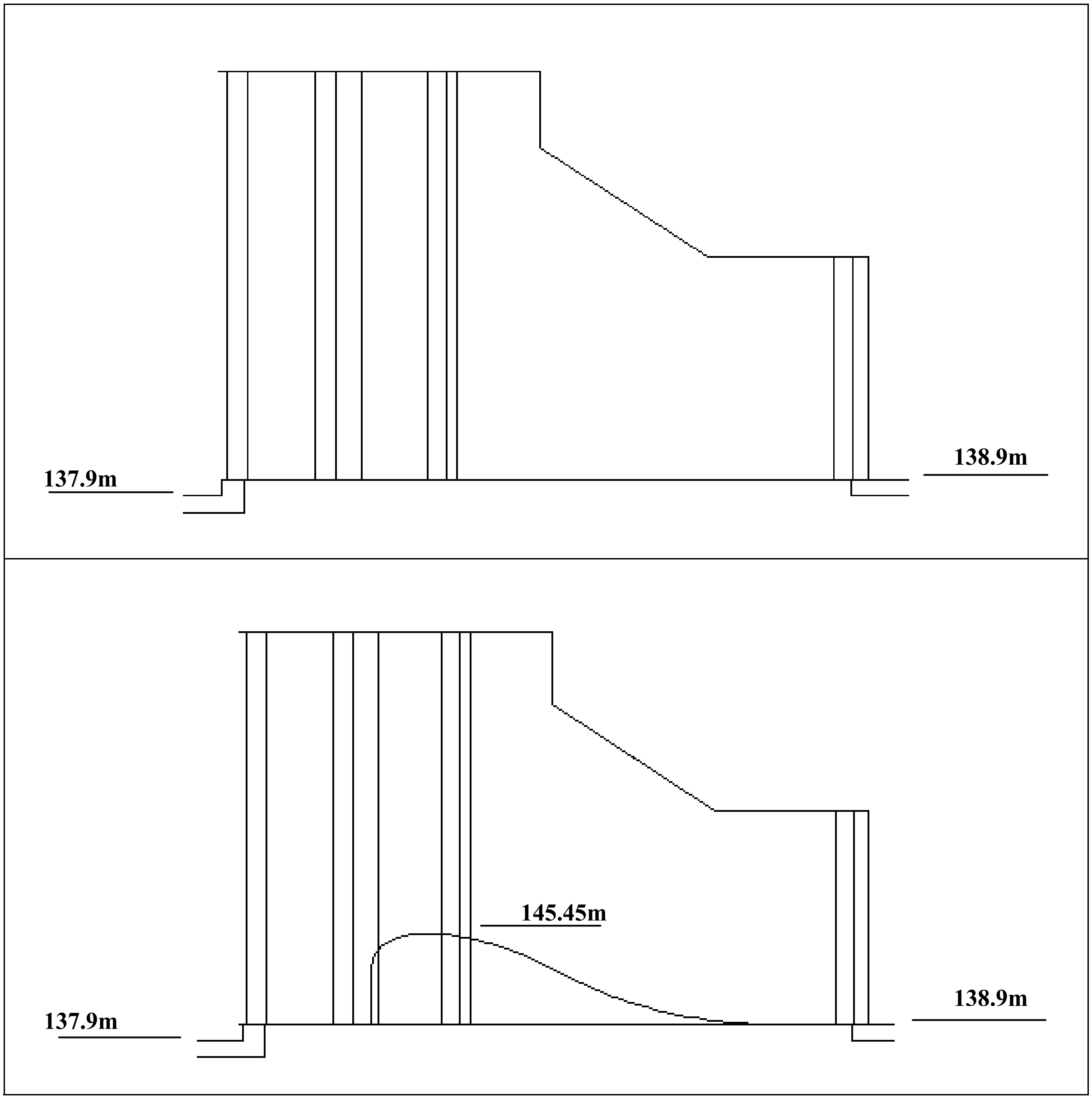

Figure 4.5: Illustration of Differences between the Diversion and Rollway Phases

The quasi-2D domain was defined with the mesh being placed at the centre of the bay containing the gate while the three-dimensional mesh was constructed in such a way as to only include the two middle bays and half of the two outer bays therefore obtaining the sectional physical model design. The following table shows the maximum extent in each direction:

Table 4.2: Maximum Extent of the Three-Dimensional Mesh

	Minimum Value (m)	**Maximum Value (m)**
X Component	-24.75*	24.75*
Y Component	-140.50**	135.55
Z Component	0	30

*replaced with -8 and -6.5 (a single mesh cell of 1.5m thickness) respectively for the quasi-2D case

**replaced with -30 (upstream of the structure) for all quasi-2D simulations and 3D rollway simulations

The maximum and minimum values in the y direction were selected to coincide with positions that the LaSalle Consulting Group termed HWL-C and TWL-B respectively as seen on the plan view of Figure 4.1 under their alternate names: pressure taps C and B. It is at these locations that the LaSalle Consulting Group recorded water level elevations, which results in a domain in Flow3D of 275.55m, which is less than the 200m approach and 175m tailrace of the physical model as described in Section 4.1. This stems from the software requiring the user to enter the fluid heights in order to obtain a flowrate.

It is important to note that the mesh configuration described in Table 4.2 was only used for the 3D simulations run on the diversion structure due to the initial uncertainty of the locations of the discharge control and hydraulic jump, therefore requiring the full tailrace and tailwater, however, it was later found that this was a conservative assumption. In fact, through trial simulations for both gated and ungated cases during diversion, the control was located at the control structure, and the gate orifice, in the presence of tailwater, as observed from video footage of the physical model, was not drowned by the hydraulic jump.

Based on the initial assumption and without the knowledge provided by the trial simulations and video, it was understood that since mesh refinement tests would be of an observational and relativistic nature, the tailwater and therefore the tailrace would not be required for these simulations despite them being performed on the diversion structure and the risk of drowned flow. In addition, the tailwater would also be excluded from rollway simulations since the control of the structure, located on the crest of the weir, is located at a higher elevation than the tailwater. This was seen to present an advantage from a computational stand point as the additional number of cells and the occurrence of the hydraulic jump (a zone of large turbulence and energy dissipation), caused by the impact of supercritical flow with the tailwater downstream of the gate, would greatly increase the computational time required for each simulation. Since this section of the physical model was eliminated from the calculations, the minimum value in the y direction is increased from -140.50 to -30, to a point which is located directly downstream of the piers. In actual fact, all simulations could have been run with this downstream boundary location since the presence of tailwater was found to have no effect on computed discharges.

The z component parameters defined the vertical direction of the computational domain: the lower z value was placed at the lowest point of the structure, along the 137.9m elevation plane and the upper value positioned 8.9m above the maximum water surface level of 159m (21.1m for the computational model datum) in order to include any splashing that could occur. Despite the sloping surfaces on either side of the control structure, the final mesh is rectangular. Through the FAVOR method, these surfaces are defined as solids and are therefore excluded from the computation. It is important to note that all length scales were reduced by a factor of 50 within Flow3D so as to obtain the geometry of the scale model and not the geometry of the prototype, as the validation data is that of the physical scale model.

Once the mesh was created, fixed points were then inserted. These fixed points represent boundaries, which are used to allow further refinement within the defined sections of the mesh so as to properly model the converging of streamlines expected at the location of the control structure. A nested mesh block, i.e. a secondary mesh that is placed within a containing mesh (the cells that define the entire computational domain), could not be used for this purpose since large pressure gradients and geometry differences are expected near the gate orifice which could cause significant truncation errors as outlined in the Flow3D User Manual.

Two fixed points placed at y = -1 and y = -2 which coincide with the upstream and downstream faces of the gate were added along the y direction and a fixed point, which was mobile and placed directly above the orifice created by the gate opening, was included in the z direction. No fixed points were however placed in the x direction during 3D simulations since further refinement in the x direction is unnecessary due to the relatively large distance between each pier. Outside the values enclosed by the three fixed points, a gradually changing coarser mesh was used as the flow became increasingly uniform.

The refinement of each section was done conserving an aspect ratio (a measure of the cubic nature of each mesh block) of less than 2 and an adjacent cell size ratio of less than 1.25 in all three directions (x-y, x-z, y-z) as specified by the Flow3D User Manual to minimize errors and increase the stability of the model. An exaggerated example of this process can be seen in Figure 4.6:

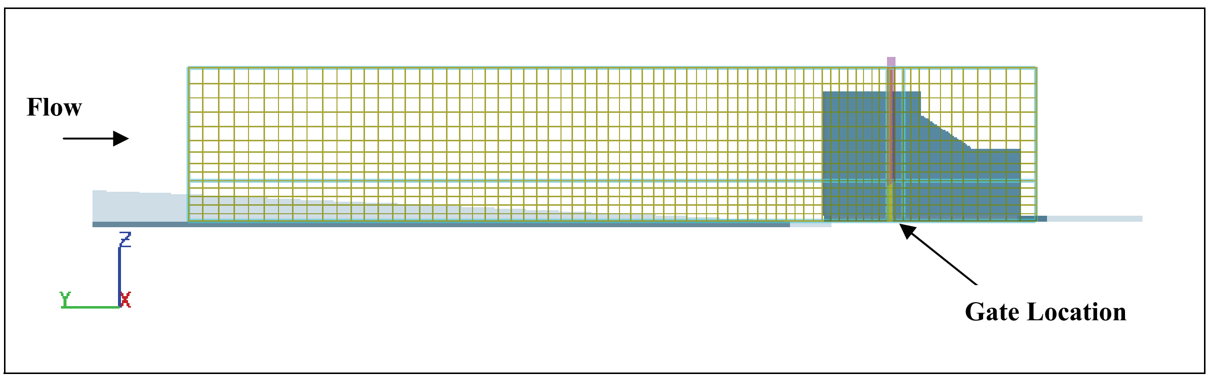

Figure 4.6: Illustration of a Quasi-2D Coarse Mesh with an Aspect Ration Equal to 2

The minimum square cell size is found at the gate location as defined by the fixed points in the y and z directions. Below the fixed z point, the height of the cell remains constant and increases above this point until it has doubled its size at the upper z boundary. Likewise, in between the two fixed points in the y direction, the cell length is smallest and remains constant. Outside of this area, the length stretches with distance from the fixed points until the final cell on both the upstream and downstream boundaries is twice the smallest length. Thus the largest possible ratio of length/height (y/z) or vis-versa is equal to 2. Note that at the upper corners of the quasi-2D mesh described above, the cells are in fact square, double the size of the smallest cells found at the gate orifice (in between the fixed points in the y direction and below the fixed point in the z direction). This reasoning also applies to 3D meshes where the maximum width of a cell is defined by the maximum allowable aspect ratio.

Three porous baffles were also included in the mesh as a means of computing the flow rate in Flow3D by defining them as flux surfaces and are arbitrarily placed at y=-30, y=30 and y=100 as shown in the Figure 4.7 below:

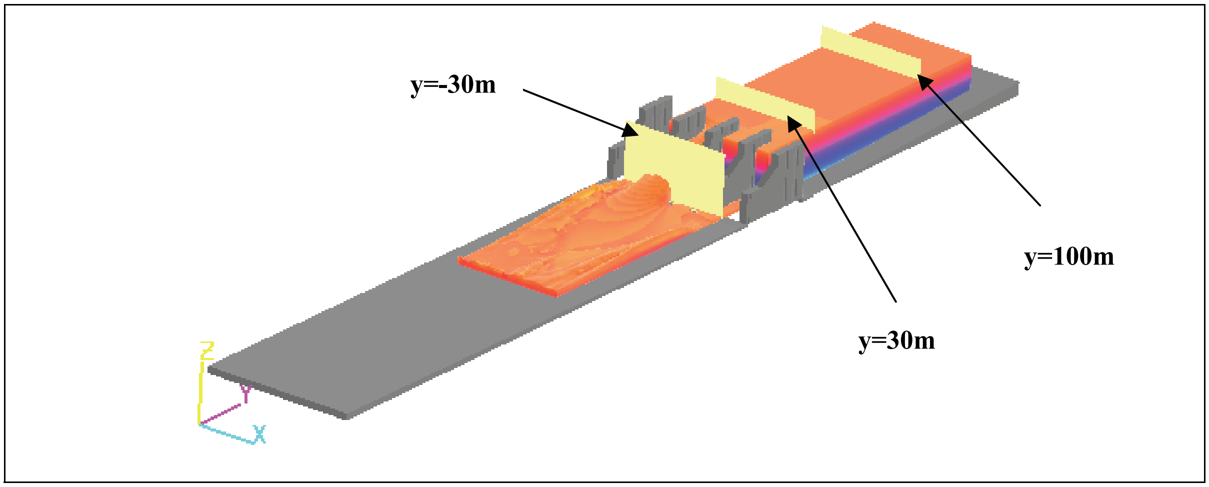

Figure 4.7: Location of Baffles in the Flow3D Model

4.2.3 Initial Conditions

In an effort to decrease the computational time required for a simulation to reach steady-state, simulations were first run on a coarse mesh and the approximate solution was then used as input data for the exact same simulated conditions with a finer mesh. This same method was used by Savage & Johnson (2001) and was employed in order to dampen the effects of a wave that is caused by a sudden motion of the fluid, which propagates along the length of the channel and reflects off the upstream and downstream boundaries of the domain until it is eventually dissipated by the viscous forces of the fluid. As a result, two sets of initial conditions are required depending on the case: a cold start initial condition for coarser grids and the results of the coarse grid for the fine grid, termed a hot start initial condition.

The initial conditions for the coarse mesh are dictated by the model test and use constant water levels located both upstream and downstream of the gate to model the reservoir and initial tailwater elevations respectively. The water levels for the simulations are defined by the water levels recorded on the physical scale model, upstream at HWL-C and downstream at TWL-B. Downstream initial conditions are not necessary in cases where the tailwater was not included. Figure 4.8 shows an example of the first set of initial conditions used on a coarse mesh for the entire computational domain:

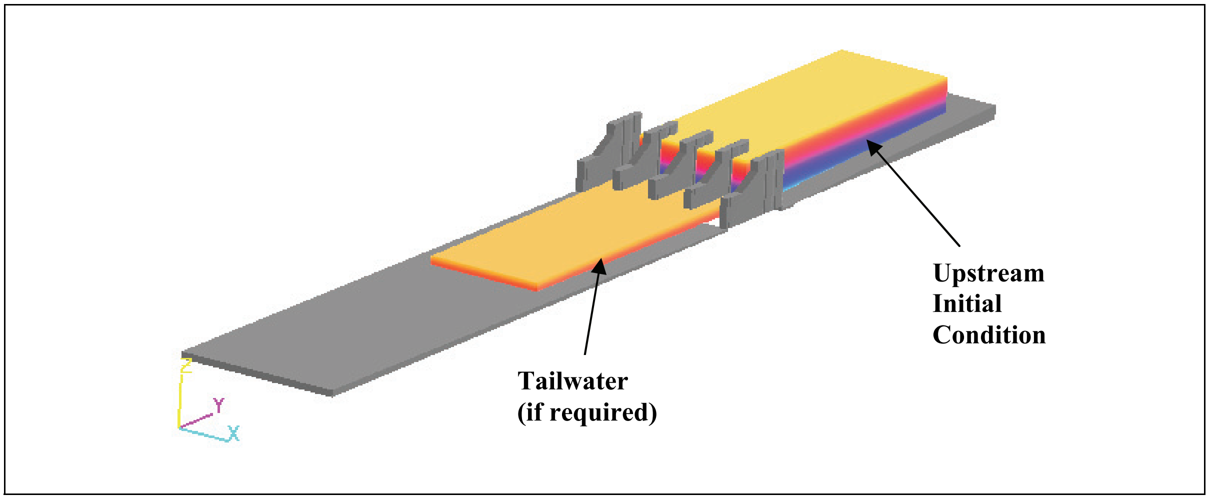

Figure 4.8: View of Coarse Grid Initial Conditions on the Diversion Structure with Tailwater

The second set of initial conditions, as described above, used the approximate solution computed by the coarser mesh and interpolated these results onto a finer mesh to reduce the amount of time required to run a simulation to steady-state where more accurate results could be obtained. The extent of refinement of the mesh depends on the size of the gate opening for which tests were performed, the solutions of which are described in Section 5.1. Further details on these initial conditions and how they relate to the model boundary conditions are described below.

4.2.4 Boundary Conditions

All simulations used the K-ε closure model (excluding the RNG comparison tests) with no-slip boundary surface conditions and used prototype k_s values equal to 0.003m and 0.00015m, as suggested by Henderson (1966) for smooth concrete and steel respectively.

The k_s values were subsequently scaled within Flow3D in order to respect the geometric similitude criterion. This, however, should not have been done for the approach and tailrace channels within the numerical model since they were constructed in concrete on the physical model. Fortunately, subsequent tests with an unscaled concrete k_s value showed that this change made no difference in results. Boundary conditions for the x and z directions were labeled as symmetry boundaries, which implies that identical flows occur on the other side of the boundary and hence there is no drag. In the y direction the boundary conditions were more complex: the upstream and downstream faces of the computational domain required functions that would allow the creation of discharge to model both the inflow and tailwater correctly while allowing the flow to exit from the downstream boundary. The type of boundary that best represented these conditions for both the entrance of the approach channel and the exit of the tailrace on the sectional model is called the "specified pressure" boundary condition. With this algorithm, Flow3D is able to model various fluid heights (specified in Section 4.3 for each test) beginning at a stagnation pressure state. It is important to note that these fluid heights coincided with the initial conditions selected for the coarse grid to perform simulations in the most time-efficient manner. For other cases where tailwater was not required, the "specified pressure" boundary condition at the downstream face of the domain was replaced with a "continuative" boundary condition, an algorithm that simply allowed the flow to exit in its current state.

The upper boundary for the z direction is 8.9 or more meters above the water surface elevation while the lower boundary is located at the bottom face of the main model geometry file. Therefore as the boundaries are either in the air phase or just below the entire structure, the symmetry condition does not affect the flow and is selected arbitrarily mainly because Flow3D defaults to this condition at start up. The computational domain including the geometry is shown in the Figure 4.9 with its boundaries labeled:

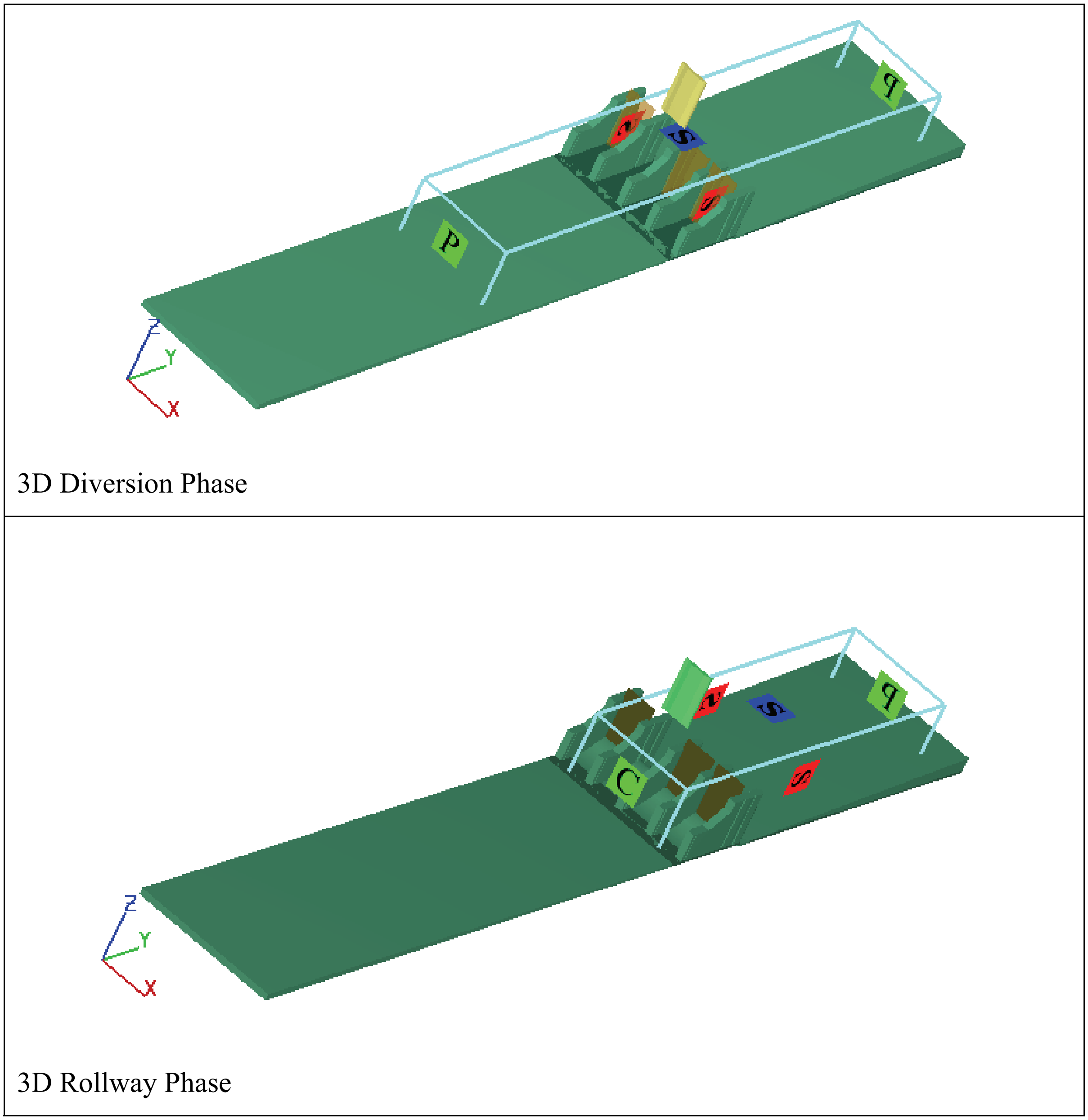

Figure 4.9: All Possible Configurations of Boundary Conditions for 3D Simulations

In the figure, “P” denotes a specified pressure boundary condition, “C” denotes a continuative boundary and “S” denotes the symmetry boundary. Not shown is the lower z limit of the computation domain, which similarly to the upper limit, has been given a symmetry boundary. The quasi-2D case has the same boundaries as those for the 3D rollway phase. It is important to note that when using the coarse grid solution as the initial condition, the boundary conditions were unchanged.

4.3 Test Program

Simulations were accomplished in several phases. The first phase completed quasi-2D simulations on the diversion structure for different gate openings to determine the level of mesh refinement required to obtain a mesh independent solution. These simulations were run on the diversion structure with an upstream water level of 159m for the fully open case, 6m, 4m, 2m and 1m gate openings however, it was later found that the fully open case required a 3D simulation for reasons explained in the results section. The latter is the only case in which tailwater was modeled.

Within the results of each gate opening, velocity profiles, water surface profiles and discharges (provided by the baffles positioned along the channel) were compared for different meshes until, with increasing refinement, subsequent results, if deemed feasible, no longer changed. Furthermore, the discharges for quasi-2D cases were integrated over the width of the operational bay so that they could be compared with the physical model results provided by the LaSalle Consulting Group. This preliminary work ensured that the final simulations were run with the maximum level of accuracy.

The second phase was a comparison between numerical simulations of the model size vs. prototype size and a comparison of simulations using the K-ε and RNG closure models. This was again accomplished with an upstream water level of 159m on the diversion structure. For both parts, only results where mesh independence is attained or nearly attained at reasonable mesh sizes, i.e. the 3D fully open gate condition and the quasi-2D 6m gate opening respectively, were examined

The third and final phase of testing included 3D simulations of the fully open case for both the diversion and rollway phases of construction. Initially, all 5 gate openings described for the first phase were to be modeled, but subsequent simulations run on the fine mesh prove that this is an impossibility given the amount of computational power available and the large amount of time required for the calculations. In addition, computations, which take large amounts of time to calculate, are of little use in the engineering world.

In this final phase, upstream water elevations of 159m, 154m and 151m were modeled in order to plot a rating curve for comparison with the LaSalle Consulting Group's results, from which operation equations were also extracted and compared. In addition, pressure at certain points and water surface profiles within the operational bay were also compared with the physical model results. Due to the previously stated conservative assumption in Section 4.2.2., tailwater was modeled for the diversion structure however, this was not done for the rollway structure since the maximum tailwater elevation is below the crest of the weir and therefore there is no risk of drowning the flow at the control.

Chapter 5

Results

The following sections present the results of the numerical model in Flow3D and the results of the physical model provided by the LaSalle Consulting Group. In order to obtain accurate results, mesh refinement tests were conducted on a quasi-2D model for the fully open case (later redone in 3D), and for partial gate openings ranging from 1m to 6m on the diversion structure for a water level of 159m upstream of the gate (at location HWL-C). The discharges, water surface profiles, velocity fields and velocity profiles for each individual gate opening will be compared while varying the degree of refinement of the mesh, which defines the computational domain in Flow3D. In addition, relative times of computations will also be presented in tabular form, as this information is important from an engineering point of view.

The results from this analysis will then be used to conduct a comparison of a full-sized numerical model and a scaled numerical model as well as a comparison of K-ε and RNG closure models for the same conditions, in 3D for the fully open case and in quasi-2D for the 6m gate opening. Finally, rating curves will be presented, derived from 3D results for the fully open gate for water levels at HWL-C of 151m, 154m and 159m for the control structure during both the diversion and rollway phases, along with pressure and water surface profiles. The meshes of these simulations will also be based on the mesh refinement tests.

5.1 Mesh Refinement

The need for mesh independence in a simulation is important for ensuring that the most accurate results are recorded and therefore, prior to any 3D calculations, quasi-2D simulations should be carried out, when possible, in order to test for mesh independence in the most time-efficient way. Mesh independence is obtained when certain indicators such as velocity profiles, water surface profiles and discharges of steady-state solutions do not change for increasingly finer meshes, which indicates that information is not missing due to the coarseness of the mesh. Table 5.1 provides a summary of all mesh refinement simulations for the quasi-2D simulations and 3D cases, which were necessary for fully open gate conditions. Note that these simulations were conducted for the diversion phase with an upstream water level of 159m bounded by the specified pressure boundary condition and the continuative boundary condition on the upstream and downstream boundaries respectively. The only exception is for the 3D simulations, in which tailwater was modeled by replacing the continuative downstream boundary with a specified pressure boundary.

Table 5.1: Summary of Simulations for Mesh Refinement on the Diversion Structure with an Upstream Water Level of 159m

Gate Opening	**Minimum Cell Size (m)**	Q_{2DP} **(m^3/s)**	Q_{3Deq} **(m^3/s)**	$Q_{LaSalle}$ **(m^3/s)**	Fr_u	Fr_d	Re_u	Re_d
Fully Open	1.5	163.5	1417	1850	0.59	1.41	312500	327500
Fully Open	0.75	163.5	1417	1850	0.56	1.57	297500	295000
Fully Open	0.5	163.5	1417	1850	0.53	1.69	302500	277500
Fully Open	2		2470	1850	0.22	1.45	147250	188500
Fully Open	1		1848	1850	0.19	1.59	95750	112750
Fully Open	0.75		1848	1850	0.18	1.86	105750	109750
6m	0.4	107.0	928	860	0.38	2.18	195250	193750
6m	0.3	101.4	879	860	0.35	2.68	190750	185250
6m	0.15	98.6	854	860	0.33	2.78	186000	181000
6m	0.075	97.9	848	860	0.34	2.74	187500	184000
4m	0.4	91.3	791	602				
4m	0.3	77.0	667	602	0.26	2.71	141750	148000
4m	0.2	73.4	636	602				
4m	0.15	71.8	626	602	0.25	3.27	135500	128500
4m	0.1	69.7	604	602				
4m	0.075	68.2	591	602	0.23	3.30	129000	127000
4m	0.05	66.9	580	602	0.23	3.30	127500	126000
2m	0.3	42.2	366	326	0.15	3.93	78250	84250
2m	0.15	39.8	345	326	0.13	4.48	71750	75250
2m	0.1	39.1	339	326	0.13	4.48	73750	72000
2m	0.075	37.9	328	326	0.13	4.36	71000	71000
1m	0.3	23.2	201	166	0.08	5.81	44000	49250
1m	0.15	22.7	196	166	0.08	5.41	43500	42250
1m	0.1	22.0	191	166	0.08	5.25	42250	39750
1m	0.075	21.2	184	166	0.07	5.57	38000	38500

In the above table, the minimum cell size represents the cell size below the gate orifice, bounded by the fixed points located at y = -2 and y = -1, which represent the downstream and upstream faces of the gate respectively (in the case of the fully open structure, the minimum cell size was extended across the entire domain). Additionally, Q_{2DP} is the flowrate of the single, 1.5m width cell of the quasi-2D simulation, $Q_{LaSalle}$ is the flowrate found from the LaSalle Consulting Group's physical model and Fr_u, Fr_d and Re_u, Re_d are the Froude and Reynolds numbers at the upstream and downstream boundaries respectively. All discharges are converted to prototype units using the Froude law given by:

$$Q_p = Q_m \left(\frac{1}{X} \right)^{\frac{5}{2}} \tag{5.1}$$

where Q_m is the scaled value of the discharge and X is the scale of the model, in this case, 1:50.

In order to compare Q_{2DP} with $Q_{LaSalle}$, another discharge, Q_{3Deq}, is introduced into the table and is defined as the equivalent discharge of the numerical model over the entire bay width or:

$$Q_{3Deq} = \frac{Q_{2DP}}{W_{cell}} W_{bay} \tag{5.2}$$

where W_{cell} and W_{bay} are the width of cell (1.5m) and width of the bay (13m) respectively. For 3D simulations such as those conducted for the fully open case, Q_{3Deq} is simply taken as the discharge of the 3D system, and Q_{2DP} is omitted.

The Froude and Reynolds numbers were determined from data in the text result files at the upstream and downstream boundaries and were calculated using the average resultant velocity, V, from a cross-section of the flow. Due to the discretization of the domain, the accuracy of the calculations increases with mesh refinement as it is impossible from the information given in the results files to determine the location of the free surface or bed of the channel within an individual mesh cell. As a result, the depth was defined as the difference between the maximum and minimum z values which were associated with non-zero velocities. Therefore, the Froude number for the model dimensions was calculated using the equation:

$$Fr = \frac{V}{\sqrt{[(z_{\max} - z_{\min})g]}} \tag{5.3}$$

and the Reynolds number for the same dimensions was calculated using the equation:

$$\mathrm{Re} = \frac{\rho V R}{\mu} = \frac{\rho V (z_{\max} - z_{\min})}{\mu} \tag{5.4}$$

For the development of the right hand side of Equation 5.4, it was assumed that the water was flowing through a channel of thickness W_{cell} in quasi-2D such that the hydraulic radius R is equal to A/P, that is the ratio of the wetted area and wetted perimeter for a rectangular channel, which for a grid bounded by symmetry boundary conditions, is simply reduced to the depth. Due to the use of the symmetry boundary condition, the equation can also be applied to the 3D case.

For all gate openings, the model Reynolds number remains above 1400 at both boundaries, therefore proving that the flow is turbulent over the entire domain. Additionally, the Froude number remains subcritical at the upstream boundary and becomes supercritical at some point along the channel. This transition is usually located at the gate position during orifice flow as this is a control, although this is most likely not true for the fully open case where the transition can be located anywhere within the piers of the open bay. Nevertheless, as the gate opening decreases, the area upstream of the gate becomes increasingly subcritical while the downstream area of the gate becomes increasingly supercritical due to increasing velocities and decreasing depths.

Mesh refinement tests were carried out for the fully open gate condition on the diversion structure. Initially, quasi-2D simulations were performed, however, Figure 5.1, which plots prototype discharges of the numerical model against the minimum cell size and the physical model's results, shows that the discharges in 2D are too low.

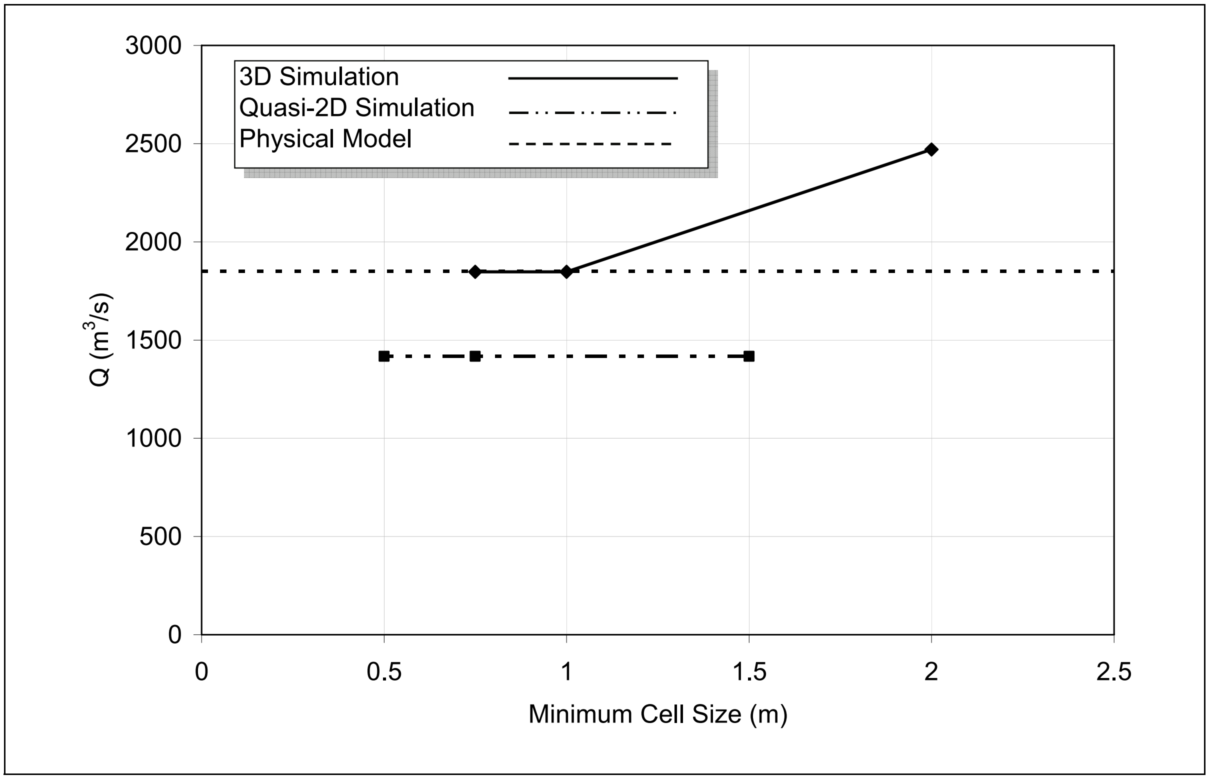

Figure 5.1: Discharge vs. Minimum Cell Size for the quasi-2D and 3D Fully Open Cases on the Diversion Structure with the Physical Model Results

The above values were extracted from the discharge vs. time curves of Figures B.1 and B.2 (Appendix B), which show the convergence of the solutions. The figure, which plots Q_{3Deq} rather than Q_{2DP}, shows that the numerical model in quasi-2D predicts a result over 400m^3/s or 23.4% less than the value of the physical model.

This discrepancy between the quasi-2D and physical models results can be explained by examining the main differences between these two systems. On the physical model, two out of three bays are blocked by Plexiglas plates while the remaining bay is operational. The extra resistance due to the contraction of the channel at the control structure causes the flow of approximately 1850m^3/s to back up behind it, effectively increasing the upstream head. This, however, cannot be the case with the quasi-2D model since the domain remains separate from the closed bays. In the quasi-2D case, a line of cells exactly one cell thick, centered within the fully open bay, extends from HWL-C to 30m downstream of the gate slots and therefore no contraction is modeled. This effect remains solely a problem related to the fully open case since the vertical contraction of the bay caused by the presence of the gate for partial gate openings in quasi-2D seems to be much more important than the horizontal contraction at the 3D level.

This hypothesis was proven by using the Bernoulli equation to verify, for the numerical model conditions, if there was enough energy to pass the required flow through the structure without any backing up. Using the depth found in the quasi-2D simulation at the entrance of the control structure (7.69m), the discharge of the physical model (1850m^3/s) and the width of the approach channel (49.5m), the upstream specific energy was calculated giving a value of 8.89m. This value is much less than the minimum allowable energy in the open bay for the given discharge, which, calculated for a critical depth of 12.73m and when including the 1m high sill, has a value of 20.10m. With this information, it becomes possible to calculate the required upstream water level to pass the flow. Equating the energy upstream of the structure to the minimum allowable energy within the open bay yields a subcritical upstream depth of 19.92m, or a water surface elevation of 157.82m. Figure 5.2 provided below illustrates the difference in water surface profiles between the physical and quasi-2D numerical models.

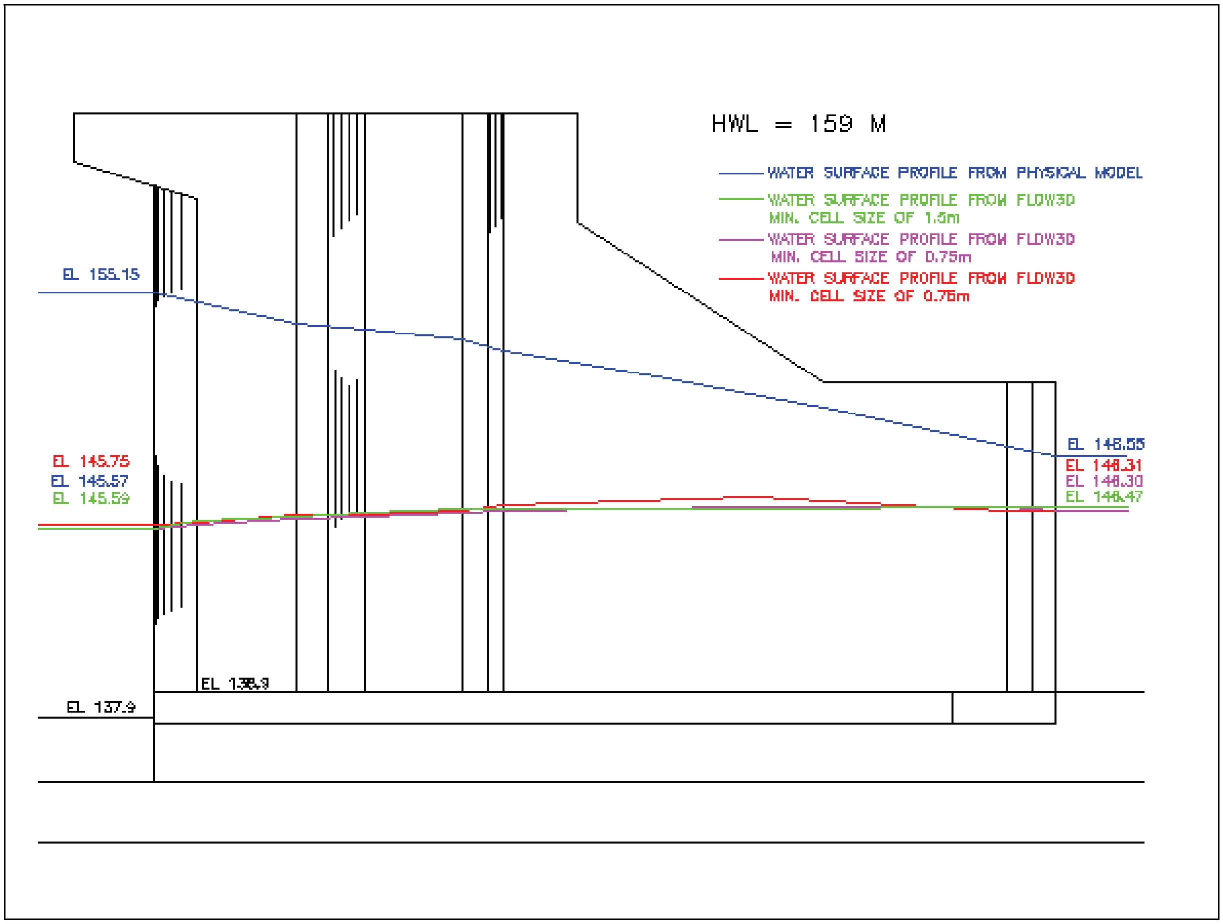

Figure 5.2: Comparison of Water Surface Profiles with increased Mesh Refinement for the quasi-2D Fully Open Diversion Case

It can be seen in the figure that the water surface elevations associated with the quasi-2D model in Flow3D, particularly at the entrance of the structure, are much lower than those found along the pier walls of the physical model suggesting that as predicted by the analytical calculation, the contraction of the channel for the case of the physical model causes the flow to back up. As a result, 3D simulations were necessary and their discharges are presented in Figure 5.1 with those of the quasi-2D simulations. The results show that there is excellent agreement (0.1% difference) between the 3D numerical model and the physical model discharges. In addition, mesh independence is reached with a minimum cell size of 1m, characterized by a horizontal line for increased refinement, representing equal discharges between the two meshes. This difference in discharges is illustrated by the markedly different water surface profiles in the 3D simulation. The water surface profiles for each mesh refinement are plotted in Figure 5.3, which illustrates that, indeed, the horizontal contraction of the physical and 3D numerical models acts as a choke.

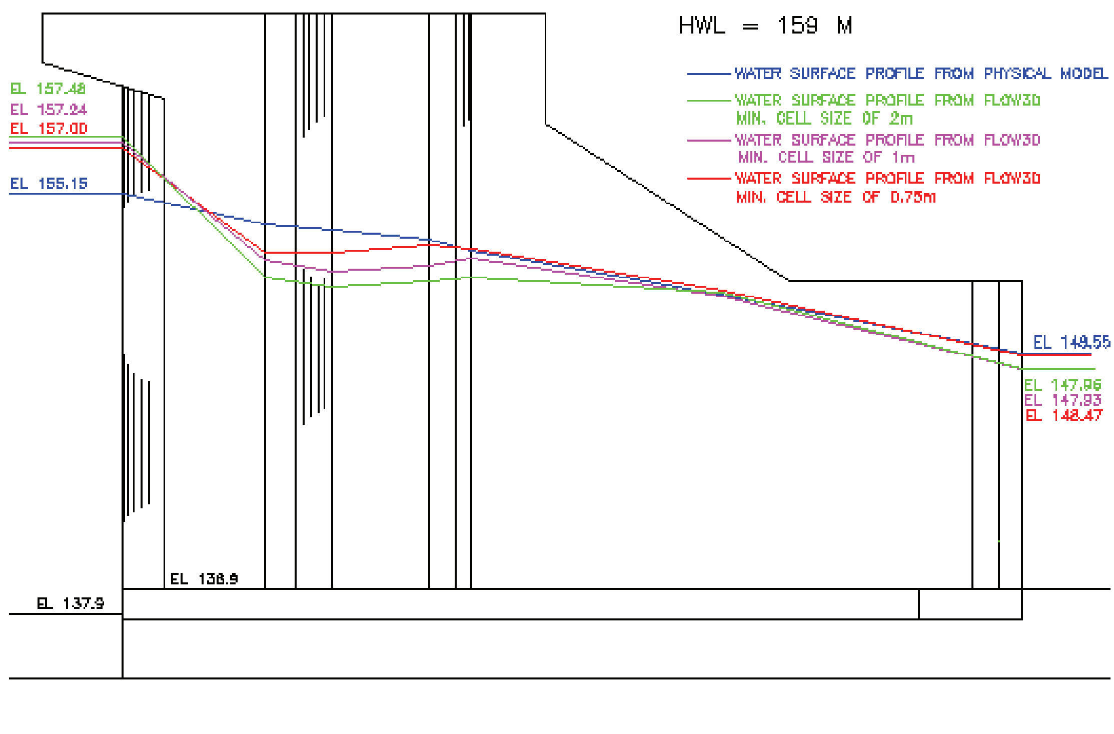

a)

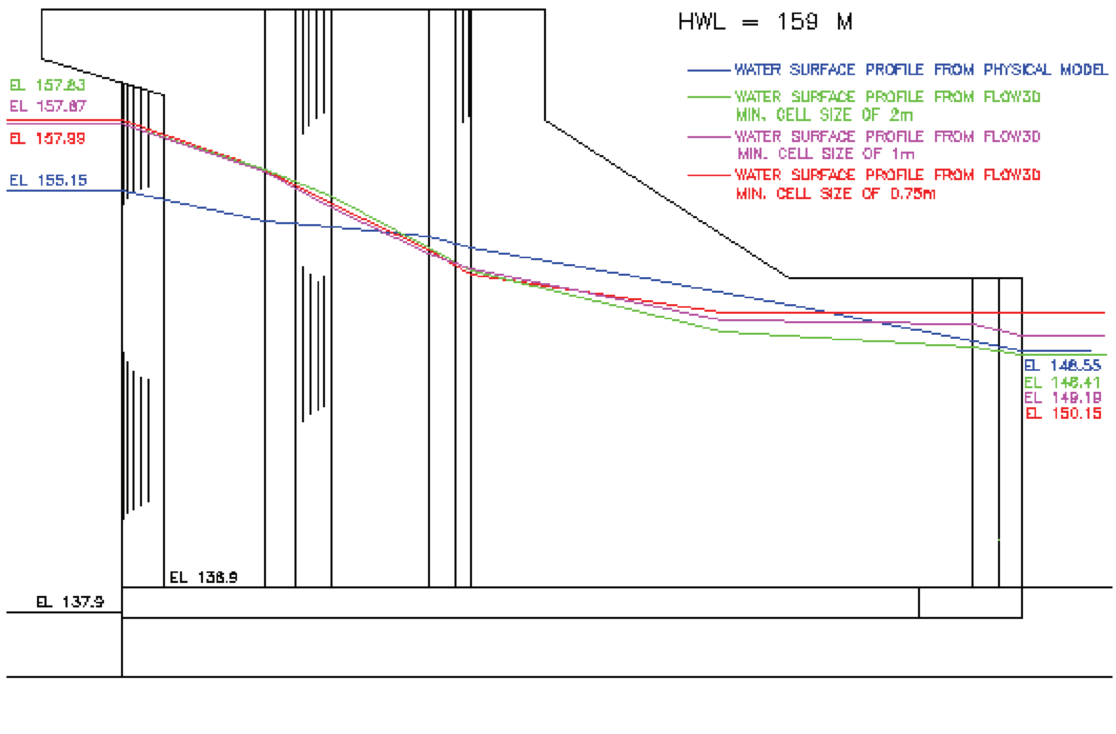

b)

Figure 5.3: Comparison of Water Surface Profiles with increased Mesh Refinement for the 3D Fully Open Diversion Case at: a) the wall, b) the centerline of the bay

Water surface profiles were extracted as close to the walls of the piers as possible (case a)), so as to reproduce the same methodology as the LaSalle Consulting Group while case b), for comparison, illustrates the water surface profiles at the centerline of the bay. In both cases, water surfaces are in better agreement to those of the physical model than the ones extracted from the quasi-2D simulations. It can immediately be seen that large differences exists between the water surface profiles extracted along the pier wall and those extracted at the centerline of the open bay. These differences are caused by the 3D nature of the flow through the structure and by shockwaves in the supercritical flow (downstream quarter), which are clearly visible in the following 3D rendering of the flow through the open bay (Figure 5.4).

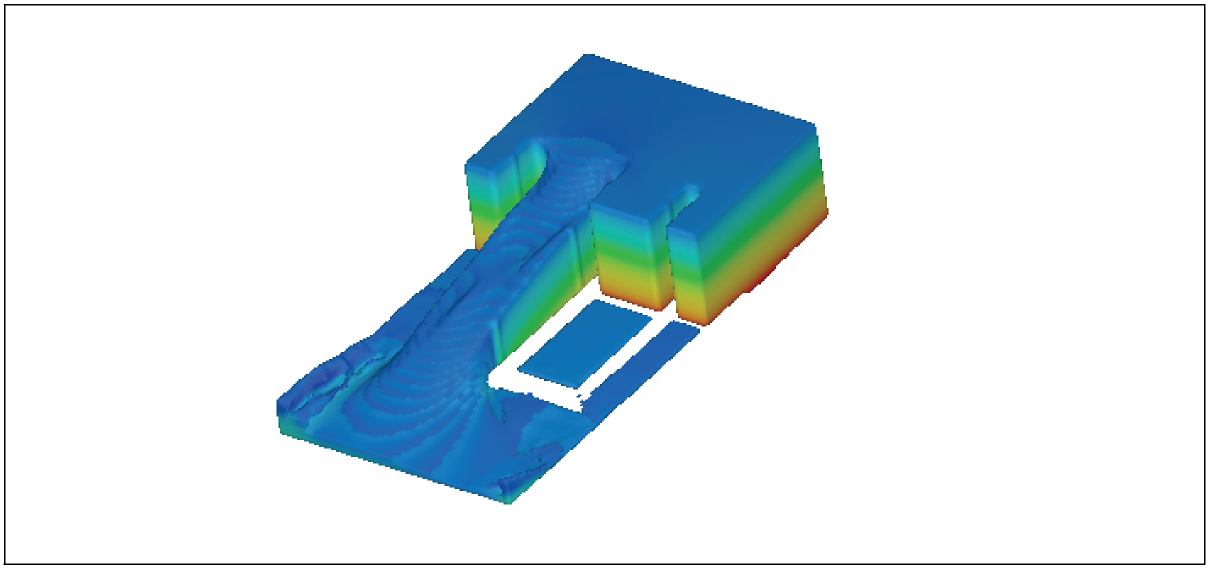

Figure 5.4: Three-Dimensional Rendering of the Water Surface through the Control Structure for the Fully Open Case on the Diversion Structure

Returning to Figure 5.3, by a comparison of case a) to the results of the physical model, differences can be seen in the water surface profiles, primarily upstream of the gate slots. All three simulations, regardless of mesh independence predict water levels that are approximately 2m above those found along the walls of the piers on the physical model. Additionally, at the first set of stoplog slots, the elevation of the water surface in the numerical model decreases by 1 to 2m as compared to the physical model. From the gate slots to the downstream extremity of the structure, both the physical and numerical models yield similar results. In case b), water surface profiles are dissimilar for the entire length of the structure, caused most notably by the three-dimensional nature of the flow. In fact, Flow3D predicts centerline water levels to be approximately 3m above those measured on the pier walls at the entrance of the control structure of the physical model. These values are in fact, very close to the value of 157.82m, previously calculated from the Bernoulli equation. Downstream of the gate slots, the water profiles of all three refinements dip below the level of the physical model and finally exit the structure either slightly below the physical model's water level or well above.

A comparison of water surfaces for each refinement is more difficult to analyze. Due to the discretization of the domain, locations at which water surfaces were extracted for each simulation cannot be duplicated due to the varying size of individual mesh cells from the different meshes. This makes it impossible to obtain results at exactly the same location for each simulation since the data is extracted up to a maximum distance of a mesh cell size away from the desired location. Therefore, water surface profiles were extracted from result files as close to the pier wall and centerline of the bay as possible, giving a maximum possible error of extraction position of 2m, reflecting the size of the cells of the coarsest mesh. In reality, it was observed that, as the coarseness of the mesh increased, the distance from the walls at which the water surface profiles were analyzed decreased. By observing Figure 5.4 in conjunction with Figure 5.3, it can be seen that the water surface increases laterally from both piers to the centre at the entrance of the control structure, therefore explaining the lower water levels seen for the two coarser meshes upstream of the gate slots in case a). The same is true for centerline water surface profiles, where finer meshes allowed for a closer extraction of data (within 0.35m) to the centerline and therefore, to the wave near the center. In conclusion, a direct comparison of water surface profiles is therefore not possible; however, an observation of the trend of the discharges with respect to minimum cell size suggests that, nevertheless, mesh independence is obtained for a cell size of 1m or less.

In order to determine if the resulting flow field is realistic and that geometry is adequately represented by the mesh, velocity fields, extracted near the centerline of the open bay of the 3D case, are presented in Figure 5.5.

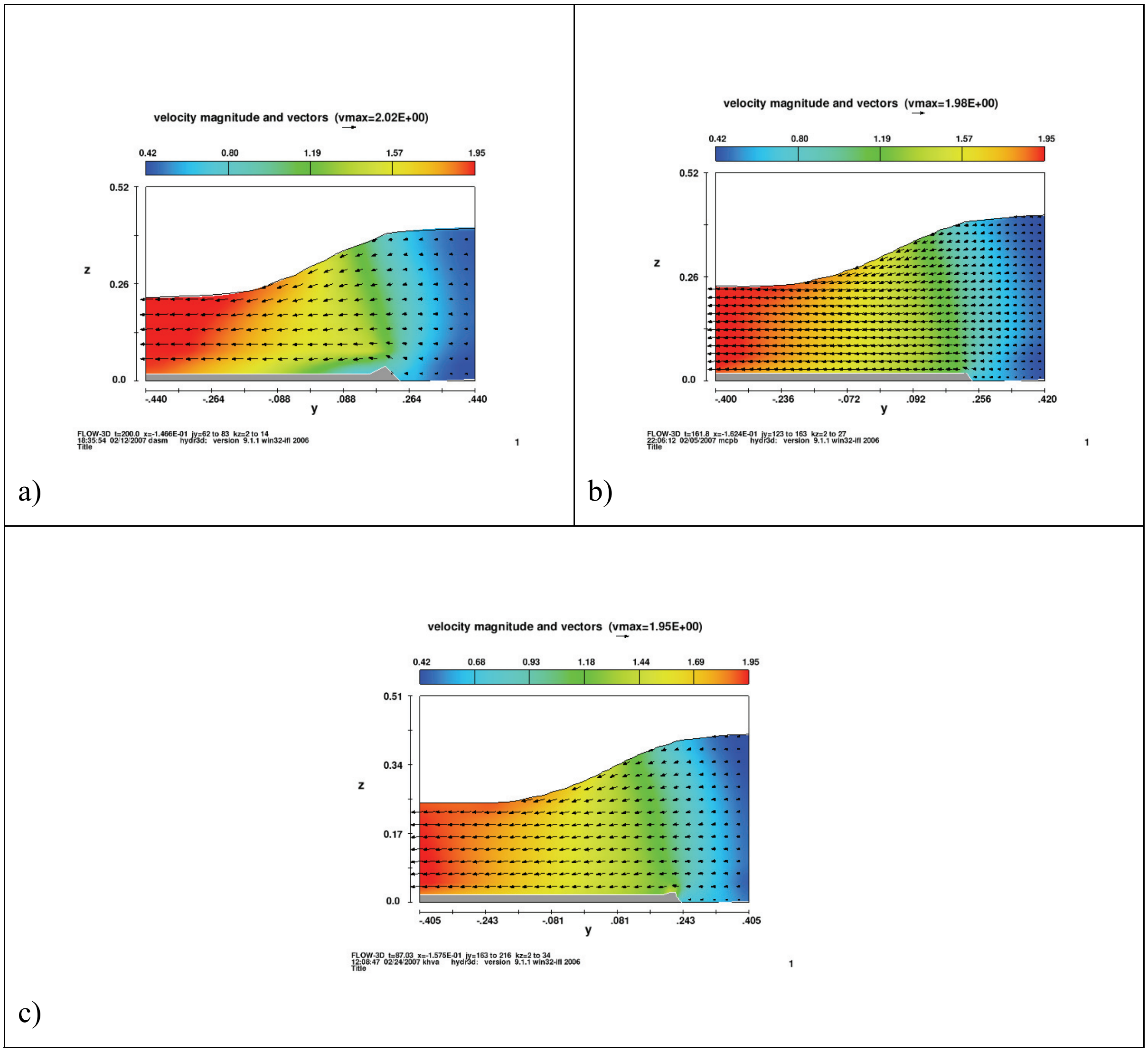

Figure 5.5: Velocity Fields for the 3D Fully Open Case on the Diversion Structure for minimum cell sizes of a) 2m, b) 1m, c) 0.75m

For each case, velocity fields are similar however; differences can be observed in the way that the FAVOR method interprets the geometry. For a mesh refinement with a minimum cell size of 2m, a large bulge can be seen at the upstream side of the 1m high sill. This bulge, while effectively increasing the sill at that location to 2m in height on the normally perfectly horizontal surface, creates an eddy of approximately 9m in length directly downstream of it. A similar yet smaller bulge is observed for the finest mesh but appears to have little effect on the flow pattern while no bulge is present for a minimum cell size of 1m.

This difference is caused by the location of the boundary between two horizontally-placed adjacent cells, i.e., for the 0.75m minimum cell size, the boundary coincides with the vertical face of the step and as a result, the step is defined by a single mesh cell in the horizontal direction rather than two, as is the case for the minimum cell size of 1m. Furthermore, the bulge for the finest mesh is limited in its height due to presence of smaller cells. The figure therefore illustrates the need to provide a mesh of adequate refinement so as to properly define the geometry of the structure.

Since it is impossible to compare the convergence of velocity fields point for point, a figure providing velocity profiles at various locations along the channel is required. These allow for a more detailed investigation of velocity magnitudes by observing, in particular, differences near the bed and near the surface.

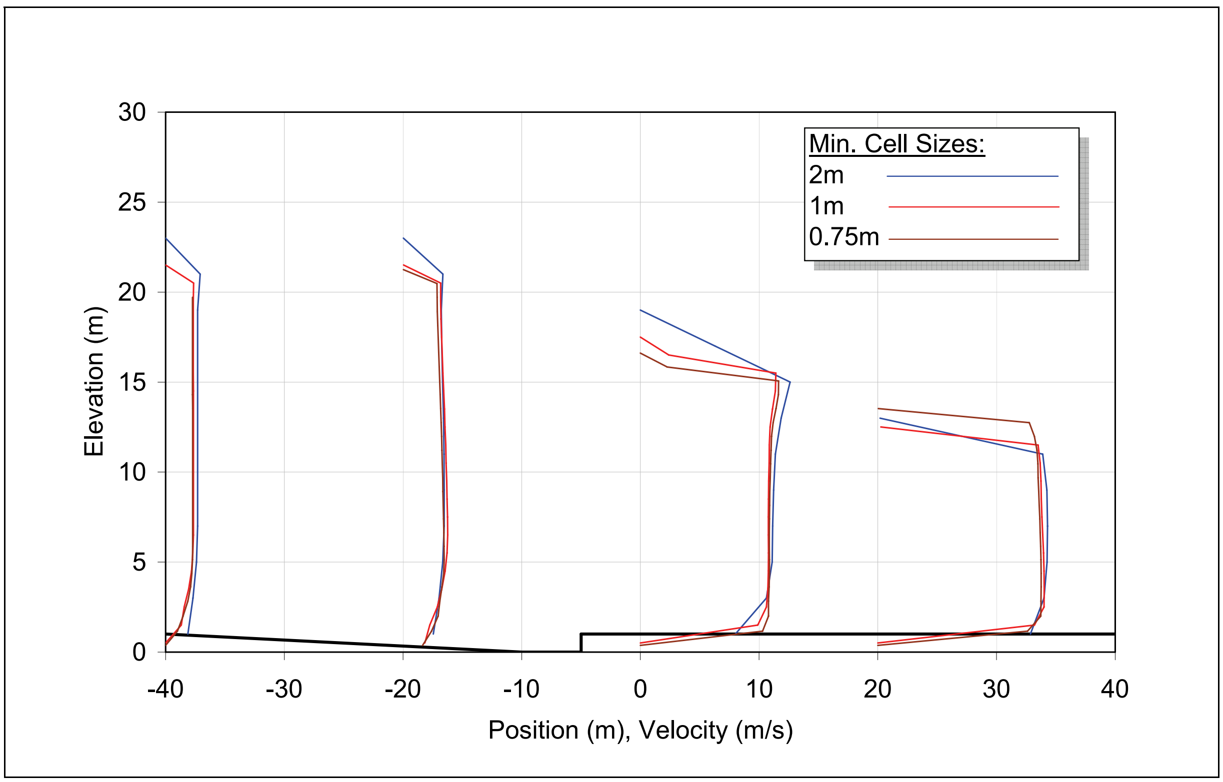

Figure 5.6: Velocity Profiles for the 3D Fully Open Case on the Diversion Structure along the Channel

The origin of the above figure is located at the upstream face of the gate, which provides velocity profiles approximately 40m upstream of the gate, 20m upstream of the gate, at the gate and 20m downstream of the gate along the approximate centerline of the open bay. Results show that velocities are in reasonably good agreement with one another, with marked differences between the solution of the coarsest mesh and the mesh independent solutions of the two other meshes. In particular, differences at the water surface and at the bed are caused by the mesh approximating the location of the geometry and water surface, which results in differences in interpolation between the non-zero velocity of adjacent cells in the flow field and the zero velocity either within the obstacle or above the water surface. These discrepancies should be minimized when a solution is mesh independent, however, differences are still present, particularly downstream of the gate slots. Similarly to the water surface profiles, these differences are caused by different extraction locations due to the discretization of the domain and can be exacerbated by the addition of a longitudinal position error component. In this case, the problem does not seem to be in the longitudinal direction since the differences in positioning diminish downstream, but are caused by the eccentricity of the sample point where the velocity profiles are off center by 0.15cm and 0.35cm for minimum cell sizes of 1m and 0.75m respectively. As a result, the water surface, located 20m downstream of the gate, is much higher for the velocity profile of the minimum cell size of 1m than it is for the minimum cell size of 0.75m, due to presence of shockwaves (see 3D rendering of water surface, Figure 5.4). Although downstream velocities are not directly comparable, velocity profiles located upstream of the control structure are and, for the two finest meshes, are very similar, suggesting mesh independence. Given the convergence of discharges and velocity profiles, a minimum cell size of 0.75m or 1m should be used for all subsequent fully open simulations.

In addition to the fully open condition, mesh independence tests for four partial gate openings of 6m, 4m, 2m and 1m were carried out in quasi-2D. The following figure presents the discharge vs. minimum cell size curves for all examined partial gate openings.

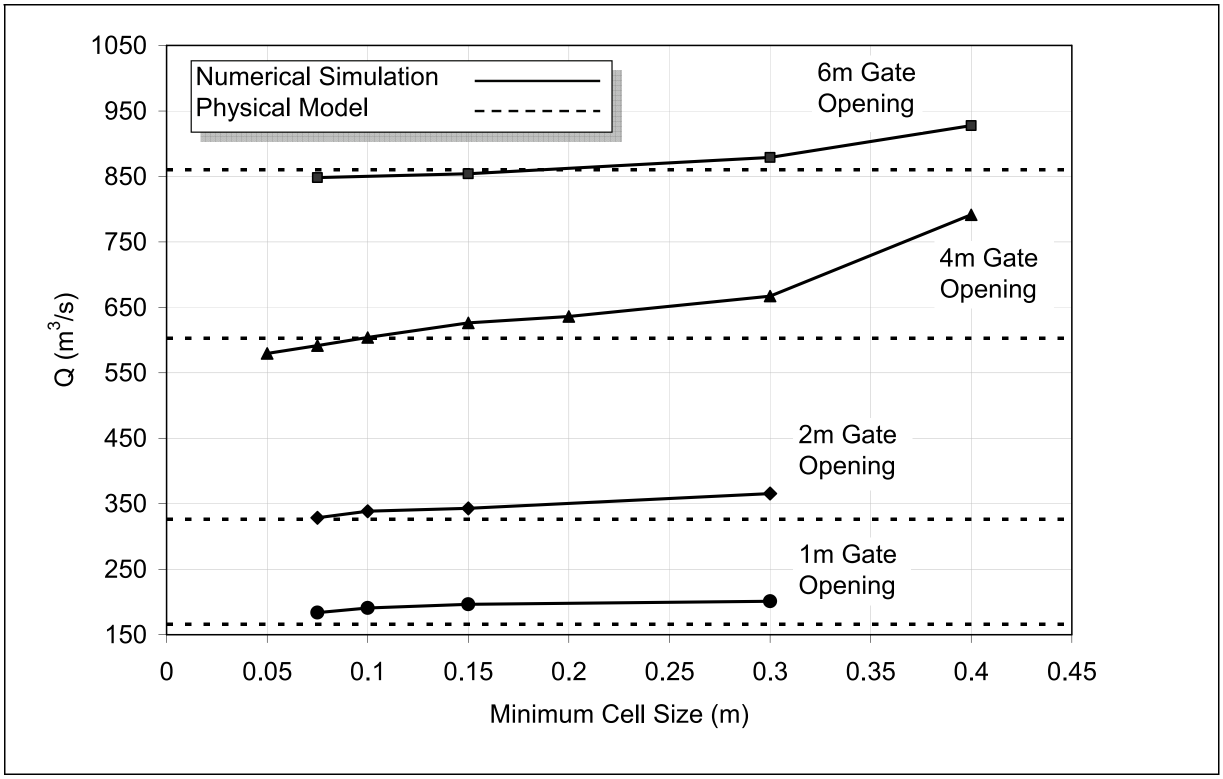

Figure 5.7: Discharge vs. Minimum Cell Size for the quasi-2D Partial Gate Openings on the Diversion Structure with Physical Model Results

For each gate opening, quasi-2D simulations were carried out with increasing mesh refinement. The quasi-2D calculations adequately represent the contraction caused by the gate as the discharges calculated by the numerical model are close to those measured on the physical scale model. The discharge vs. time curves showing convergence of the solutions from which flowrates were extracted and analyzed using Equations 5.1 and 5.2 can be found in Figures B.3 to B.6. It can be seen from discharges plotted in the above figure that none of the partial gate openings have yet attained mesh independence since individual curves do not attain a constant discharge. In fact, given the trend of the curves, only the 6m gate opening seems to be converging towards mesh independence, while the other gate openings are diverging with increased mesh fineness, as seen by the increasing slope between each data point. This difference is most likely caused by the need for increased refinement below smaller gate openings in order to properly define the velocity profiles and therefore, to verify this hypothesis, further mesh refinement is required. Unfortunately, this is unfeasible given the available computing power and time as even decreasing the minimum cell size to 0.05m, as was done for the 4m gate opening, requires approximately two weeks of computation to reach steady-state.

For the 6m gate opening mesh refinement resulted in the flowrates converging to a discharge approximately equal to that measured in the physical scale model. It can be seen in Figure 5.7, that a reduction in minimum cell size by 33% (0.4 m to 0.3 m), by 50% (0.3 m to 0.15 m) and again by 50% (0.3 m to 0.15 m) resulted in a reduction in the calculated discharge of 5%, 2.8% and 0.7% respectively. All but the coarsest mesh are within the engineering norm of 5% from the physical model result (differing by +8.8%, +2.2%, -0.7% and -1.3%) and the smallest mesh size is near mesh independence as the discharge converges close to the physical model result and changes by less than 1% from the previous refinement.

Several additional meshes were tested for the 4m gate opening in order to observe their effects on the divergence of discharges. The minimum cell sizes used for these observations are 0.4m, 0.2m and 0.1m. For these cases, only discharges are presented while velocity fields, velocity profiles, water surface profiles, Fr and Re numbers and computation times were not recorded. No new information was extracted from these additional simulations except that at coarser meshes, the solution appears to convergence only to diverge for finer meshes.

In order to examine the efficiency of each gate opening, discharge coefficients are frequently favored over discharges by engineers. Thus, Table 5.2 provides a comparison of numerical and physical model discharge coefficients for all four partial gate openings along with their relative errors. Note that only the coefficients from the finest meshes for each gate opening are presented.

Table 5.2: Summary of Discharge Coefficients for all Partial Gate Openings

Gate Opening (m)	$\mathbf{Q_{3Deq}}$ **(m^3/s)**	$\mathbf{Q_{LaSalle}}$ **(m^3/s)**	$\mathbf{C_{F3D}}$	$\mathbf{C_{LaSalle}}$	**% Error**
6m	848	860	0.54	0.55	-1.42
4m	580	602	0.55	0.57	-3.65
2m	328	326	0.62	0.62	0.61
1m	184	166	0.70	0.63	10.84

In the above table, C_{F3D} and $C_{LaSalle}$ represent the two dimensionless discharge coefficients for the two sets of results and are both computed using the following equation:

$$q_{bay} = CG_o\sqrt{2gy_u} \tag{5.5}$$

where q_{bay} is the discharge per unit width of the bay, G_o is the gate opening and y_u is the water level directly upstream of the gate. Furthermore, the % error for each simulation is given by:

$$\%error = \frac{Q_{3Deq} - Q_{LaSalle}}{Q_{LaSalle}} x100\% \tag{5.6}$$

Since discharge coefficients are related to discharges through a set of known values, the % error calculations used the flowrates rather than the coefficients due to a larger number of significant figures in the former.

With these discharge coefficients, flowrates can be predicted with reasonably good accuracy for a small range of headwater levels, as long as the gate orifice is not drowned by tailwater. It can be seen in Table 5.2, that there is relatively good agreement between the numerical and physical models for the three larger gate openings while the numerical model value for the 1m gate opening is well above the physical model value. Unfortunately, given the current trend in discharges, the coefficients for the 4m, 2m and 1m gate openings will decrease with increased mesh refinement at the same rate. As a result, these values are not reliable however, since the 6m gate opening is observed to have a converging discharge trend, the discharge coefficients from either the numerical or physical models can be used in design. For this reason, the 6m gate opening will be used for full sized vs. scaled and K-ε vs. RNG comparisons.

To further examine the trend towards mesh independence of the 6m gate opening and the general characteristics of gated flow, Figure 5.8 provides an illustration of the comparison of the water surface profiles with those of the physical model.

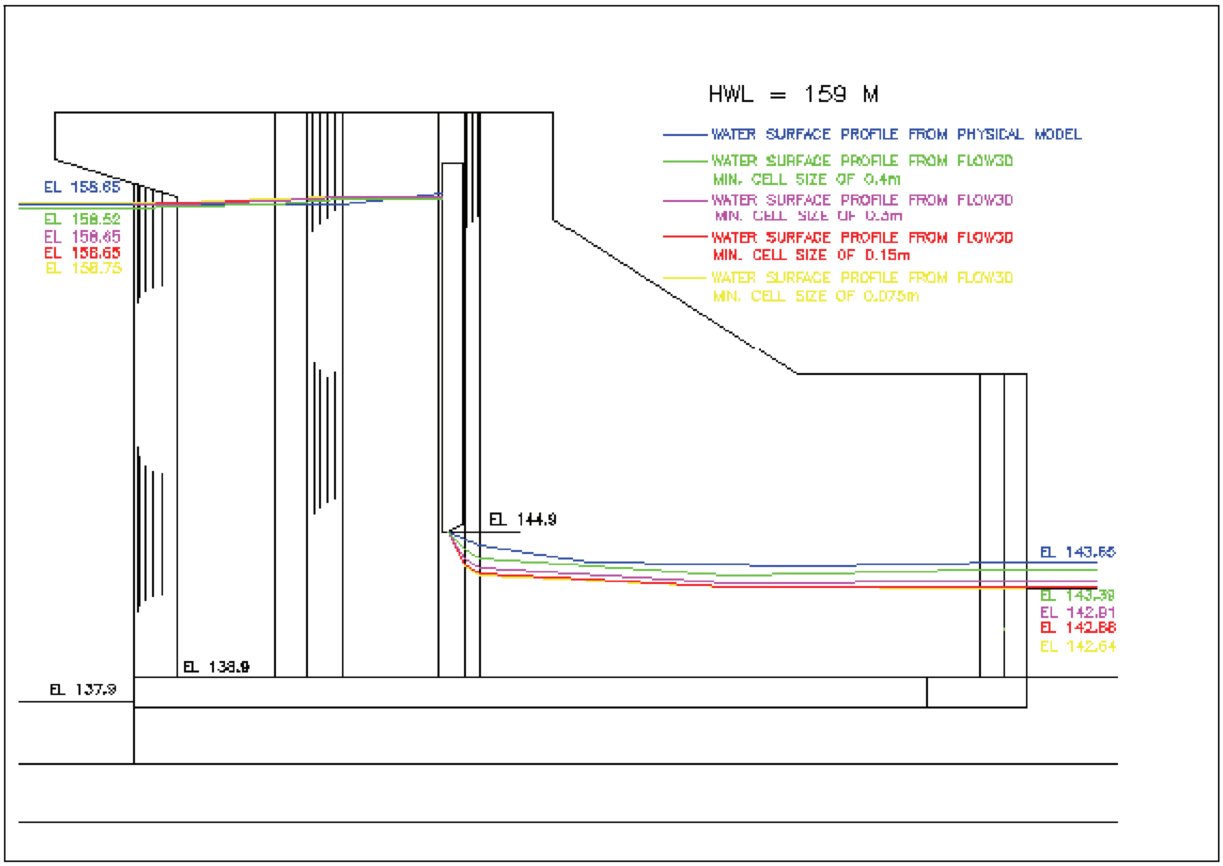

Figure 5.8: Comparison of Water Surface Profiles with increased Mesh Refinement for the quasi-2D 6m Gate Opening Diversion Case

The above figure shows that, for the 6m gate opening, water surface profiles for each mesh refinement are in good agreement with those of the physical model, differing by a maximum of 0.13m upstream of the gate in the subcritical region and under predicting the water surface by up to 1m downstream of the gate in the supercritical regime. Similarly, for the 4m gate opening (Figure B.7), the upstream water surface profiles differ by a maximum of 0.08m while downstream levels are again under predicted by a maximum of approximately 1.5m. Due to differing water levels at HWL-C for which water surfaces from the physical model were plotted, water surfaces for the 2m and 1m gate openings (Figures B.8 and B.9) cannot be directly compared however, similarly to the other gate openings, downstream water levels are again under predicted. The underlying trend is that Flow3D adequately predicts the upstream water levels while significantly under predicting downstream levels. There are several possibilities that could cause this discrepancy in the results. First of all, the exclusion of the lip in the numerical model could influence the contraction of the jet downstream of the orifice. Another source of error could be the exclusion of the tailwater in the quasi-2D model, and thus, the higher water levels downstream of the gate in the physical model could be caused by an M3-type curve prior to the hydraulic jump which is located further downstream. A more probable source of the discrepancy could be caused by the location at which the water surface profiles were measured on the physical model. Since the water levels are measured along the walls of the piers, a certain amount of friction is present which would cause the supercritical flow downstream of the gate to lose energy and therefore have an increased depth along the pier walls. The quasi-2D simulation on the other hand, being an idealized case where the flow is bounded on both sides by a frictionless environment would not display this energy loss, resulting in a lower depth with a higher velocity. Finally, the discrepancy could simply be caused by the inability of the software to model these flows.

In order to further examine differences in downstream water levels, contraction coefficients were calculated from the water surface profile figures provided by Flow3D and the LaSalle Consulting Group's report, using the following relationship:

$$C_c = \frac{y_d}{G_o} \tag{5.7}$$

where C_c is the contraction coefficient and y_d is the depth directly downstream of the gate. For each gate opening, the coefficient from the finest mesh of the numerical model will be presented followed by the coefficient from the physical model in parentheses. Respective contraction coefficients for the 6m, 4m, 2m and 1m gate openings are as follows: 0.63 (0.78), 0.60 (0.85), 0.715 (0.875), 0.73 (0.87). In all 4 cases, the contraction of the flow of the numerical model is much larger than the contraction of the physical model despite the two systems having similar discharges. Furthermore, only the 6m and 4m gate openings have values near the standard of 0.60-0.61 for sharp-edged gates, as outlined by Lin et al. (2002) while the contraction coefficients for the two other gate openings are much larger, suggesting that these values may be different due to the non mesh independence of the solutions. To verify the effects of the omission of the gate lip on the numerical model and the effects due to the pier walls on the physical model, it is possible to calculate approximate theoretical values for contraction coefficients of the physical model in order to compare them to the values of the numerical model, by using the following equation:

$$q_{bay} = C_c G_o \sqrt{2 g y_u \frac{y_u}{y_u + y_d}} \tag{5.8}$$

For lack of additional information, y_d takes the same values as it did in Equation 5.7, despite there being the possibility that the flow depth is affected by the friction of the pier walls. As a result, the calculated contraction coefficients will be slightly larger than in reality. With all other variables known, for the 6m, 4m, 2m and 1m gate openings, the approximate theoretical coefficients for the physical model are 0.60, 0.61, 0.64 and 0.62 respectively, suggesting that discrepancies in actual measured downstream depths are caused by frictional effects from the pier walls. Furthermore, these values confirm those that were measured on the numerical model for the 6m and 4m gate openings and suggest that, for these cases, the omission of the gate lip has no effect on flow contraction, however, it may be concluded that smaller gate openings still require further mesh refinement in order to properly model the flow.

By observing the water surface profiles provided by Flow3D in Figure 5.8, a trend can be observed: the coarser the mesh, the larger the water surface elevation downstream of the gate. Convergence is seen from coarser to finer meshes where the water surfaces for the two finer meshes appear to coincide with one another. While the water surface profile for the minimum cell size of 0.3m is similar to two finer cases, its discharge and velocity profiles, as will be seen later, dictate that it is not close enough to mesh independence so as to be used for comparison tests. A similar converging trend is also observed for smaller gate openings; however, differences in water surface profiles, particularly for the 2m and 1m gate openings, are increasingly difficult to see due to slower velocities in the approach channel and smaller jets downstream of the gate orifice. It is, therefore, difficult to determine whether the convergence is as a result of mesh independence or the general geometric characteristics of the problem.

The velocity fields provide a way to assess if the flow qualitatively correct. The velocity fields for the 6m gate opening, as calculated by Flow3D, for each mesh refinement are presented below in Figure 5.9:

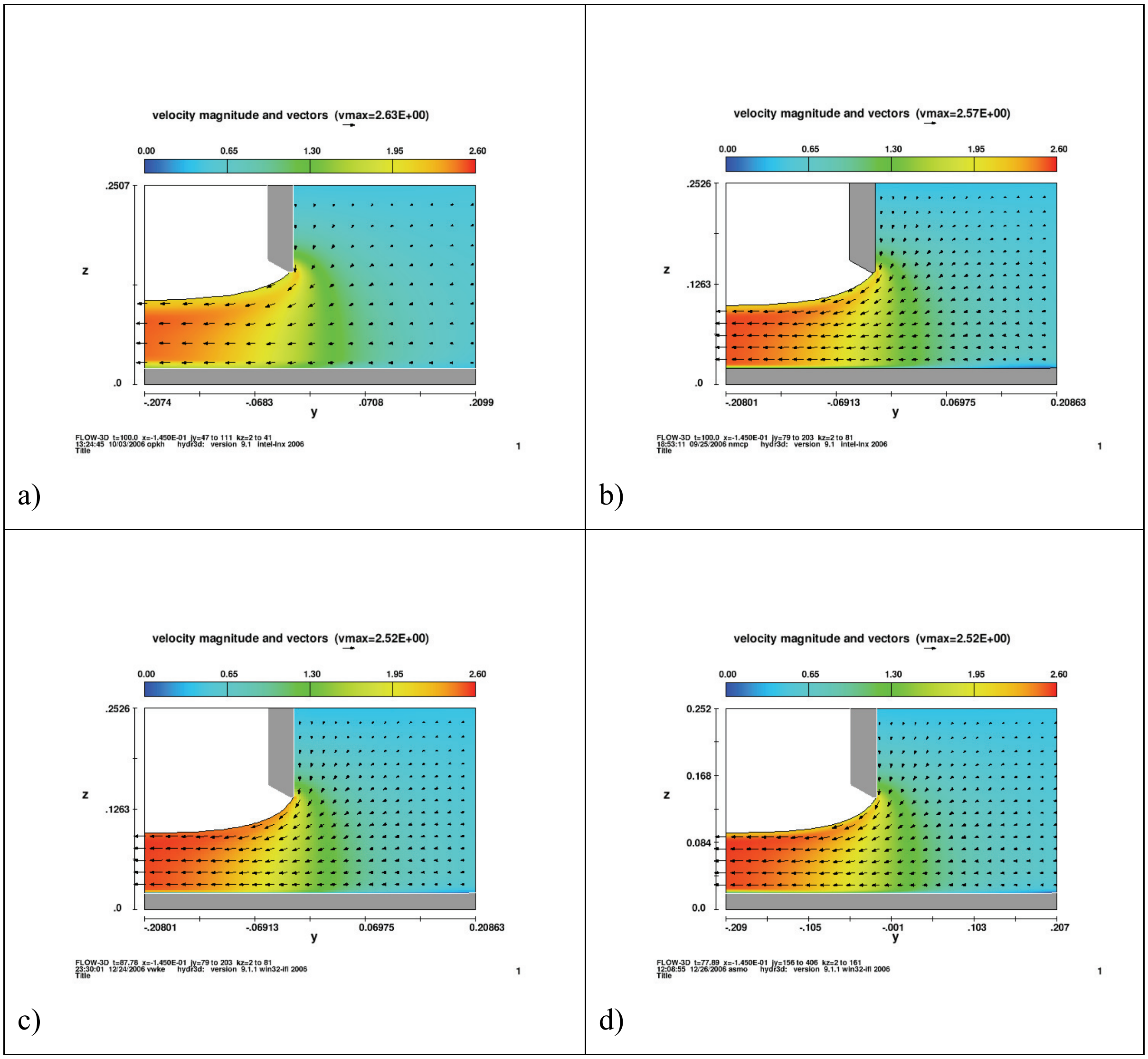

Figure 5.9: Velocity Profiles for the quasi-2D 6m Gate Opening on the Diversion Structure for minimum cell sizes of a) 0.4m, b) 0.3m, c) 0.15m, d) 0.075m

For each case, velocity fields are similar and the geometry is well defined by the mesh with perfect similitude of the gate lip as drawn in AutoCAD being attained in cases c) and d). The slight differences in the gate lip cause the dissimilarity of the velocity fields along the water surface and increase the downstream depth however; the gate orifice size remains essentially the same. This is seen mostly in cases a) and b) where Flow3D interprets the flat surface of the gate as being curved or beveled. A similar trend is observed for the velocity fields of the other gate openings, found in Figures B.10 to B.12. The velocity field figures demonstrate the importance of using an adequate mesh refinement, in order to ensure that the FAVOR method interprets the model geometry correctly so as to obtain valid results.

A more accurate means of determining mesh independence is found in a comparison of the velocity profiles along a segment of the channel, as shown in Figure 5.10.

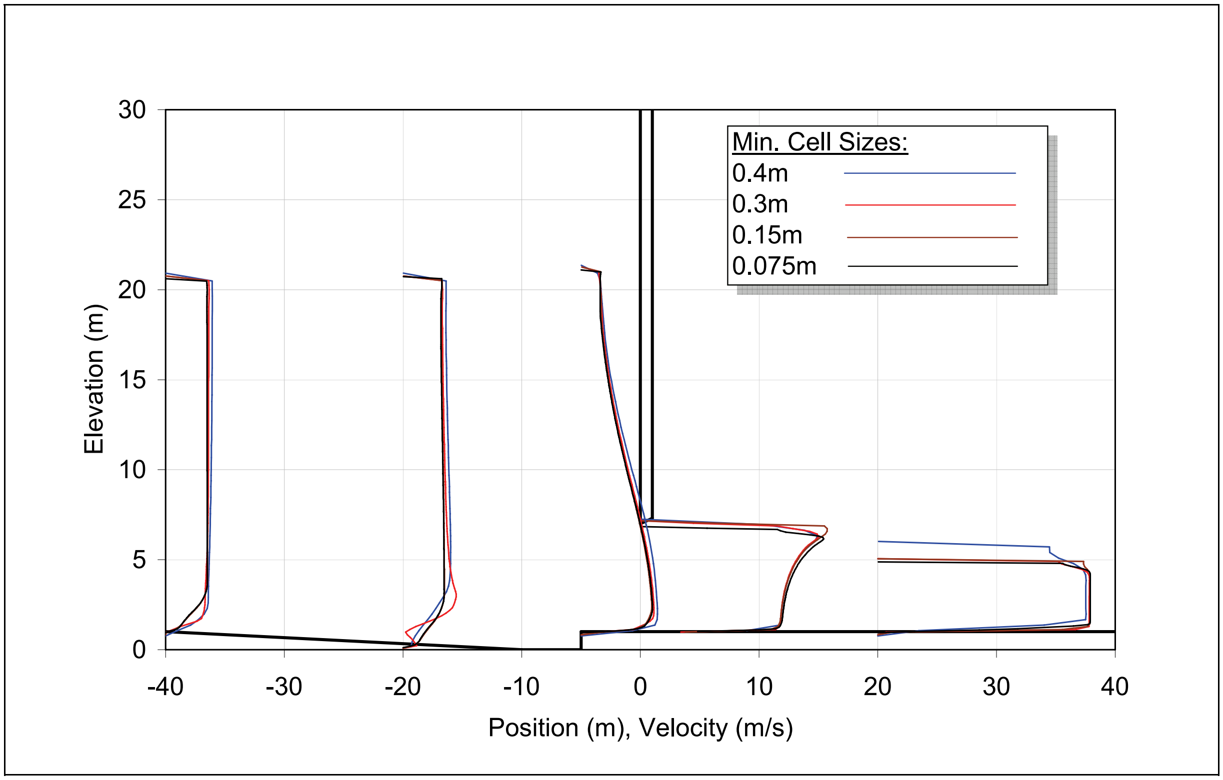

Figure 5.10: Velocity Profiles for the quasi-2D 6m Gate Opening on the Diversion Structure along the Channel

Similarly to 3D fully open case, velocities are plotted at the same positions along the channel with the addition of velocities 5m upstream of the gate. Furthermore, the exact location of extracted velocity data is more accurate due to the increased mesh refinement of the simulations while the discrepancies that exist are solely confined to the longitudinal direction since the domain of the quasi-2D simulation is 1-cell wide. This having been said, the velocity profiles shown above are in agreement with the trend observed in the discharge vs. minimum cell size curve and water surface profiles. Velocity profiles for minimum cell sizes of 0.3m and 0.4m are dissimilar in shape and magnitude to the two other mesh refinements, which are so similar that it is difficult to differentiate one from the other. Slight differences between the latter two are seen at the gate opening position, where both velocity profiles should have equal heights since the velocities are constrained by the bottom of the channel and the gate above them. Nevertheless, both velocity profiles are smaller than the gate opening which suggests that the location at which the velocity data was extracted is slightly downstream from the gate, causing the profile of the minimum cell size of 0.075m to be smaller than that of 0.15m since its location is 7.5cm further downstream. Despite this discrepancy, it can be concluded from the discharges, velocity profiles and water surface profiles, that for the 6m gate opening, a mesh with a minimum size of 0.15m or 0.075m would be adequate to obtain realistic results.

Figures B.13, B.14 and B.15 present the velocity profiles for the 4m, 2m and 1m gate openings respectively. A converging trend is also observed for these, despite the fact that the discharges are diverging. In fact, in all three cases, the velocities for at least the two finest meshes appear to almost coincide with each other, especially upstream of the gate. This, however, could be caused by the masking of fluctuations due to non mesh independence by the relatively small velocities in this portion of the channel due to smaller gate openings and as a result, major changes in profile shape could be minute in size. Additionally, profiles in which velocities are much higher, such as at the gate or further downstream, are generally not good candidates for comparison because any discrepancies that are caused by increased mesh refinement would be masked by dissimilar data extraction points. Although, similarly to the water surface profiles, a converging trend is observed, definitive conclusions from these profiles cannot be drawn without further refinement, which is impractical given the current available resources.

Since relative times of computation are important from an engineering point of view, Table 5.3 provides all relevant information related to the time required for computing all gate openings, including the fully open case in 3D, on the diversion structure for varying mesh refinements.

Table 5.3: Required Time for 3D Fully Open and quasi-2D Partial Gate Opening Simulations

Gate Opening	Min. Cell Size (m)	No. of Processors*	Initial Conditions	T_{ss} (s)**	T_{rt} (days)***
Fully Open	2	1	Cold Start	50	0.05
Fully Open	1	1	Cold Start	50	0.63
Fully Open	0.75	1	Cold Start	50	2.75
6m	0.4	1	Hot Start	80	0.25
6m	0.3	1	Hot Start	80	1.95
6m	0.15	1	Hot Start	45	0.75
6m	0.075	1	Hot Start	45	5.00
4m	0.3	1	Hot Start	80	0.5
4m	0.15	1	Hot Start	90	4.1
4m	0.075	1	Hot Start	45	5.0
4m	0.05	1	Hot Start	40	12.7
2m	0.3	1	Hot Start	90	0.7
2m	0.15	1	Hot Start	100	4.7
2m	0.1	1	Hot Start	50	2.7
2m	0.075	1	Hot Start	50	5.8
1m	0.3	1	Hot Start	125	0.3
1m	0.15	1	Hot Start	125	2.1
1m	0.1	1	Hot Start	80	3.5
1m	0.075	1	Hot Start	60	7.0

* Intel Core 2 Duo, 2.13 GHz
** the time in the software required to obtain steady-state conditions
*** the time in real-time required to obtain steady-state conditions

The data presented above shows that for increased refinement, there is an increase in time required to reach steady-state for all gate openings. The rate of time increase is not a linear function due to the relationship of the mesh size to the time-step: as mesh refinement increases, the time step must decrease in order to keep the Courant number at a reasonable value so that the simulation can remain stable.

As can be seen, there is great variability in the amount of simulation and real-time required to reach steady-state. These differences are dependent on the gate opening and the result files used as input for the initial conditions (hot start) for the partial gate opening simulations. For the 6m, 4m and 2m gate openings, the two coarsest meshes used the solution given by a mesh of minimum cell size of 2m while the 1m gate opening's two coarsest meshes used the solution by a mesh of minimum cell size of 1m. As a result, since the information used to hot start the simulations was far from mesh independence, more in-simulation time was required to obtain a steady-state solutions in comparison to the two finer meshes of each gate opening. This, however, does not necessarily translate in a longer amount of real-time.

As for the two other simulations of each partial gate opening, each computation used the previous simulation's results as initial conditions. For example, for the 6m gate opening, the solution for a minimum cell size of 0.3m was used as input for the simulation with a minimum cell size of 0.15m, which after completion, was then used as the initial conditions for the simulation with a minimum cell size of 0.075m. The net result is that simulations required less in-software time to calculate their results as compared with the two coarser mesh refinements of each gate opening, which translated on occasion, as in the case of the 6m and 2m gate openings for the minimum cell sizes of 0.15m and 0.1m respectively, with less real-time being required to calculate the solution as compared to their adjacent coarser meshes. Given the trend observed with the two coarsest meshes, both the finer meshes would have taken a much longer time to reach steady-state and therefore, the finest mesh possible should be used as input for similar computations.

An additional trend is observed concerning the size of the gate orifice: as the gate opening decreases, an increased amount of time is required to reach steady-state. This is most likely caused by additional time required to dissipate excess energy present in the coarser solutions due to the smaller orifice of the gate, which increases the reflection of shockwaves in the upstream reach.

To conclude this section, it should be stated that divergence of discharges for the 1m, 2m and 4m gate openings occurred for unknown reasons. Investigations were conducted to observe the effects of coarser meshes on the 4m gate opening and select simulations beginning with cold start initial conditions with equal minimum cell sizes to the ones presented were also performed yielding equal solutions. Therefore, it is possible that discharges will converge with further mesh refinement, although further tests must be conducted to verify the veracity of this statement. Consequently, the reader should view the results for the 4m, 2m and 1m gate openings cautiously. Given the presented results for the fully open case and the 6m gate opening, minimum cell sizes of 0.75m or 1m and either 0.075m or 0.15m should be used for comparison tests respectively.

5.2 Comparison of Scaled and Full-Sized Models

To ensure that the results of simulations run with the model dimensions were dynamically similar to those obtained for the prototype dimensions, tests were conducted on the diversion structure for the fully open case and 6m gate openings in order to compare the model/prototype velocity profiles, water surface profiles and discharges. Similarly to the mesh refinement tests, the upstream water elevation for each simulation was selected as being equal to 159m above sea level or 21.1m above the datum (z = 0) of the numerical model. The mesh was constructed following the description outlined in Table 4.2 (see explanations in Section 4.2.2) and using mesh refinements determined in the previous section in order to increase the accuracy of solutions.

The discharge convergence curves for both the 3D fully open and the quasi-2D 6m gate opening obtained by the three baffles are available in Figures B.16 and B.17 of Appendix B respectively. For the fully open case, each simulation was computed with a minimum cell size of 0.75m and began with a cold start initial condition, i.e., a reservoir of water was placed from the upstream boundary to the gate slot with an initial elevation of 159m. The flowrate found on the prototype is the true discharge and is equal to approximately 1848m^3/s while the flowrate found on the 1:50 scaled model is a scaled discharge with a value near 0.1045m^3/s. Since the flow is turbulent for both cases, the discharges can be related to each other by using the Froude law through Equation 5.1. Performing the appropriate calculations yields an equivalent value of 1848m^3/s for the scaled model and therefore, the discharges for model and prototype dimensions are equal.

Due to the relatively short time required to reach steady-state in each case, the simulations for the 6m gate opening were carried out with a minimum cell size equal to 0.075m rather than 0.15m. Similarly to the fully open case, the flowrate extracted from the full-sized curves is the true discharge and is approximately equal to 96.4m^3/s. This discharge is the value calculated by the two upstream baffles. For unknown reasons, the baffle furthest downstream calculated a flow approximately 0.3m^3/s smaller, which represents an approximate 0.3% relative difference. Nevertheless, both of the values, regardless of the choice of baffle, are more than 1.4m^3/s smaller than the prototype value of the 1:50 scaled model. The related curve shows a discharge of 0.005537m^3/s which, through Equation 5.1, is equal to 97.9m^3/s. Although this slight discrepancy exists, it is only equivalent to a maximum difference of 1.5% between the scaled and full-sized models and could be caused by scaling effects and the increased complexity of the flow of the gated case.

A noticeable difference can be observed on the x axis of the two figures: the full-sized model seems to take a much longer time to reach steady-state within Flow3D. The scaled and full-sized results for the fully open condition are directly comparable since both are initiated by a cold start initial condition. The full-sized model requires 270s compared to the 45s required for a 1:50 scaled model. This, however, does not translate in additional computing time, with each simulation requiring almost two thirds of a day to compute. By using the Froude relationship for time provided in Table 4.1, the equivalent times for the model/prototype can be calculated. Dividing 270s by a factor of 7.07 yields 38.2s, a value which is close to 45s and therefore, the scaling of the 1:50 model provides a reasonable explanation for this discrepancy.

Unfortunately, for the 6m gate opening, both simulation times and real-time values cannot be directly compared for both simulations since their initial conditions are different. While both the simulations began with a "hot start" initial condition (i.e. used a previous simulation to begin the computation), the scaled model used a solution from a much finer mesh (min. cell size of 0.15m). Since there was no previous simulation to begin the full-sized computation, a coarse grid, with a minimum cell size of 0.5m was first computed and was subsequently used for its results. A total amount of simulation time of 560s was required for the full-sized model while only 50s was required for a model of 1:50 scale. By multiplying the value of 560s by the root of this scale (Froude law, factor of 1/7.07), a value of 79.2s is obtained, which is similar to results presented in Table 5.3. Both these simulation times translate to real-time values of 5 days and 8.5 days respectively, which is to be expected since using an initial condition which is further from the true solution would result in longer computational times to reach steady-state.

Water surface profiles of the two fully open cases are provided in Figure 5.11.

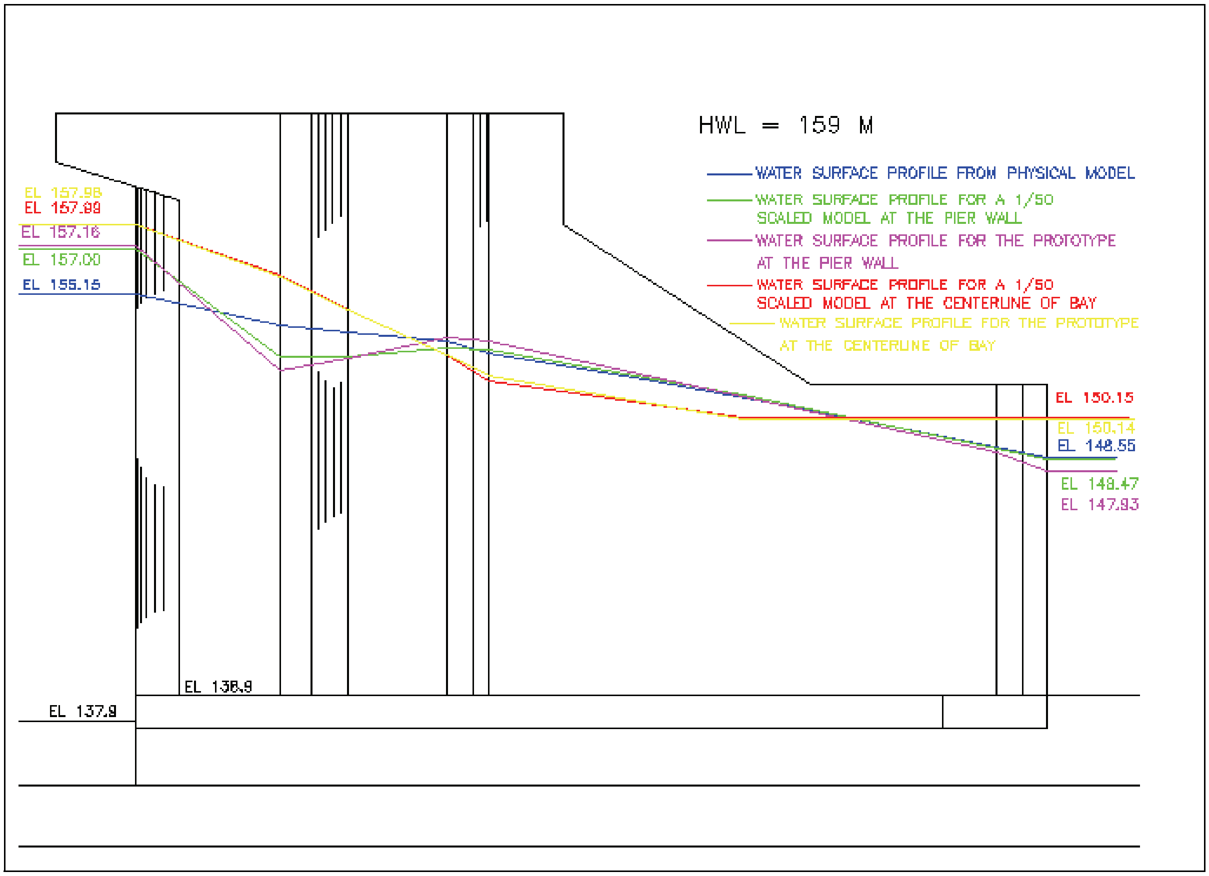

Figure 5.11: Comparison of Water Surface Profiles for Scaled and Full-Sized Fully Open Diversion Cases

As can be seen in the above figure, maximum differences of approximately 0.5 m are observed between the two systems, specifically along the pier wall, even though the profiles were extracted at exactly the same locations. The primary reasons for differences are scaling effects caused by increased air entrainment in the full-sized case in combination with viscous effects along the wall of the structure where these results were extracted, caused by the use of the same fluid on the scaled model. Despite this, both systems for both sets of profiles exhibit the same dissimilarities when compared with the results of the physical model, as previously described in the mesh refinement tests section.

Figure B.20 shows a comparison of the 6m gate opening for prototype and model dimensions. Similarly to the fully open case, both the water surface profiles of the scale model and prototype are comparable in shape with slight dissimilarities caused, in this case, by a combination of small differences in discharges, velocities, and scale effects caused by less air entrainment at scale. Nevertheless, the profiles, both upstream and downstream of the gate are in good agreement with each other, with a maximum difference of 8cm occurring at the entrance of the control structure however, this is not the case when compared with the downstream water surface of the physical model, the causes having been previously discussed.

Figure 5.12 presents a comparison of velocity profiles for the fully open scaled and full-sized diversion structures.

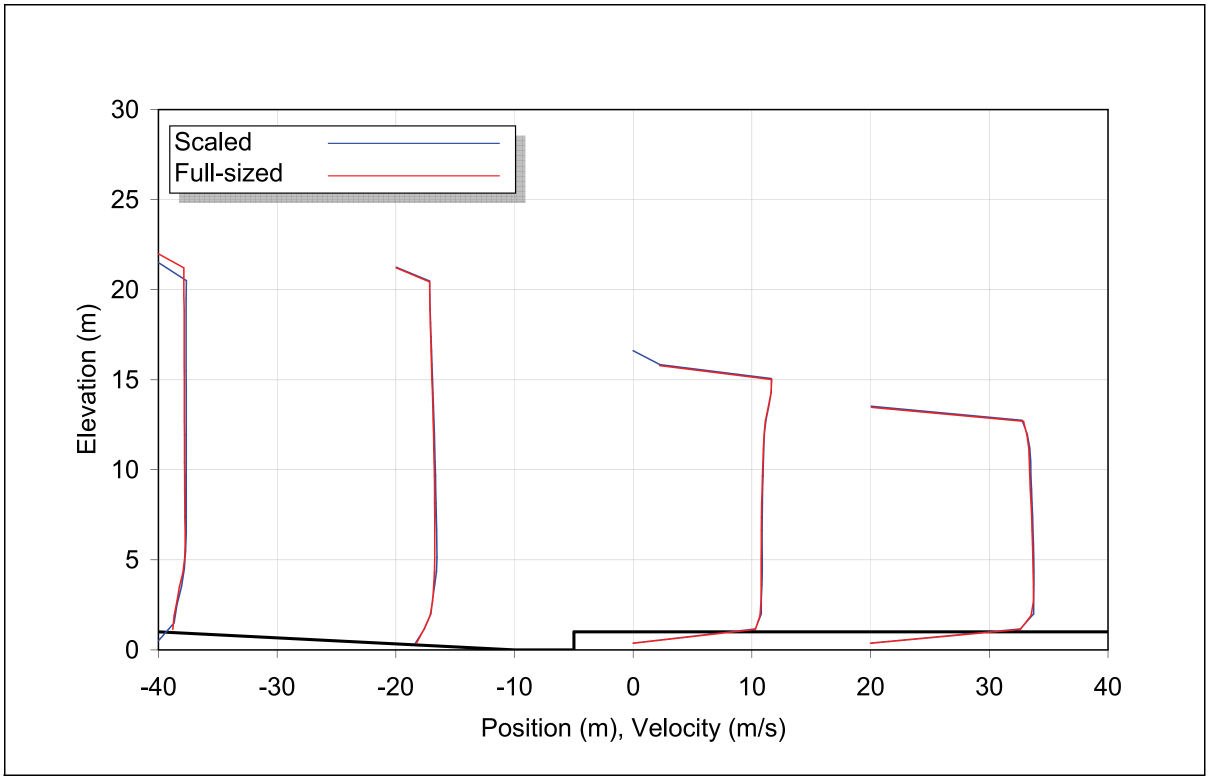

Figure 5.12: Velocity Profiles for the Scaled and Full-Sized Fully Open Case on the Diversion Structure

The profiles for the full-sized model were extracted at the closest possible locations to the ones previously extracted during the mesh refinement tests for the scaled model. The above figure, in combination with the previously presented discharges and water surfaces, indicates that the two systems are kinematically similar, despite there being a slight discrepancy at the furthest upstream profile. This difference is most likely caused by the variation in extraction points which are 30cm apart and is therefore of little consequence since all other velocity profiles at subsequent locations further downstream are almost indistinguishable from one another.

Figure B.21 presents the velocity profiles for the scaled and full-sized model for the 6m gate opening. Similarly to the fully open case, velocities appear to be kinematically similar despite there being bigger differences along the headrace bed, and near the surface of the flow below the gate. These differences are seen, for example, with the velocity profile located furthest upstream for the full-sized model which contains an inverted “S” shape near the bed of the channel while the scaled velocity profile is parabolic in appearance. Furthermore, at a distance of 20m upstream of gate, velocities on the full-sized model appear to be larger near the bed than their scaled counterparts. Differences in velocity can also be seen at the gate orifice and 20m downstream of the gate, where velocities appear to be slightly higher near the surface for the full-sized case.

Due to the proximity in results, both systems can be considered dynamically similar for both gate openings since only small differences in results are observed.

5.3 Comparison of K-ε and RNG Closure Models

In the RANS approach to simulating fluid flows, a closure model is required so as to obtain an additional set of variables to allow the system of equations to become solvable. These models are generally based on experimental data, with the most important being the K-ε viscosity model of Launder et al. (1972) which is often used as a standard in industry. Although the standard K-ε model is more than adequate for purposes of this thesis, the RNG model, uses different coefficients based on renormalization analysis (see Section 3.2 for more details). Since both formulations are readily available in Flow3D and that the RNG model is not extensively tested, this section provides a comparison of the results obtained by the two models for their uses in sluiceway design.

The comparison of K-ε and RNG closure models were done in a similar way to the comparison of scaled and full-sized models: results from the mesh independence tests were used to define the mesh, and the turbulence closure models were tested for both the 3D fully open case and the quasi-2D 6m gate opening with an upstream water elevation at HWL-C equal to 159m on the diversion structure. Furthermore, tailwater was included only for the fully open case.

The fully open gate condition used a minimum cell size of 1m for both simulations. The discharge convergence curves obtained by the three baffles are available in Figure B.22

of Appendix B. Both simulations used a cold start initial condition and it can be seen, that both yield identical convergence curves. As a result, the discharges are equal, giving a scaled value of 0.1045m^3/s, which, through Equation 5.1, is equivalent to 1848m^3/s in prototype units. Additionally, both simulations reach steady-state at 45s of simulation time, which translates in approximately 15 hours of real-time computation.

In contrast, discharge curves for the 6m gate opening, found in Figure B.23, appear to be dissimilar in shape. Both simulations were conducted on a mesh with a minimum cell size of 0.075m and used a hot start initial condition with the solution for the minimum cell size of 0.15m which was computed with the K-ε model during the mesh refinement tests. For the restart of the RNG model, turbulent energy and average kinetic energy parameters were excluded from the initial interpolation on the new mesh and were recomputed using the RNG model constants within Flow3D. Thus, the initial conditions of the simulation were similar to a simulation with a minimum cell size of 0.15m that had been computed using the RNG model over its entirety. The computed discharges for each simulation are 97.88m^3/s and 96.12m^3/s in prototype values for the K-ε and RNG models respectively, which is equivalent to a difference of approximately 1.8% between the two systems. Furthermore, both simulations reached steady-state near 45s of in software time, which, in both cases, was equivalent to approximately 5 days in real-time.

Since the water surface profiles and velocity profiles for the fully open case are almost indistinguishably similar for both turbulence closure models (see Figures B.26 and B.27 in the Appendix B), the remainder of the section will focus on the 6m gate opening where slight differences can be observed, mainly due to the increased complexity of the flow patterns. The water surfaces are plotted below, in Figure 5.13.

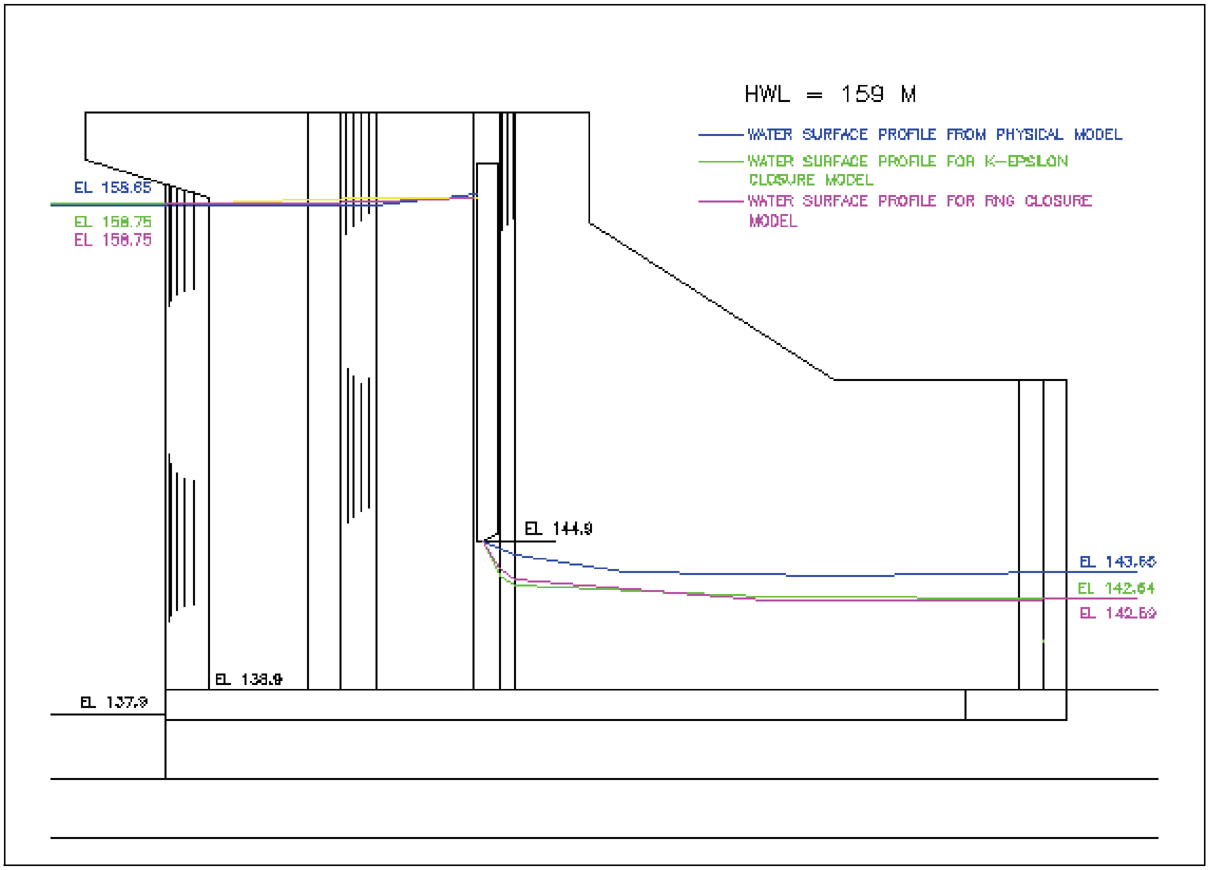

Figure 5.13: Comparison of Water Surface Profiles for the K-ε and RNG Models for the quasi-2D 6m Gate Opening Diversion Case

Water surfaces for the 6m gate opening appear to be almost identical, with slight discrepancies caused by the different turbulence models. Furthermore, both turbulence models exhibit dissimilar downstream water levels when compared to the results of the physical model and show a much larger contraction of the flow, as was documented in the mesh refinement tests section.

The velocity profiles of both turbulence models are presented in Figure 5.14.

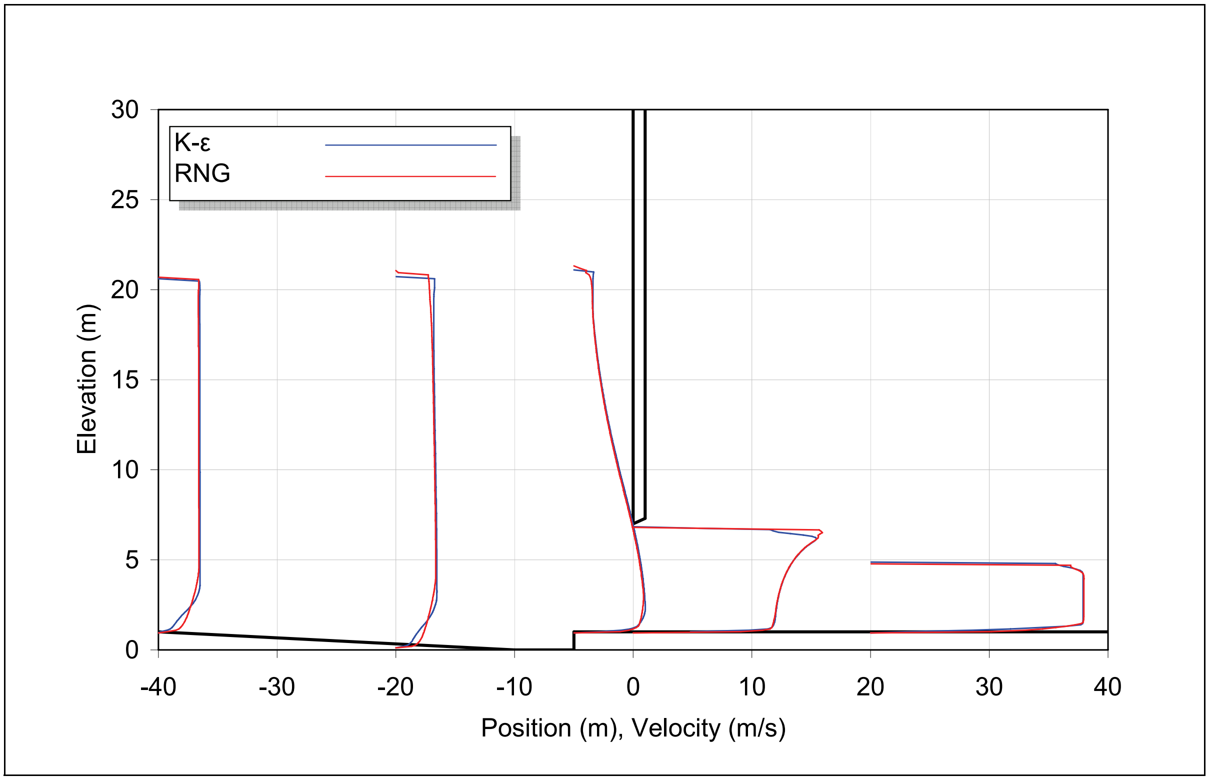

Figure 5.14: Velocity Profiles for K-ε and RNG Models for the quasi-2D 6m Gate Opening Diversion Case

Data was extracted from text result files at the exactly the same locations for both sets of results. Differences in velocity profiles for the 6m gate opening are observed particularly near the bed of the approach channel where the K-ε model has a tendency to compute lower velocities. In addition, slight differences are observed near the water surface in the subcritical region and below the gate orifice while the downstream most profiles are identical.

It can be concluded, that although slight differences in results caused by the vertical contraction of the gate for the 6m gate opening case exist, the RNG and K-ε closure models yield similar results and are identical for the fully open case.

5.4 Comparison of 3D Simulations and Physical Model Measurements

Simulations in 3D were computed for the fully open gate condition on both the control structure during diversion and rollway phases for water levels of 151m, 154m and 159m. While the diversion simulations included a tailwater of 6.1m depth, the rollway simulations did not due to the presence of a control on the rollway crest. Furthermore, all simulations used a mesh with a minimum cell size equal to 1m, as specified by the mesh refinement tests. In this section, results from numerical simulations such as discharges, discharge coefficients and design equations are compared to those of the physical model along with water surface profiles at the centerline of the bay and at the pier wall and pressure profiles along the centerline of the bay and at the pier walls, 2m above the rollway or bed of the structure. In some cases, information from the physical model was never recorded, and consequently, instead of a comparison, the results from Flow3D will be presented. Table 5.4 provides a summary of the results of the simulations and a comparison with measured results including relative times of computation.

Table 5.4: Summary of Discharges, Discharge Coefficients and Computation Times for 3D Fully Open Simulations

Structure Type	Level at HWL-C (m)	Q_{F3D} (m^3/s)	$Q_{LaSalle}$ (m^3/s)	$C_{d\text{-}F3D}$ ($m^{1/2}/s$)	$C_{d\text{-}LaSalle}$ ($m^{1/2}/s$)	% Error	T_{ss} (s)	T_{rt} (days)
Diversion	159	1848	1850	1.58	1.58	-0.10	45	0.63
Diversion	154	1211	1213	1.59	1.59	-0.11	42	0.59
Diversion	151	858	858	1.57	1.57	~ 0	40	0.56
Rollway	159	1412	1430	1.96	1.98	-1.24	42	0.59
Rollway	154	790	781	2.06	2.04	1.15	40	0.56
Rollway	151	421	434	1.93	1.99	-2.98	38	0.53

In the table, Q_{F3D} is defined as the flowrate obtained from the discharge vs. time convergence curves from Flow3D (Figures B.28 and B.29) transformed to prototype values. Note that, unlike the discharge coefficients of the partial gate openings presented in Section 5.1, the coefficients presented above include constants (See Chapter 2) and, as a result, are not dimensionless. They were calculated using a variation of Equation 2.2, which has the following form:

$$Q = C_d W_{bay} \left(z_{HWL-C} - z_{crest} \right)^{\frac{3}{2}} \tag{5.9}$$

where $z_{HWL\text{-}C}$ and z_{crest} is the water level at HWL-C and the elevation of the crest at the control structure respectively. The elevation of the crest is considered to be equal to 144.45m for the rollway case and 138.9m for the diversion case. Furthermore, the % error is calculated by using Equation 5.6 where Q_{3Deq} is replaced with Q_{F3D}.

The rating curves for the two structures are presented in Figure 5.15.

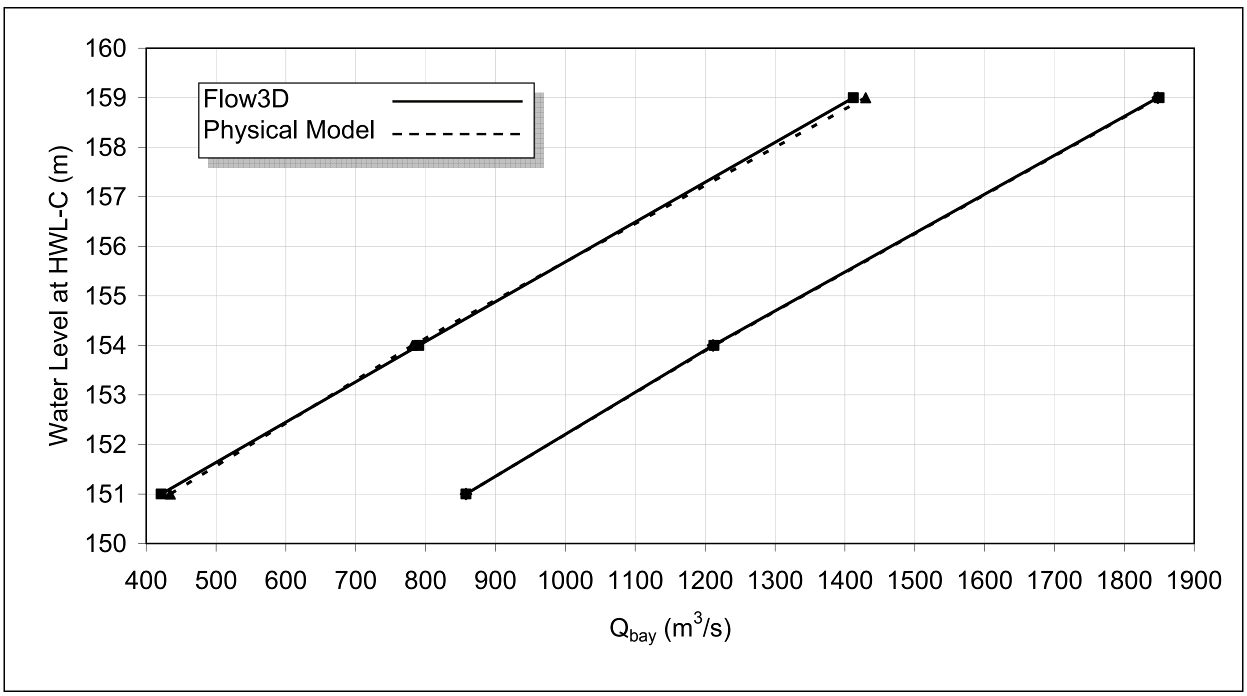

Figure 5.15: Comparison of Rating Curves for the Physical and Numerical Models during Diversion and Rollway Phases for the Fully Open Gate Condition

Results show that discharges between the two systems are in good agreement, especially for the diversion case, where a maximum error of 0.11% is observed. The error is slightly higher for the rollway case with a maximum of 3% for the lowest upstream water level which is nevertheless, within the engineering norm of 5%.

Similarly to the partial gate openings, the values of the discharge coefficients in Table 5.4 are directly related to the flowrates as given by Equation 5.9 through a set of known values, hence the discharge coefficients have the same error percentage. It can be seen that the discharge coefficients are much lower during diversion than during the rollway phase, due to a broader crest which creates positive pressures and inhibits the flow. Discharge coefficients for the rollway phase are, within the range as outlined by Smith (1995), which predicts coefficients at design head equal to 1.99, 2.08 and 2.19 for water levels at HWL-C equal to 159m, 154m and 151m respectively. The difference in the coefficient for the last water level is caused by a decrease in efficiency in the numerical and physical models, caused by a flowrate that is much lower than the design capacity of the spillway.

In order to aid both gate operators and engineers, equations of best fit of the form $q = aH^b$, derived from the rating curves, are frequently used to describe the trends of discharges and discharge coefficients. The discharge and discharge coefficient equations for the fully open gate condition during diversion are presented below:

$$Q_{F3D} = 1.53 W_{Bay} \left(z_{HWL-C} - 138.9 \right)^{1.510} \tag{5.10}$$

$$Q_{LaSalle} = 1.53 W_{bay} \left(z_{HWL-C} - 138.9 \right)^{1.512} \tag{5.11}$$

$$C_{d-F3D} = 1.534 \left(z_{HWL-C} - 138.9 \right)^{0.011} \tag{5.12}$$

$$C_{d-LaSalle} = 1.534 \left(z_{HWL-C} - 138.9 \right)^{0.011} \tag{5.13}$$

and equations during the rollway phase are:

$$Q_{F3D} = 1.93W_{bay}\left(z_{HWL-C} - 144.45\right)^{1.513} \quad (5.14)$$

$$Q_{LaSalle} = 2.04W_{bay}\left(z_{HWl-C} - 144.45\right)^{1.492} \quad (5.15)$$

$$C_{d-F3D} = 1.901\left(z_{HWL-C} - 144.45\right)^{0.017} \quad (5.16)$$

$$C_{d-LaSalle} = 2.038\left(z_{HWL-C} - 144.45\right)^{-0.008} \quad (5.17)$$

These equations, in particular those of the diversion structure, demonstrate the proximity of the two models. Variations are seen in each a,b constant for both dependent variables with large variations between the discharge and discharge coefficient equations for the rollway structure. Nevertheless, resulting calculated values for these remain in good agreement with one another.

Returning to Table 5.4, it can also be seen that decreasing upstream water levels cause a slight decrease in computational time due to less time required to reach steady-state. Similarly, rollway cases require slightly less time for similar water levels than the diversion cases. It can be concluded for these cases, that discharge, or specifically, volume flux plays a role in the stability of the model: with higher water levels and increased flow, more time is required to reach steady-state.

Figure 5.16 presents a comparison of the water profiles and pressure profiles for the diversion structure with a water level of 159m at HWL-C.

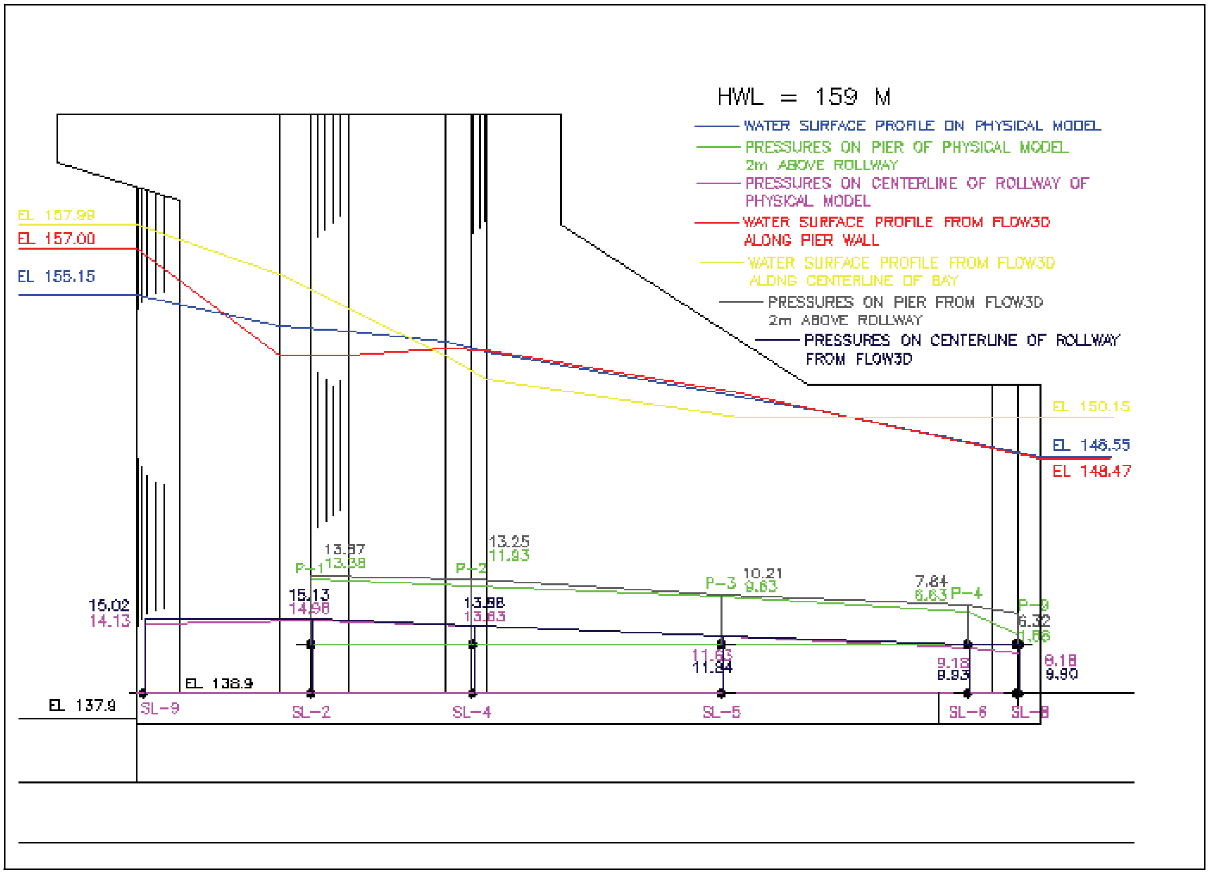

Figure 5.16: Comparison of Water Surfaces and Pressures of the Physical Model and the Numerical Model for an Upstream Water Level of 159m on the Diversion Structure

This figure is similar to the Figure 5.3 presented in the mesh refinement section and so, only the pressure profiles will be discussed since the water surface profiles have previously been addressed. Profiles were extracted from the results as close to the pier wall and centerline of the bay as possible. As was the case with previous comparisons, it was impossible to extract the data at the exact location in which the LaSalle Consulting Group obtained their measurements, since the domain of the numerical model is discretized into 1m cubes. As a result, data was extracted within 1m of the desired location in all three directions. Pressure profiles, computed through the relationship of Table 4.1 and in terms of pressure head in meters, appear to be in good agreement with one another, with the results from the numerical model, in most cases, slightly exceeding those of the physical model. A major difference is, however, seen towards the exit of the structure where measurements differ by over 5m at the pier wall, a value which is too great to be attributed to discrepancies in data extraction location.

Figures B.30 and B.31 present the water surface and pressure profiles of the diversion structure for the water levels of 154m and 151m respectively. Similar tendencies to the 159m water level are exhibited in both of these cases with slight differences being seen in the water surfaces near the downstream end of the structure. For the water level of 154m at HWL-C, water surfaces along the pier wall diverge from those of the physical model approximately 10m upstream of the exit of the structure. In fact, it is observed, that the centerline profile better matches the exit water level for this simulation. In contrast, for the water level of 151m, exit water levels, both along the wall and along the centerline are under predicted by approximately 2m in the numerical model. Nevertheless, in all three cases, water profiles extracted along the pier are in much better agreement than those extract along the centerlines. Furthermore, pressures for all three diversion simulations are similar to those measured on the physical model except at the exit of the structure, where they are over predicted.

Unfortunately, due to the lack of measured data from the physical model for the rollway phase, only the case with a head water level of 159m can be compared with the physical model. Nevertheless, Figures B.32 and B.33 present the results from Flow3D for the rollway phase with HWL-C levels of 154m and 151m respectively. Figure 5.17 presents the water surface profiles and pressure profiles for the 159m water level.

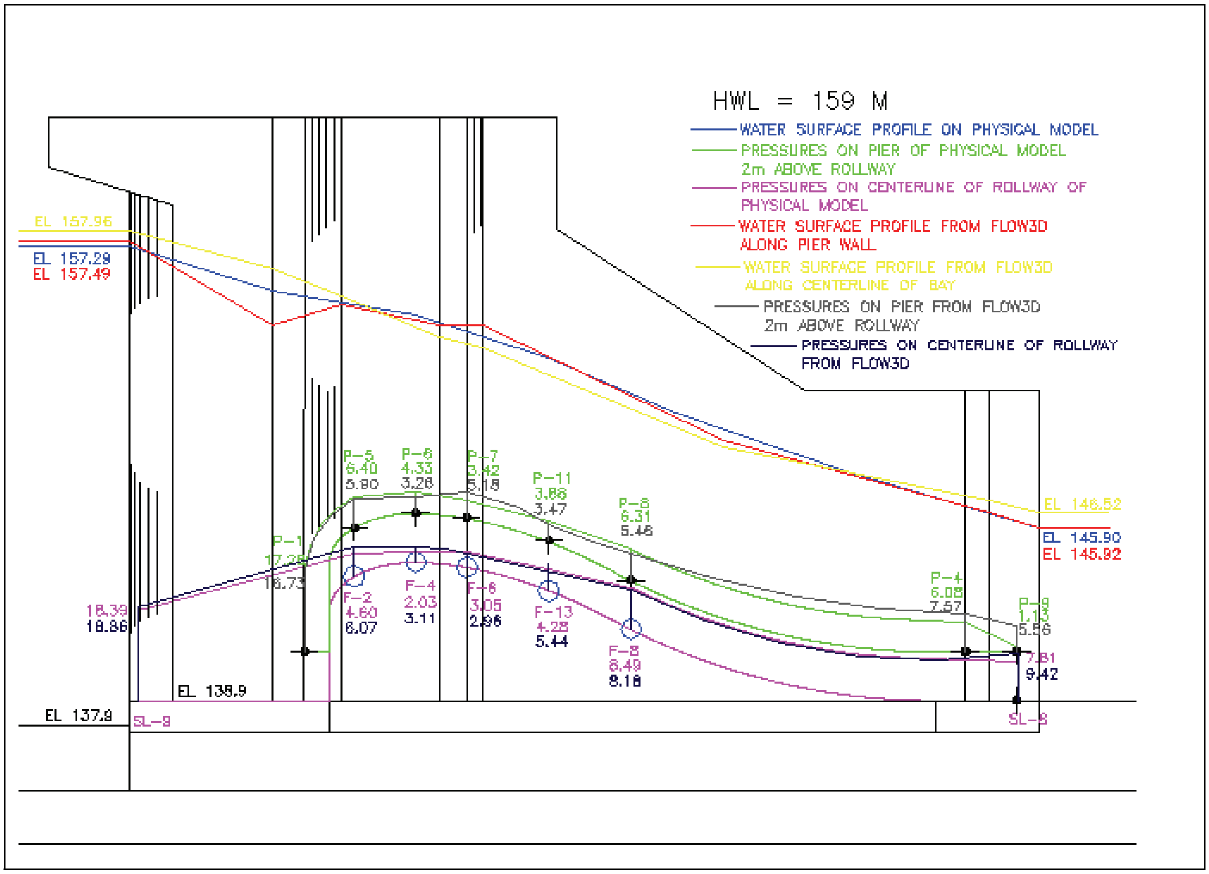

Figure 5.17: Comparison of Water Surfaces and Pressures of the Physical Model and the Numerical Model for an Upstream Water Level of 159m on the Rollway Structure

Water surface profiles exhibit, once again, the same type of behavior that was prevalent on the diversion phase. Both water levels extracted at the wall and along the centerline of the open bay are higher at the entrance of the structure than the measured results of the physical model, however, the profile along the wall seems to in much better agreement, with similar entrance and exit levels. Furthermore, after the first drop in level, just downstream of the stoplog slots, the pier wall water surface profile seems to closely follow that of the physical model.

Pressure profiles are in relatively good agreement, however, not as good as the diversion phase. Maximum differences of about 1m can be found, either in the positive or negative direction, along the length of structure, both at the wall and along the centerline of the bay except at the exit of the structure, where, similarly to the diversion phase, Flow3D largely over predicts the pressures.

Since a comparison with the physical model cannot be made for the head water levels of 154m and a 151m, a general trend can observed between the Flow3D results. Similarly to all other 3D fully open water surface profiles, centerline profiles tend to have a higher entrance elevation than that of the pier wall profiles. Furthermore, with decreasing head water levels, pressures also decrease, both along pier walls and at the centerline of the bay.

Flow3D generally predicts adequate results for the range of data that was compared. Discharges and discharge coefficients are in very good agreement with each other, differing by a maximum of approximately 3%. Furthermore, water levels at the entrance of the structure are generally higher than those on the physical model, with tailwater levels being under predicted for the smaller water levels. Pressures tend to be in good agreement with one and other, except towards the downstream end of the structure which is largely over calculated. No negative pressures were observed on either the numerical or physical models, which adequately predict that the concrete surface of the rollway or bay floor will not suffer from cavitation damage when the gate is fully open.

Chapter 6

Discussion

In the previous chapter, the results from a physical model of a diversion/spillway structure provided by the LaSalle Consulting Group were used for comparison with a numerical model within the commercially available software package Flow3D. Results were obtained in quasi-2D for gate openings of 6m, 4m, 2m and 1m as part of mesh refinement tests which were conducted in order to determine the level of refinement necessary to attain mesh independence. Furthermore, fully 3D results, encompassing the domain of the physical model, were conducted for varying upstream water levels for the uncontrolled cases (fully open gate). The following chapter discusses the results of the quasi-2D 6m gate opening, the only partial gate opening for which near mesh independence was reached, and the fully open 3D results and their agreement and relevance to the existing literature. The chapter is divided into two sections: ungated cases and gated cases.

6.1 Ungated Cases

As seen in the literature review, many studies, in one, two and three-dimensions have been performed on uncontrolled crests of ogee weirs and spillways. Although 1D models can be used to adequately predict discharge coefficients and water levels upstream and downstream of the ogee crest, such as in the case of Guercio & Magini (1998) and Khan & Steffler (1996b), these lack the details present in 2D and 3D models that are capable of calculating the locations of surface disturbances, shock waves, hydraulic jumps, velocities from several directions, etc. In other words, 1D models only represent vertically averaged results but are, nevertheless, still of some importance when no further detail is required and quickly computed results are desired.

For the fully open case, modeled in three-dimensions in Flow3D, parameters that may be directly compared to previous studies are discharges/discharge coefficients, water surface profiles and pressure profiles. Unfortunately, a direct comparison can only be made for the 159m water level at HWL-C for the rollway structure since there is no information (other than discharges and discharge coefficients) provided by the LaSalle Consulting Group for the other water levels on the same structure and since the diversion structure does not contain an ogee weir. Nevertheless, diversion results will still feature in the discussion since flow over a flat bed is less difficult to model than flow over a curved surface, where pressure distributions are significantly non-hydrostatic (Khan & Steffler 1996a).

Both Berger & Carey (1998) and Unami et al. (1999) attempted to model spillway flow in 2D in order to compare measurements from their respective physical models to the lateral water surface profiles of their respective numerical models for given discharges. Unami et al. (1999) provided additional information by plotting the mean calculated and measured water profiles. Both studies provide similar results in comparison to the physical models, and, Unami et al.'s mean profiles seem to be in excellent agreement with one another. This differs from the model in Flow3D for both the diversion and rollway cases. For the diversion case, water levels at the control structure entrance, extracted at the pier wall and at the centre of the bay, are always greater than the measured profiles from the physical model for all head water levels. These differences are as high as 2m at the wall, and 3m along the centerline of the bay, for the maximum water level at HWL-C. Furthermore, large fluctuations in water levels of up to 2m are observed further downstream before the gate slots, for results along the pier wall, for the both diversion and rollway cases. It is also observed that rollway results seem to be in much better agreement with the previously published literature, where extracted entrance and exit data appear to closely match measured results, despite water level fluctuations within the structure. These water level fluctuations are in fact caused by 3D effects, where stoplog slots and gate slots cause boundary layer separation along the walls of the pier. Therefore, if a 2D rollway simulation was conducted, it could be expected that calculated water levels within the control structure would be much smoother in appearance.

In the study conducted by Chatila & Tabbara (2004), a commercially available software package called ADINA-F was used to compare 3D water surface profiles of an ogee overflow spillway with those of a geometrically similar physical model. No piers were modeled and water surfaces were measured along the centerline of the physical model. The findings show that, although qualitative results are consistent with general flow patterns, discrepancies were found along the entire length of the spillway, with water levels being in good agreement upstream of the crest of the spillway and at the toe. ADINA-F, in all three modeled discharges, predicted water levels that were much lower than those measured on the sloping surface of the physical model. These discrepancies were mostly attributed to air entrainment effects which were not accounted for in the numerical model. This same phenomenon was observed in the study of Song & Zhou (1999) due to the use of the marker and cell method to track the free surface. In contrast, the results provided by Flow3D for the modeling of the Keeyask spillway, include the effects of air entrainment due to the use of the VOF method and therefore, despite differences at the entrance and exit of the structure for diversion, and fluctuations caused by measurements taken along the wall of the pier for both structures, computed results are in much better agreement with those measured on the physical model.

Of more importance to this thesis are the findings of Savage & Johnson (2001) who used Flow3D in both 3D and quasi-2D in order to compare ten different discharges and pressure profiles along the centerline of the crest of a single ogee overflow spillway with the measurements of a physical model. Results show that Flow3D is more accurate than analytical calculations of the U.S. Army Corps of Engineers and the U.S. Bureau of Reclamation formulae and curves. Furthermore, results were in excellent agreement with the measurements of the physical model. These results are in line with those of Olsen & Kjellesvig (1998) who studied a structure of similar geometry with a similar numerical model yet, differ slightly from the results provided in Chapter 5. Although discharges and discharge coefficients are in good agreement for the diversion and rollway cases, calculated pressures are much less accurate. Generally, for diversion, pressures are over predicted at the exit of the structure with reasonably good results being obtained upstream. The rollway case exhibits the same tendencies at the downstream end of the structure; however, pressures along the ogee weir tend to be nearly equal at some locations and fluctuate by approximately +/- 1m at others. A possible cause for the discrepancy between the two studies is the differences associated with the two modeled structures. While Savage & Johnson (2001) modeled an overflow ogee spillway, in which upstream velocities are negligible, the Keeyask spillway has a long approach channel, in which significant velocities develop. In addition, unlike the study of Savage & Johnson (2001), the Keeyask spillway also includes piers which significantly increase the amount of turbulence within the fully open bay. These pressure fluctuations are not accounted for in the K-ε closure model and rather, pressure spikes that are present on the physical model, are averaged in the numerical model in order to get a statistically stable solution. Therefore, a large discrepancy in pressures can be expected when dealing with more turbulent flows.

Flow3D appears to provide results that are in reasonably good agreement with the currently available literature. The main causes of differences are caused by the type of structure modeled. Most previous studies examined simple cases, where the spillway was represented by a vertical or sloped upstream face with a curved sloping surface, with no piers and no approach channel. The inclusion of these significantly alters flow patterns and pressures and therefore increases the complexity of the problem.

6.2 Gated Cases

The modeling of partial gate openings is important in the hydraulic engineering field since it allows the engineer to compute rating curves for various head water levels in order to better manage floods. A better management of floods allows the hydro-electric facility to produce electricity more efficiently by keeping the water in the reservoir at a constant level.

Currently, there exists very little literature on the numerical modeling of flows under gates and generally, the modeling of spillways has been confined to uncontrolled crests. Although some literature exists, these are mostly confined to 1D and 2D models since, as seen in the previous chapter, a 3D simulation of a gated spillway structure would require a large amount of time to reach steady-state due to the requirement of a much finer computational grid.

In the cases of Yost & Rao (2000) and de León-Moiarro et al. (2007), a 1D numerical model was used to calculate the upstream effects of dynamic gate maneuvers on the flow through an open channel and an irrigation canal respectively. Although gates were modeled in these two studies, no data is available downstream of the gate orifices. In contrast, Daneshmand et al. (2000) modeled 2D gravity flow through a conduit ending with a radial gate, which discharged along a highly curved surface. Results from the numerical model were compared to measurements taken from a Froude similitude physical model. Discharges and water levels appear to be in good agreement for both models however, there is no specification on where the free surface was measured on the physical model. Since the water levels of the numerical model are close to those measured on the physical model, it can be assumed that the latter was probably measured at the middle of the flume, away from the frictional effects of the model walls.

In the case of the quasi-2D numerical model within Flow3D, the water surface profiles for all four partial gate openings (6m, 4m, 2m and 1m) were plotted against the results of the physical model. The water profile of the latter case was measured along the pier walls, and therefore includes the effects of friction on the flow of water. As a result, depths are larger downstream of the gate orifice on the physical model than on the 2D numerical model which does not include the pier wall effects. This is the reason why the measured contraction coefficients are much smaller in the numerical model than on the physical model for approximately the same discharges, as was proved in Chapter 5. Even so, it is observed that the 2m and 1m gate openings in the numerical model have contraction coefficients of the order of 0.75, a value that is much larger than those of the 6m and 4m gate openings which are near 0.61, the coefficient for sharp-edged gates (Lin et al. 2002). Since flowrate is a function of the contraction coefficient, it can be assumed that with increased mesh refinement, the contraction coefficients for the two smallest gate openings should decrease as a function of the discharge.

Other discrepancies were also witnessed for the 4m, 2m and 1m gate openings. In these cases, although water surface and velocity profiles appeared to converge with each mesh refinement, for unknown reasons, discharges were observed to diverge. Further mesh refinement, although unfeasible given the available computing power, is required in order to determine if the discharges will eventually converge as they did for the 6m gate opening. These tests, although of a preliminary nature, will provide information about mesh refinement for future researchers in the field.

Flow through the partially gated bay of the spillway was observed to be highly two-dimensional in nature, despite there being slight 3D effects caused by the pier walls. As a result, fully 3D simulations may not be required for proper study of the spillway unless pressure measurements are necessary. For example, by integrating the 1 cell thick discharge of the 6m gate opening over the entire bay, a relatively good estimate of physical model discharge is obtained. The difference between the two systems is only equal to -1.4% for the minimum cell size of 0.075m. Furthermore, fully open conditions dictate the height of the piers to avoid overtopping at the downstream half of the structure, and therefore, 3D effects along these need not be modeled since the extra run up caused by the additional friction is most certainly less than the depth through the uncontrolled structure at high water levels. Nevertheless, a difficulty arises in determining what mesh sizes should be used for these calculations since none of the partial gate openings reached mesh independence. As a result, errors will be introduced into the estimates and there is no way in determining how accurate a simulation will be without validation data from a physical model. With increasing advances in computing technologies, mesh independent numerical simulation of controlled flow over a spillway should become feasible in the near future; at least at the 2D level for larger gate openings however, 3D simulations are far beyond foreseeable computing power.

Chapter 7

Conclusion

Numerical models play an increasingly important role in the design of hydraulic structures however; these often require some form of validation in order to ensure that the results are as realistic as possible. This validation is generally obtained by comparing the results of the model to the results of a physical model.

In this study, results from the 3D modeling software, Flow3D, were compared with those of a 1:50 scale sectional physical model of the Keeyask Generating Station spillway and diversion works, constructed by the LaSalle Consulting Group. The structure was constructed in a concrete channel, with 300m of approach and tailrace, modeled 3 out of the 7 bays of the prototype, separated by piers, and included a self-closing vertical gate in the operational bay while the remaining bays were blocked by Plexiglas plates. Simulations were run using a standard personal computer utilizing an Intel Core 2 Duo 2.13Ghz processor with 4Gb of memory, and the software was programmed to use the RANS approach coupled with the K-ε closure model in order to model turbulence.

Initially, mesh refinement tests were conducted for a fully open gate condition and four partial gate openings of 6m, 4m, 2m and 1m for the diversion structure with a single upstream water level. The purpose of these tests was to determine the mesh refinement required in order to obtain a mesh independent, steady-state solution. These were conducted at the 2D level in order to increase the time efficiency of the computations. It was found that this could not be done for the fully open case due to the horizontal contraction of the physical model and therefore, tests were confined to the 3D level. In contrast, the vertical contraction caused by the partial gate openings seemed to be much more important than the horizontal contraction caused by the blocked bays, and, as a result, these remained in 2D.

The trend towards mesh independence was observed by analyzing the discharges, velocity fields, velocity profiles and water surface profiles. It was assumed that these would converge to a single solution once mesh independence had been reached, which was subsequently proven by these tests. Additionally, for each simulation, the required time to reach steady-state was recorded. Only the fully open case was capable of attaining mesh independence within a reasonable time-frame and mesh refinement. Partial gate openings required much finer meshes, with the size of individual cubic cells sometimes decreasing by more than 13 times compared to those found on fully open case mesh. As a result, only the 6m gate opening was seen to converge towards mesh independence while the other gate openings diverged for unknown reasons. Further mesh refinement is required in order to verify if these will eventually converge and the reader should view the results of the 4m, 2m and 1m gate openings cautiously.

It was also found that the quasi-2D partial gate opening results, for the finer meshes that were closer to mesh independence, could be compared to the results of the physical model. Generally, discharges and discharge coefficients were found to be in good agreement with each other, with increasing error for decreasing gate orifice size due to non mesh independent solutions. For example, for the 6m gate opening, discharges and coefficients were within 2% of those found on the physical model. It was also found that, for all gate openings, upstream water levels were in good agreement with those measured on the physical model; however, downstream water levels were under predicted, since measurements were taken along the pier wall rather than along the centerline of the operational bay. Therefore, for partial gate opening cases that exhibit highly 2D flows, it could be advantageous to perform 2D simulations rather than 3D simulations.

Using the information from the mesh refinement tests, comparative simulations were conducted in order to observe differences caused by changing the turbulence closure from the standard K-ε to the RNG model at the physical model scale and by using prototype units. These were conducted in 3D for the fully open gate condition and in quasi-2D for the 6m gate opening on the diversion structure for a single upstream water level. In both cases, simulations required the same amount of real-time and results agreed with each other however, discrepancies in results between each set of comparison tests for the 6m gate opening were much higher than the fully open case, most likely due to the presence of the gate which results in a more complex flow.

Final comparative tests were conducted in 3D for the fully open gate condition for both the diversion and rollway (spillway) structures for three different water levels. Discharges, discharge coefficients, rating curves, water surface profiles and pressure profiles were compared with those of the physical model. In addition, times of computation were also documented. Results show that discharges and discharge coefficients are generally within 3% of those found on the physical model, with more accurate results being found for the diversion structure, which has a simpler flow. Additionally, water levels, particularly at the entrance of the structure, tend to be over predicted for both structures however, the rollway water levels appear to be in much better agreement than the diversion water levels which can be over predicted by up to 3m. Upstream water levels are found to better match those of the physical model for lower water levels while, for the same conditions, downstream water levels are under predicted. Pressure profiles for both structures are in good agreement for all three water levels, with better results for diversion, however, in both cases, pressures near the exit of the structure are grossly over predicted. Given the pressures observed on the numerical and physical models, cavitation will not occur along the rollway or the bay floor of the structures.

It may be concluded, from the range of tests that were conducted, that Flow3D adequately models the fully open case, but does not properly model the partial gate openings, which in most cases exhibit diverging discharges and require too great a computational time with increased mesh refinement. Results also indicate that complex 3D flow is not always adequately modeled, particularly when comparing water surface profiles for the diversion structure to those of the physical model. Furthermore, simulations can be run with RNG or K-ε closure models or scaled or prototype dimensions without any major differences. This study has shown that Flow3D is sufficiently advanced so as to model the general characteristics of the flow through the ungated structures while a much more powerful computer is necessary for partial gate openings. It should be noted that these findings are valid for this particular case, and should be used as a guide when studying other designs.

References

Anastasiou, K., Chan, C.T. (1997) Solution of 2D Shallow Water Equations using Finite Volume Method on Unstructured Triangular Meshes. Int. J. Numer. Methods Fluids 23. 1225-1245

Berger, R.C., Carey, G.F. (1998) Free-Surface Flow over Curved Surfaces Part II: Computational Model. Int. J. Numer. Methods Fluids 28. 201-213

Berger, R.C., Stockstill, R. (1993) A 2D Numerical Model for High Velocity Channels. Hydraulic Engineering 93, Proc., 1993 Nat. Hydr. Conf., New York. 1085-1090

Boes, R.M., Hager, W.H. (2003a) Hydraulic Design of Stepped Spillways. J. Hydr. Engrg. 129(9). 671-679

Boes, R.M., Hager, W.H. (2003b) Two-Phase Characteristics of Stepped Spillways. J. Hydr. Engrg. 129(9). 661-670

Bureau of Reclamation (1958) Hydraulic Laboratory Practice. Engineering Monographs No. 18. U.S. Government Printing Office.

Bureau of Reclamation (1974) Design of Small Dams. U.S. Government Printing Office.

Causon, D.M., Mingham, C.G., Ingram, D.M. (1999) Advances in Calculation methods for Supercritical Flow in Spillway Channels. J. Hydr. Engrg. 125(10). 1039-1050

Chanson, H., Gonzalez, C.A. (2005) Physical Modeling and Scale Effects of Air-Water Flows on Stepped Spillways. J. Zhejiang University 6(3). 243-250

Chatila, J., Tabbara, M. (2004) Computational Modeling of Flow over an Ogee Spillway. Computers and Structures 82. 1805-1812

Chen, C.J., Bernatz, R., Carlson, K.D., Lin, W. (2000) Finite Analytic Method in Flows and Heat Transfer. Taylor & Francis.

Chen, Q., Dai, G., Liu, H. (2002) Volume of Fluid Model for Turbulence Numerical Simulation of Stepped Spillway Overflow. J. Hydr. Engrg. 128(7). 683-688

Christodoulou, G.C. (1993) Energy Dissipation of Stepped Spillways. J. Hydr. Engrg. 199(5). 644-650

Daneshmand, F., Sharan, S.K., Kadivar, M.H. (2000) Finite-Element Analysis of Double-Free-Surface Flow through Slit in Dam. J. Engrg. Mech. 126(5). 515-522

Date, A.W. (2005) Introduction to Computational Fluid Dynamics. Cambridge University Press.

De León-Moiarro, B., Prado-Hernández, J.V., Verdier, J., Fuentez-Ruiz, C. (2007) Numerical Simulation of Control Structure Movement in Irrigation Canals. Agroncienca 41. 75-86

Drikakis, D. (2003) Advances in Turbulent Flow Computations using High-Resolution Meth. Prog. Aerospace Sci. 39(6-7). Elsevier Ltd. 406-408

Ferziger, J.H., Perić, M. (2002) Computational Methods for Fluid Dynamics. Springer-Verlag.

Flow Science Inc. (2005) Flow3D User's Manual Version 9.0

Gatski, T.B. (2004) Constitutive Equations for Turbubulent Flows. Theoretical and Computational Fluid Dynamics 18. Springer-Verlag. 345-347

Guercio, R., Magini, R. (1998) Modeling Side Channel Spillways. Hydropower & Dams 4. 60-63

Guo, Y., Wen, X., Wu, C., Fang, D. (1998) Numerical Modelling of Spillway Flow with Free Drop and Initially Unknown Discharge. J. Hydr. Res. 36(5). 785-801

Hager, W.H. (1985) Equations for Moderately Curved Open Channel Flow. J. Hydr. Engrg 111(3). 541-546

Hager, W.H. (1989) Supercritical Flow in Channel Junctions. J. Hydr. Engrg 115(5). 595-616

Hager, W.H., Hutter, K. (1984) Approximate Treatment of Plane Channel Flow. Acta Mechanica 51. 31-48

Hanjalić, K. (1970) Two Dimensional Assymetrical Turbulent Flow in Ducts. PhD Thesis, University of London.

Harlow, F.H., Nakayama, P.I. (1967) Turbulence Transport Equations. Phys. Fluids 10(11). 2323-2332

Harlow, F.H., Welsh, J.E. (1965) Numerical Calculation of Time Dependant Viscous Incompressible Flow with Free Surface. Phys. Fluids 8(1). 2182-2189

Henderson, F.M. (1966) <u>Open Channel Flow</u>. Prentice-Hall Inc.

Henderson, F.M., Tierney, D.G. (1963) Flow at the Toe of a Spillway, II – the Solid Toe Spillway. La Houille Blanche 18(1). 42-50

Hirt, C.W., Nicholls, B.D. (1981) Volume of Fluid (VOF) Method for Dynamics of Free Boundaries. J. Comp. Physics. 39(1). 201-221

Hirt, C.W., Sicilian, J.M. (1985) A Porosity Technique for the Definition of Obstacles in Rectangular Cell Meshes. Proc. 4th Int. Conf. Ship Hydro. Washington D.C. 1-19

Ippen, A., Dawson, J. (1951) Design of Channel Contractions: High Velocity Flow in Open Channels (symposium). Trans. ACSE, 116, 326-346

Jaw S.Y., Chen, C.J. (1991) On the Determination of Turbulence Model Coefficients. Symp. Adv. Appl. Comp. Fluid Dyn., Winter Annual Meeting. ASCE.

Jaw S.Y., Chen, C.J. (1998) Present Status of Second-Order Closure Turbulence Models. I: Overview. J. Engrg. Mech. 124(5). ASCE. 485-487

Jones, W.P., Launder, B.E. (1972) The Prediction of Laminarization with a Two-Equation Model of Turbulence. Int. J. Heat Mass Trans. 15, 301-314.

Khan, A.A., Steffler, P.M. (1996a) Vertically Averaged and Moment Equations Model for Flow over Curved Beds. J. Hydr. Engrg. 122(1). 3-9

Khan, A.A., Steffler, P.M. (1996b) Modeling Overfalls Using Vertically Averaged and Moment Equations. J. Hydr. Engrg. 122(7). 397-402

Kjellesvig, H.M. (1996) Numerical Modelling of Flow over a Spillway. Hydroinformatics 96.

Kobus, H. (1984) Local Air Entrainment and Detrainment. Proc. from the Symp. on Scale Effects in Modelling Hydr. Structures. H. Kobus 4(10). 1-10

Kvincinsky, S., Longatte, F., Kueny, J.-L., Avellan, F. (1999) Free Surface Flows: Experimental Validation of Volume of Fluid (VOF) Method in the Plane Wall Case. ASME. 1-8

Laible, J.P., Lillys, T.P. (1997) A Filtered Solution of the Primitive Shallow-Water Equations. Adv. In Water Res. 20(1). 23-25

LaSalle Consulting Group (2005) Keeyask Generating Station Stage IV: Sectional Model Study, Final Report R.1584

Launder, B.E., Morse, A., Rodi, W., Spalding D.B. (1972) A Comparison of Performance of Six Turbulence Models. NASA Conf. on Free Shear Flows, Nat. Aeronautics Space Admin., Washington D.C.

Launder, B.E., Spalding, D.B. (1974) The Numerical Computation of Turbulent Flows. Comp. Meth. Appl. Mech. and Engrg. 3. 269-289

Lesieur, M., Métais, O. (1996) New trends in Large-Eddy Simulations of Turbulence. Ann. Rev. Fluid Mech. 28. 45-48

Lewin, J. (2001) Hydraulic Gates and Valves. Thomas Telford Ltd.

Lin, C.H., Yen, J.F., Tsai, C.T. (2002) Influence of Sluice Gate Contraction Coefficient on Distinguishing Condition. J. Irr. Drg. Engrg. 128(4). 249-252

Lumley, J.L. (1983) Turbulence Modelling. J. Appl. Math. 50, 1097-1103

MacDonald, I., Baines, M.J., Nichols, N.K., Samuels, P.G. (1997) Analytic Benchmark Solutions for Open Channel Flows. J. Hydr. Engrg. 123(11). 1041-1045

Matthew, G.D. (1991) Higher Order One-Dimensional Equations of Potential Flow in Open Channels. Proc., Institution of Civil Engineers, London, England 2(91). 187-201

Montes, J.S. (1994) Potential-Flow Solution for 2D Transition from Mild to Steep Slope. J. Hydr. Engrg., ASCE, 1(5), 601-621

Muralidhar, K., Biswas, G. (2005) Advanced Engineering Fluid Mechanics. Alpha Science International.

Ng, N.H., Spalding, D.B. (1972) Some Applications of a Model of Turbulence to Boundary Layers near a Wall. Phys. Fluids 15. 20

Olsen, N.R.B., Kjellesvig, H.M. (1998) Three-Dimensional Numerical Flow Modelling for Estimation of Spillway Capacity. J. Hydr. Res. 36(5). 775-784

Petankar, S.V. (1980) Numerical Heat Transfer and Fluid Flow. Taylor & Francis.

Potter, M.C., Wiggert, D.C., Hondzo, M, Shih, T.I.-P. (2002) Mechanics of Fluids. Brooks/Cole.

Reinauer, R., Hager, W.H. (1998) Supercritical Flow in Chute Contraction. J. Hydr. Engrg. 124(1) 55-64

Rodi, W., Spalding, D.B. (1970) A Two-Parameter Model of Turbulence and its Application to Free Jets. Warme-und Stoffubertragung 3(2). 85-95

Saffman, P.G. (1970) A Model for Inhomogeneous Turbulent Flow. Proc., Royal Society, London A317. 417-433

Savage, B.M., Johnson, M.C. (2001) Flow over Ogee Spillway: Physical and Numerical Model Case Study. J. Hydr. Engrg. 127(8). 640-649

Smith, C.D. (1995) Hydraulic Structures. University of Saskatchewan Printing Services.

Song, C.C.S., Zhou, F. (1999) Simulation of Free Surface Flow over Spillway. J. Hydr. Engrg. 125(9). 959-967

Spalding, D.B. (1982) The Vorticity-Fluctuations (kω) Model of Turbulence. Early Papers' Imperial College. CFDW Rep. CFD 82/17, Imperial College London.

Steffler, P.M., Jin, Y. (1993) Depth Averaged and Moment Equations for Moderately Shallow Flow. J. Hydr. Res. 31(1). 5-17

Strelkoff, T.S., Moayeri, M.S. (1970) Pattern of Potential Flow in a Free Overfall. J. Hydr. Div. 96(4). 879-901

Tabbara, M., Chatila, J., Awwad, R. (2005) Computational Simulation of Flow over Stepped Spillways. Comp. Structures 83. 2215-2224

Taruya, H., Ishino, S., Okushima, S., Kato, T. (1986) Hydraulic Model Study of the Spillway of Goi Dam. Tech. Rep. Nat. Res. Inst. Agri. Engrg. Japan, 172, HE-5, 33-46

Unami, K., Kawachi, T., Munit Babar, M., Itagaki, H. (1999) Two-Dimensional Numerical Model of Spillway Flow. J. Hydr. Engrg. 125(4). 369-375

U.S. Army Corps of Engineers (1995) Hydraulic Design of Spillways. ASCE.

Vischer D.L., Hager, W.H. (1998) Dam Hydraulics. John Wiley & Sons Inc.

Warsi, Z.U.A. (2006) Fluid Dynamics: Theoretical and Computational Approaches. CRC press.

Webber, N.B. (1965) Fluid Mechanics for Civil Engineers. William Glowes and Sons Ltd.

Wei, C.Y., De Fazio, F.G. (1982) Simulation of Free Jet Trajectories for Design of Aeration Devices on Hydraulic Structures. In Finite Elements in Water Resources: Proc. 4th Int. Conf., Hanover, Germany, June 1982. 17/45-17/55

Yakhot, V., Orszag S.A. (1986) Renormalization Group Analysis of Turbulence. I. Basic Theory. J. Scientific Computing 1(1). 3-51

Yan, J., Mockett, C., Thiele, F. (2005) Investigation of Alternative Length Scale Substitutions in Detached-Eddy Simulation. Flow, Turbulence and Combustion 74. 85-102

Yen, B.C. (1973) Open Channel Flow Equations Revisited. J. Engrg. Mech. Div. 99(5). 979-1009

Yen, B.C., Wenzel, H.G. (1970) Dynamic Equations for Steady Spatially Varied Flows. Proc. ASCE 96.

Yost, S.A., Rao, P. (2000) A Multiple Grid Algorithm for One-Dimensional Transient Open Channel Flows. Adv. Wat. Res. 75. 645-651

Zarrati, A.R., Jin, Y.-C., Shanehsaz-zadah, A., Ahadi, F. (2004) Potential Flow Solution for a Free Surface Flow Past a Sudden Slope Change. Can. J. Civ. Engr. 31. 553-560

Appendix A

Additional Geometry

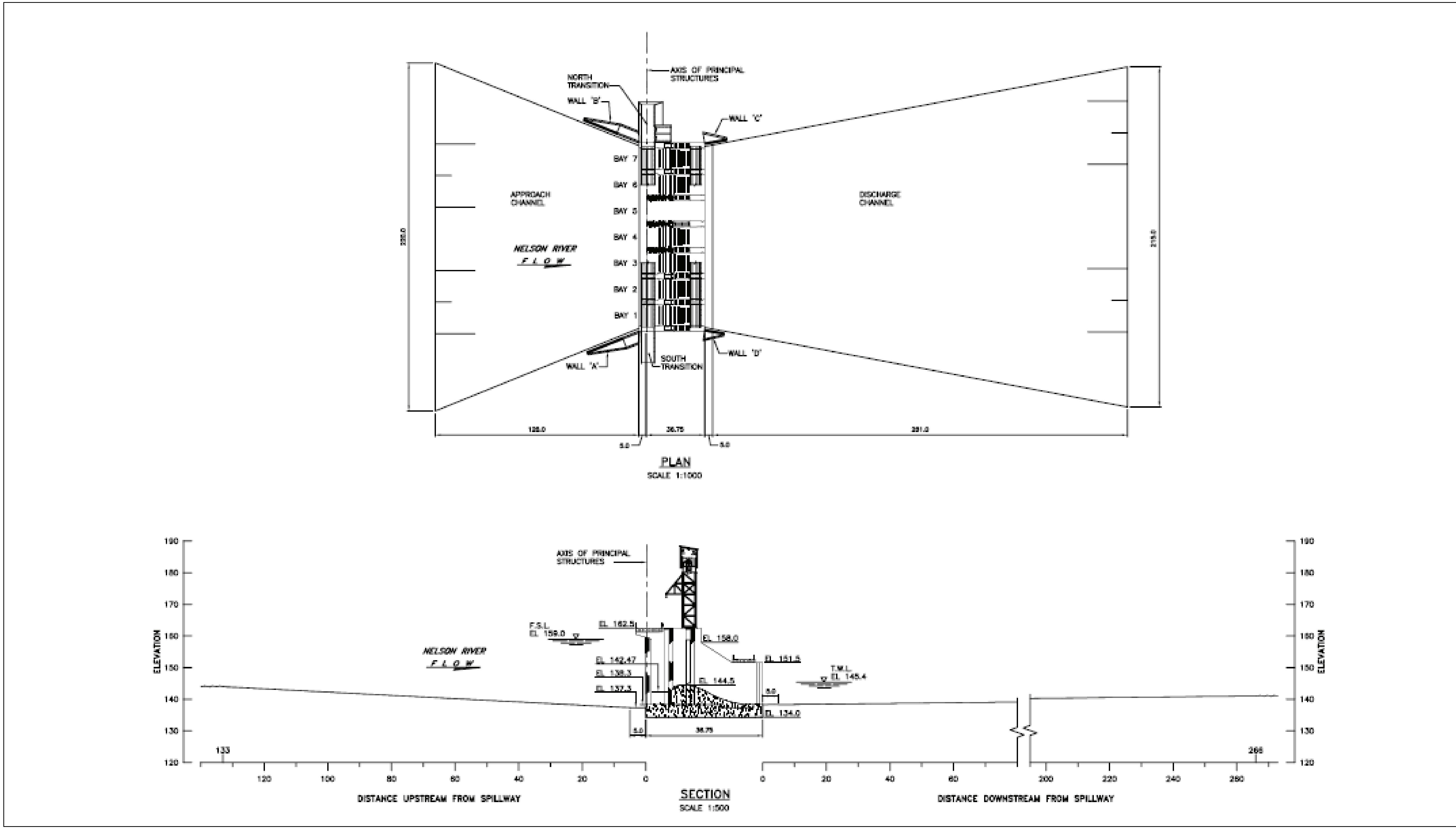

Figure A.1: Spillway Design for the Keeyask Generation Station (LaSalle Consulting Group 2005)

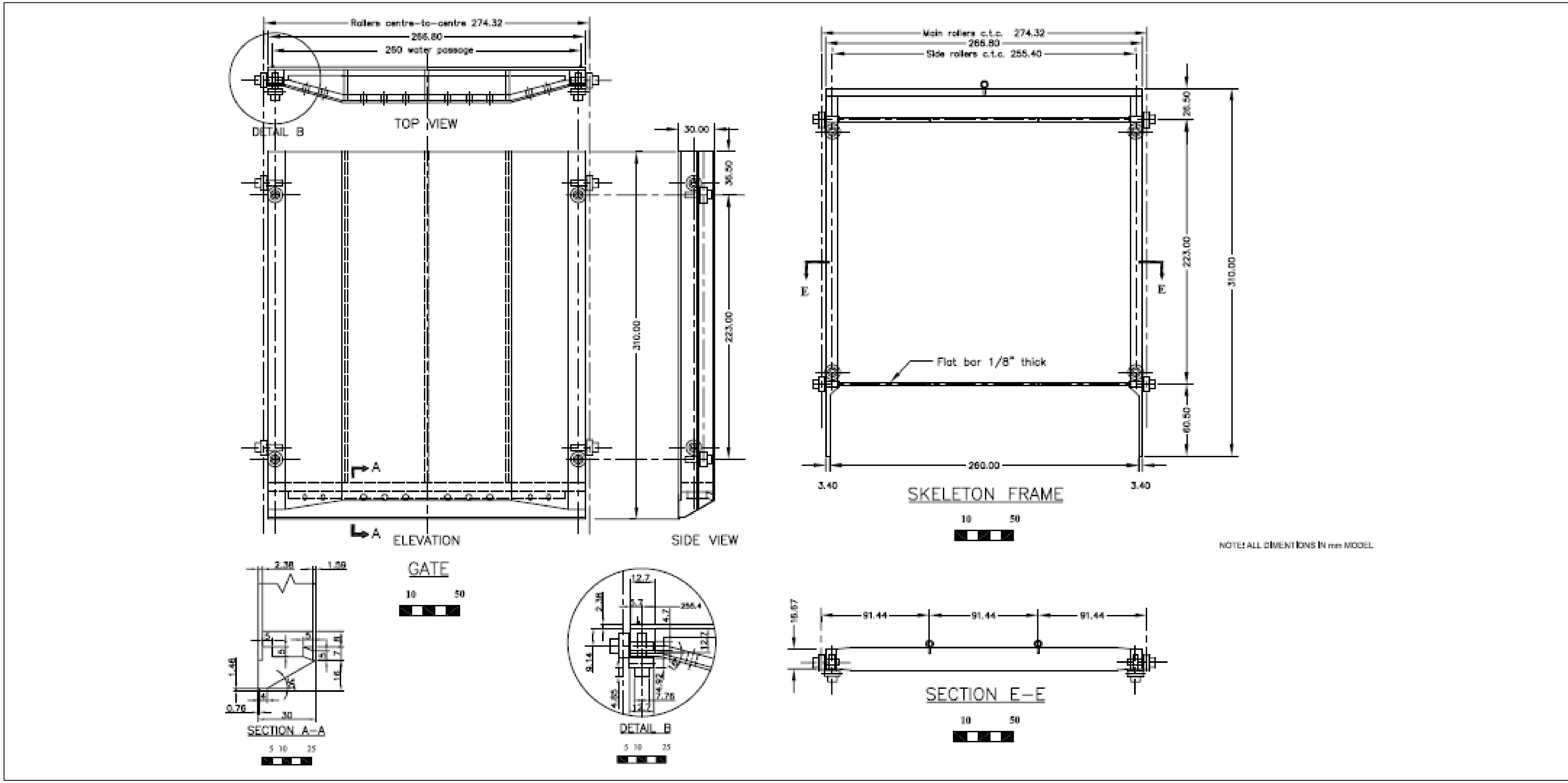

Figure A.2: Gate Geometry in Model Dimensions (LaSalle Consulting Group 2005)

Appendix B

Additional Results

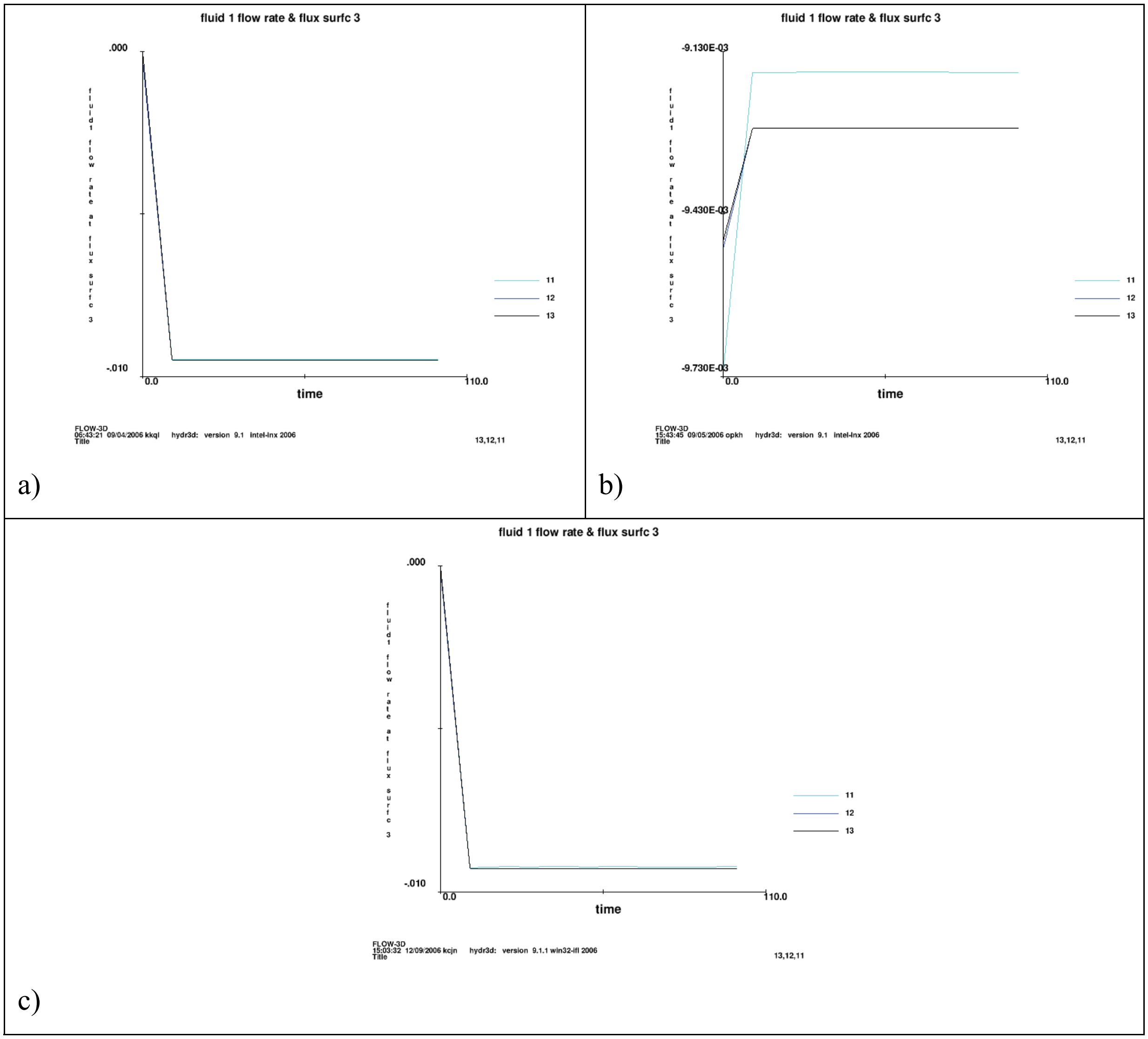

Figure B.1: Discharge vs. Time Curves for the quasi-2D Fully Open Case on the Diversion Structure for minimum cell sizes of a) 2m, b) 1m, c) 0.75m

N.B. By comparison of the three graphs, it is interesting to note that all three yield the same discharge but differ only in shape. This dissimilarity is due to the use of different initial conditions. For cases a) and c), a cold start approach was used, i.e. the simulation began with a discharge of 0 by using the coarse mesh initial conditions described in Section 4.2.3. In the case of the simulation with a minimum cell size of 0.75m, the solution of the coarser of the two other simulations was used as the initial condition obtaining essentially a “zoomed in” version of the two other graphs.

Each individual baffle is denoted by a double digit indicator. The first digit identifies the fluid whose volume flux the baffle is calculating over the simulation period, i.e. the period equivalent to a physical model running in real time. Since this study uses the original form of the VOF method, there is only one fluid being modeled which was assigned to Fluid 1 with the properties of water at 20ºC. The second digit identifies the location of the baffle where the value 1 represents the baffle located at y = -30, the value 2 represents the baffle located at y = 30 and the value 3 represents the baffle located at y = 100. Thus, the curve associated with the double digit indicator 12 is the baffle calculating the flowrate of Fluid 1 at location 2, or y =30.

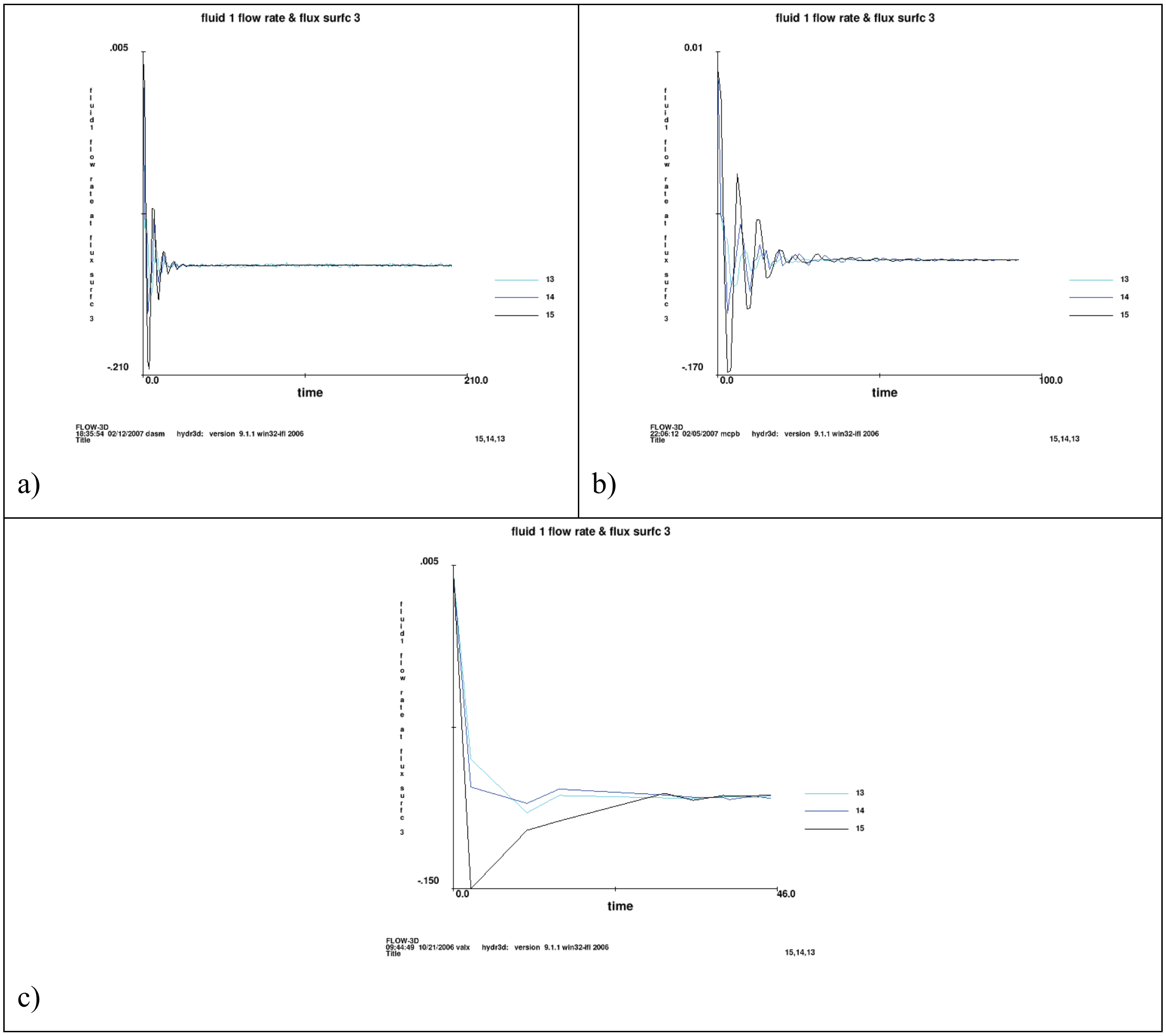

Figure B.2: Discharge vs. Time Curves for the 3D Fully Open Case on the Diversion Structure for minimum cell sizes of a) 2m, b) 1m, c) 0.75m

N.B. By observing the figure provided above, it is interesting to note that all three graphs are dissimilar in appearance. This is due to the use of different data recording techniques. Case c) is much simpler in appearance than cases a) and b) because the interval of time between each data recording, where results were saved to file, was increased for the latter. Therefore, the two first graphs have more recorded information, which allows the viewing of more fluctuations that are masked by the comparatively smoother graph of case c). Despite these fluctuations that are present at the end of the calculation, the solution remains steady as all global parameters including the discharge fluctuate by less than a fraction of a percentage point. Similar differences in other figures are present for the same reasons.

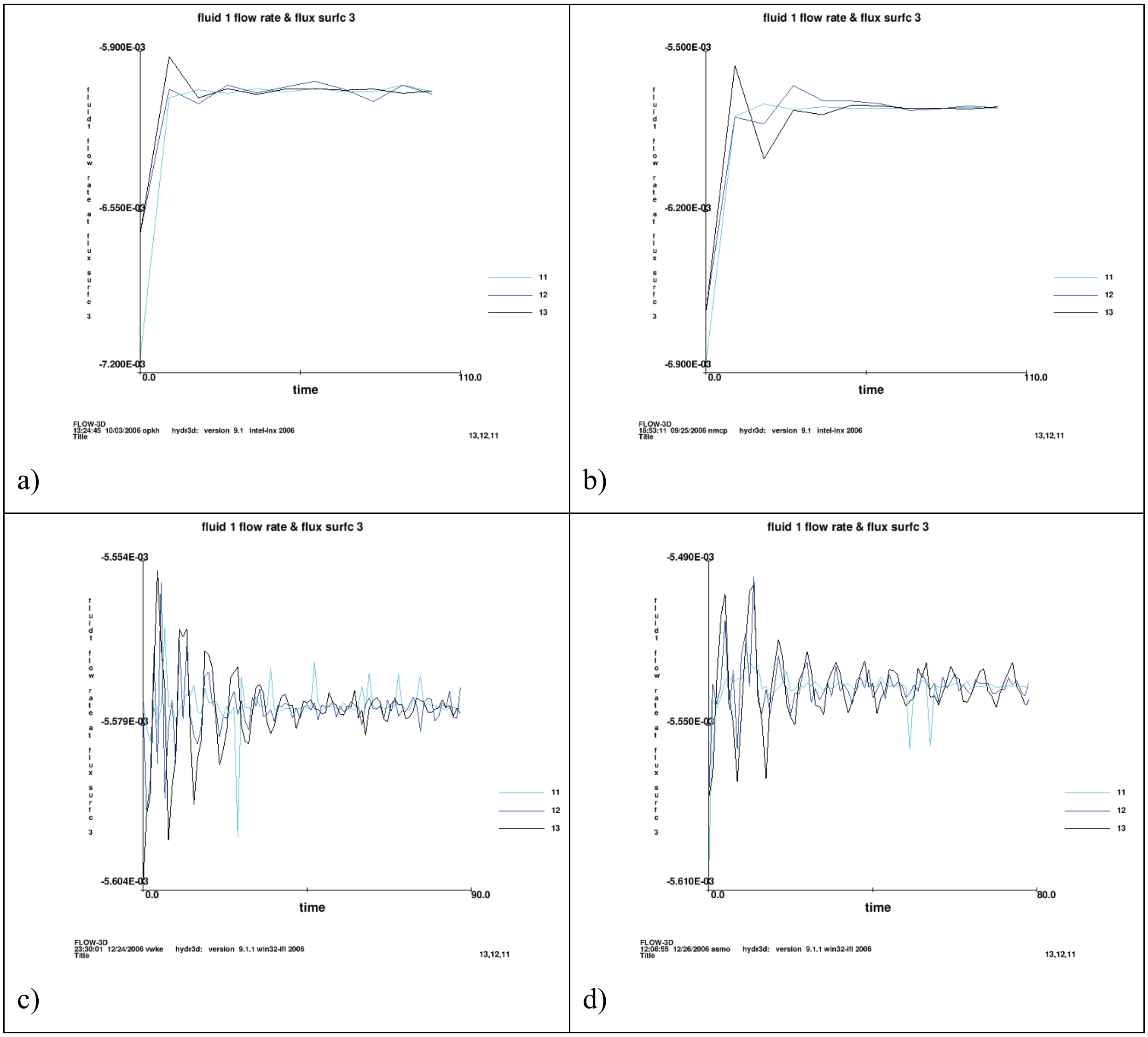

Figure B.3: Discharge vs. Time Curves for the Quasi-2D 6m Gate Opening on the Diversion Structure for minimum cell sizes of a) 0.4m, b) 0.3m, c) 0.15m, d) 0.075m

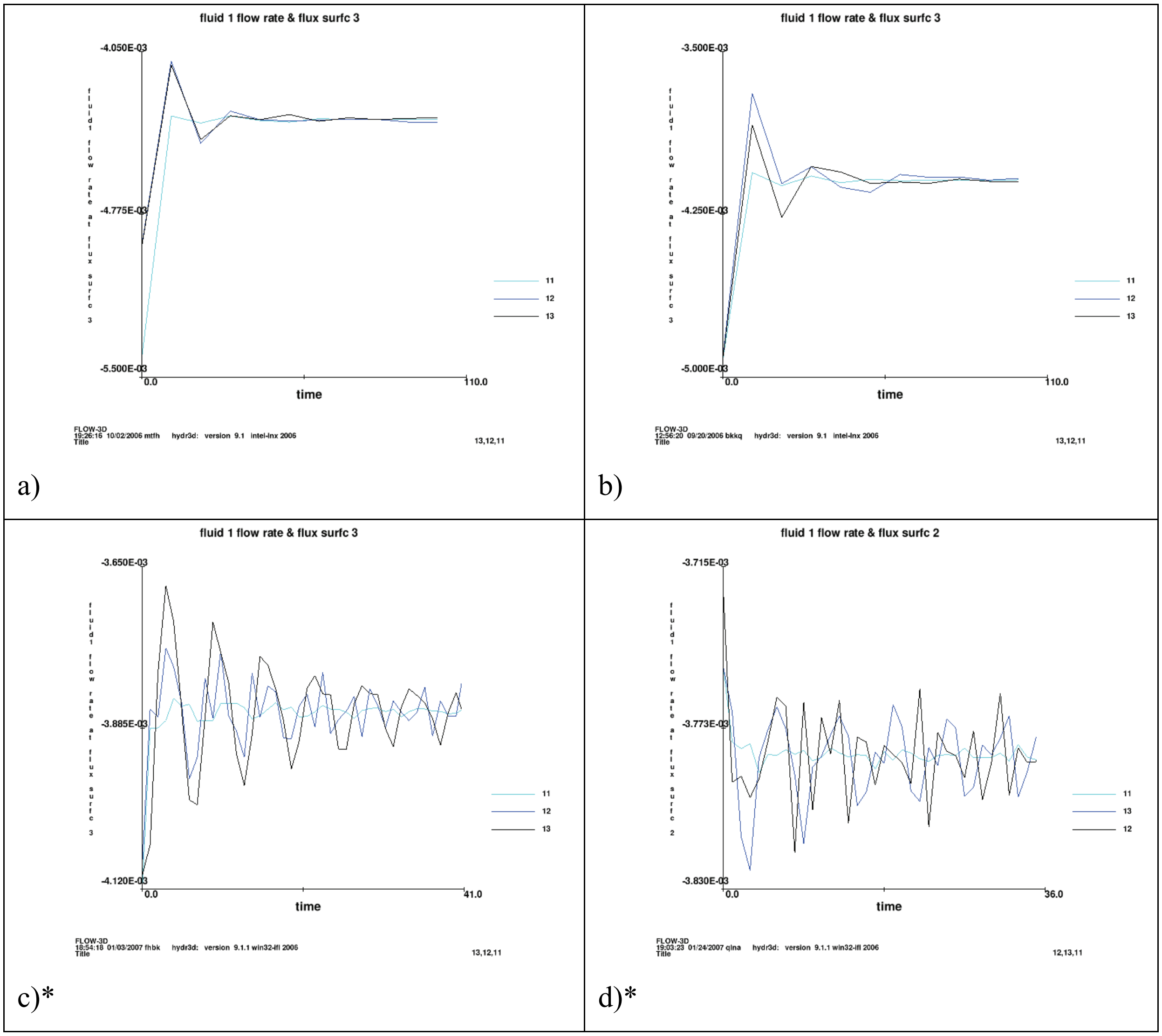

Figure B.4: Discharge vs. Time Curves for the Quasi-2D 4m Gate Opening on the Diversion Structure for minimum cell sizes of a) 0.3m, b) 0.15m, c) 0.075m, d) 0.05m

*simulations were restarted due to power failures and therefore, the x axis does not reflect the full amount of time of the simulations.

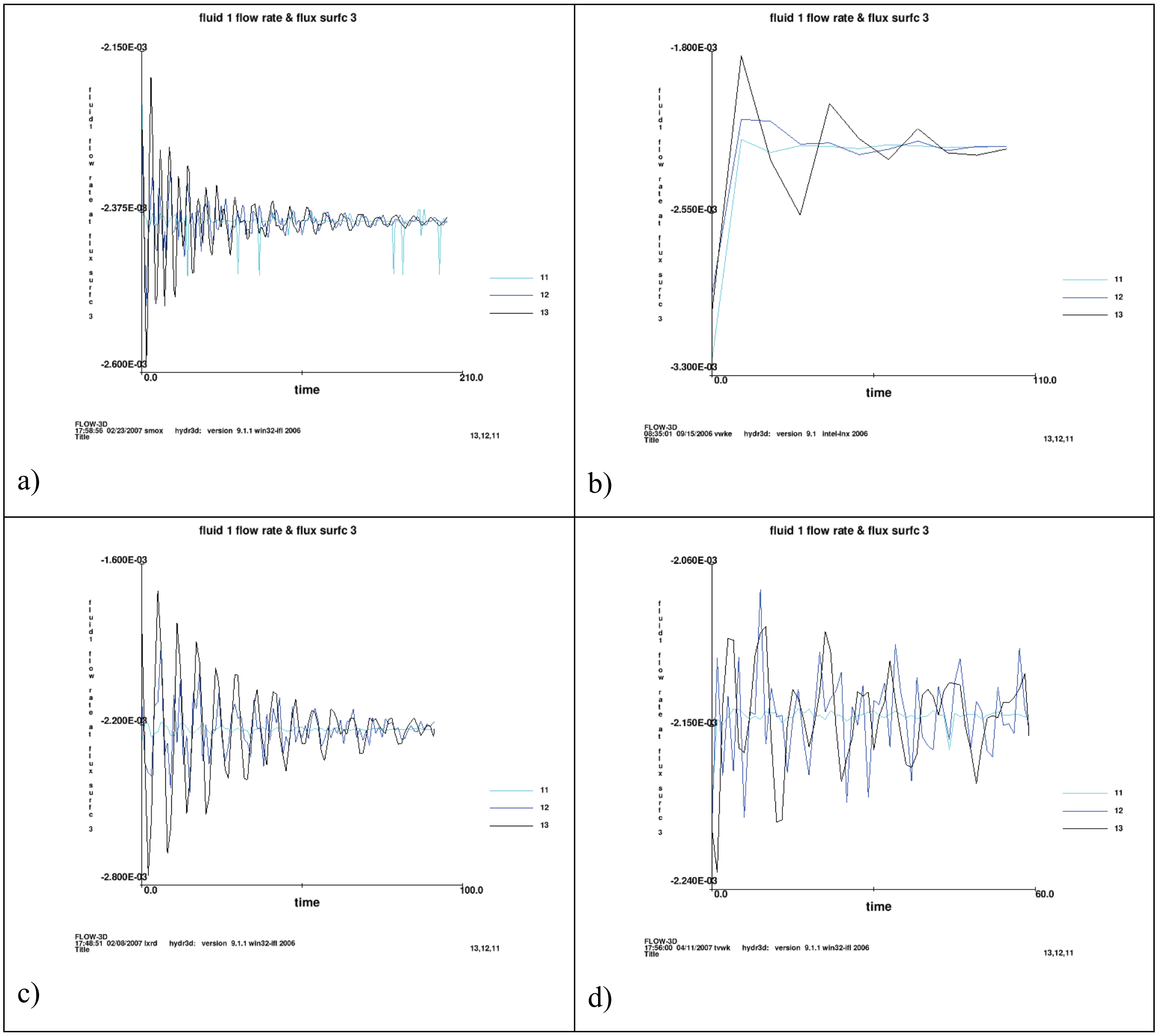

Figure B.5: Discharge vs. Time Curves for the Quasi-2D 2m Gate Opening on the Diversion Structure for minimum cell sizes of a) 0.3m, b) 0.15m, c) 0.1m, d) 0.075m

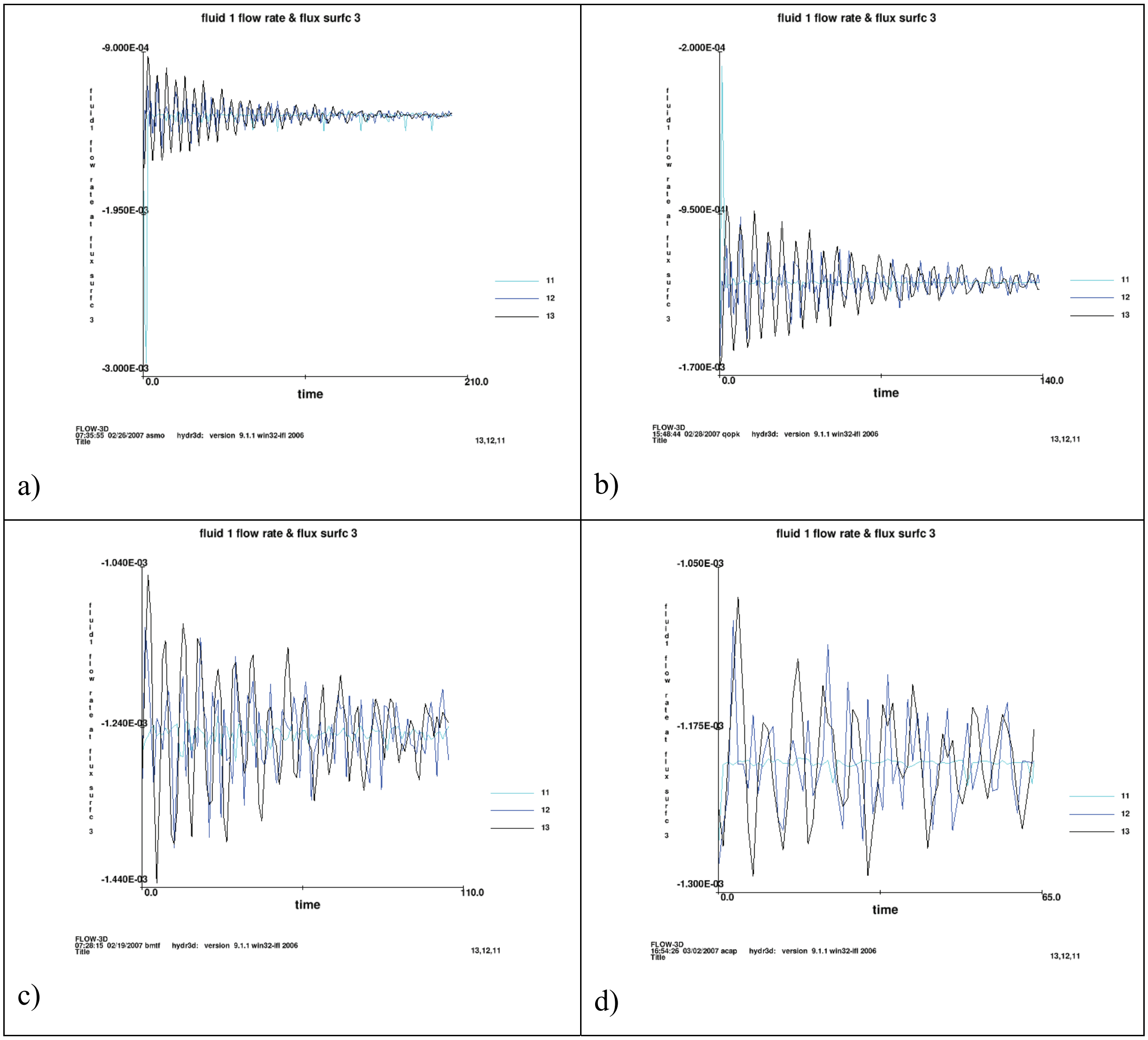

Figure B.6: Discharge vs. Time Curves for the Quasi-2D 1m Gate Opening on the Diversion Structure for minimum cell sizes of a) 0.3m, b) 0.15m, c) 0.1m, d) 0.075m

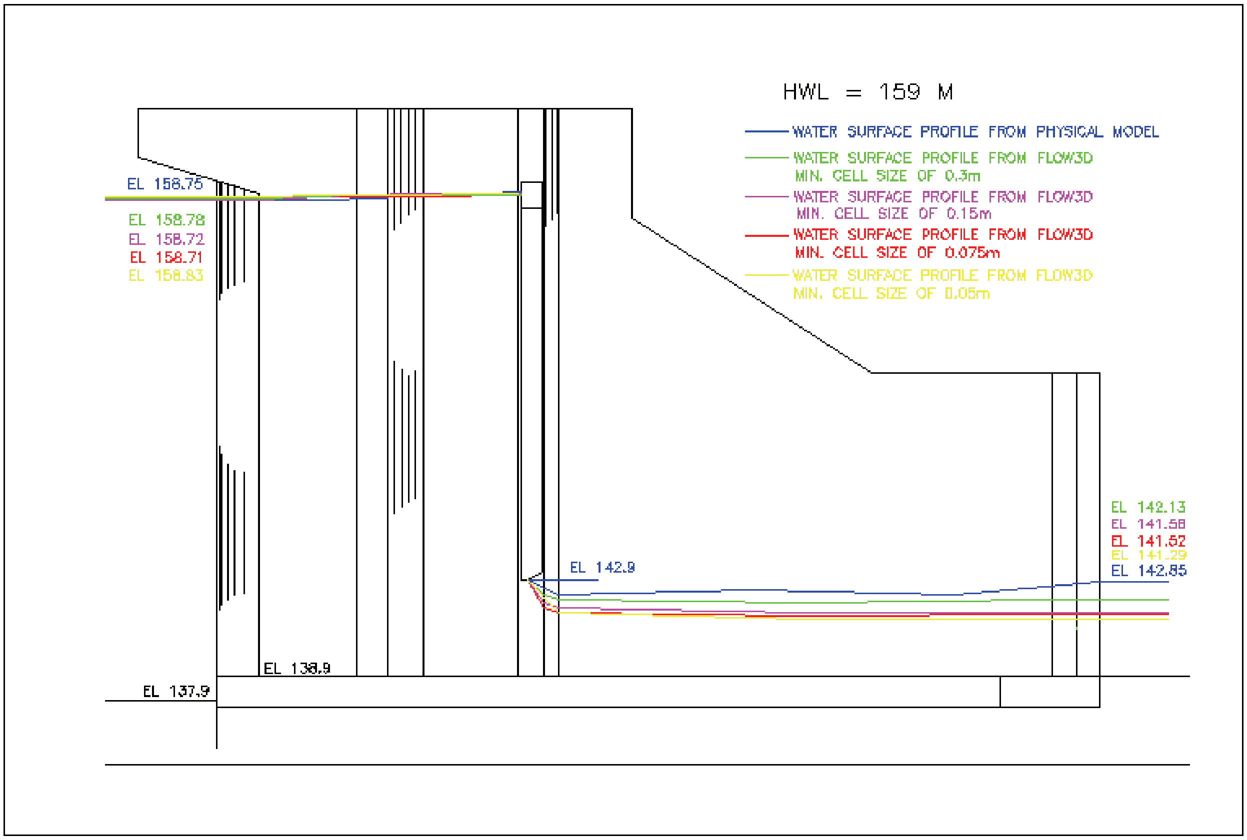

Figure B.7: Comparison of Water Surface Profiles with increased Mesh Refinement for the quasi-2D 4m Gate Opening Diversion Case

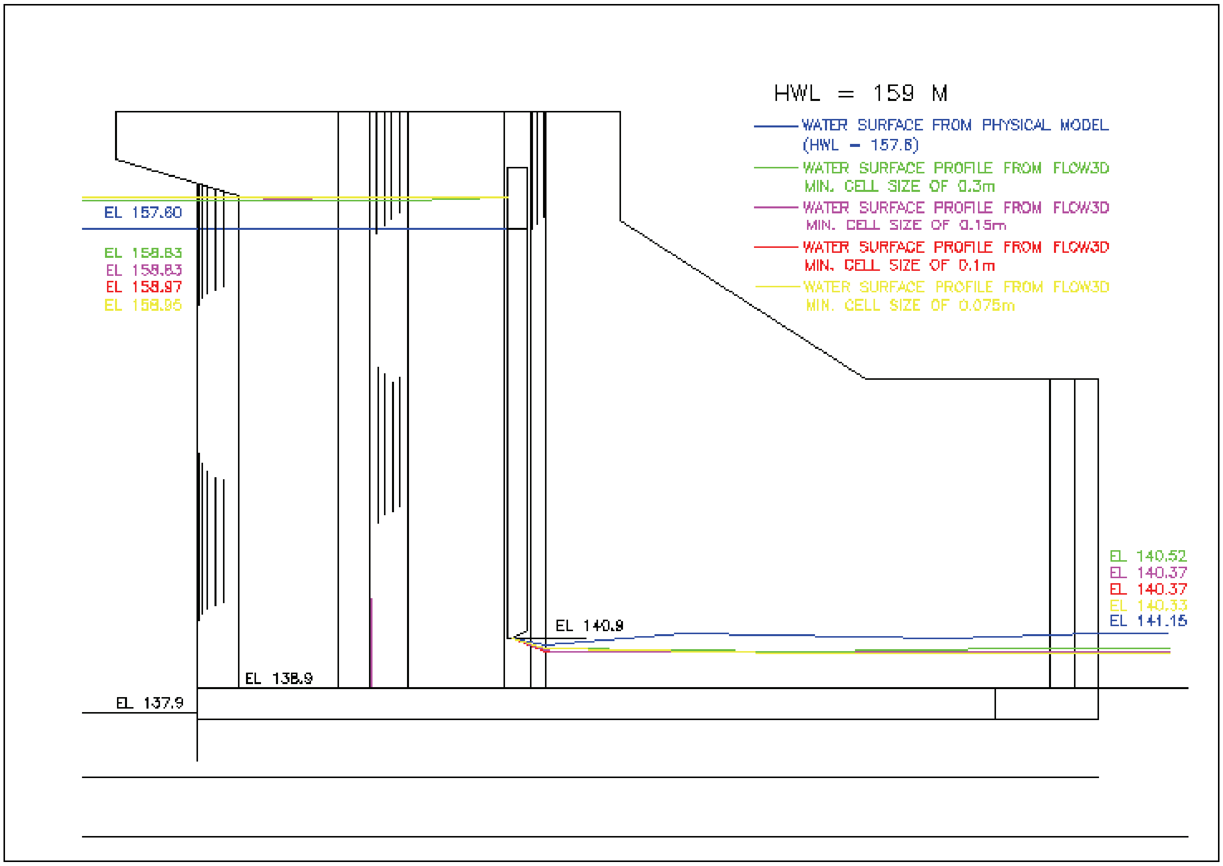

Figure B.8: Comparison of Water Surface Profiles with increased Mesh Refinement for the quasi-2D 2m Gate Opening Diversion Case

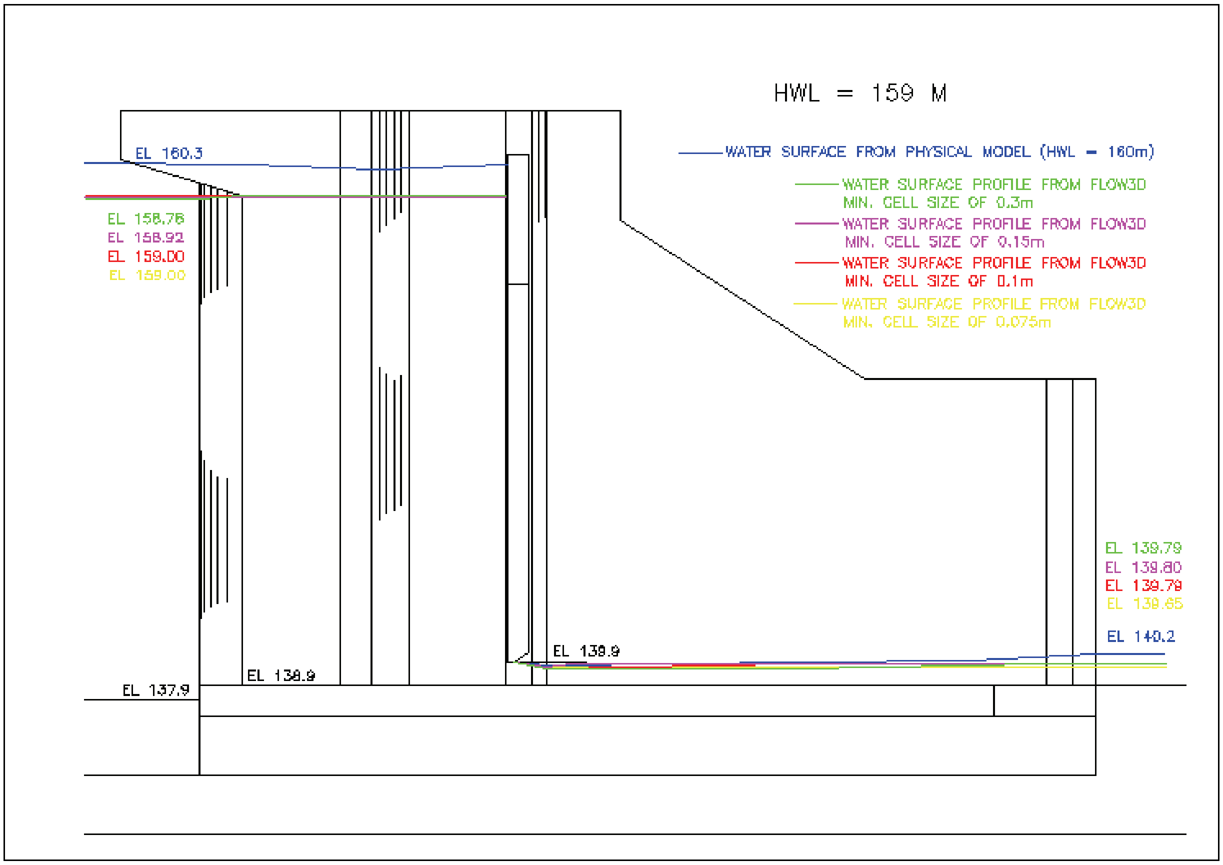

Figure B.9: Comparison of Water Surface Profiles with increased Mesh Refinement for the quasi-2D 1m Gate Opening Diversion Case

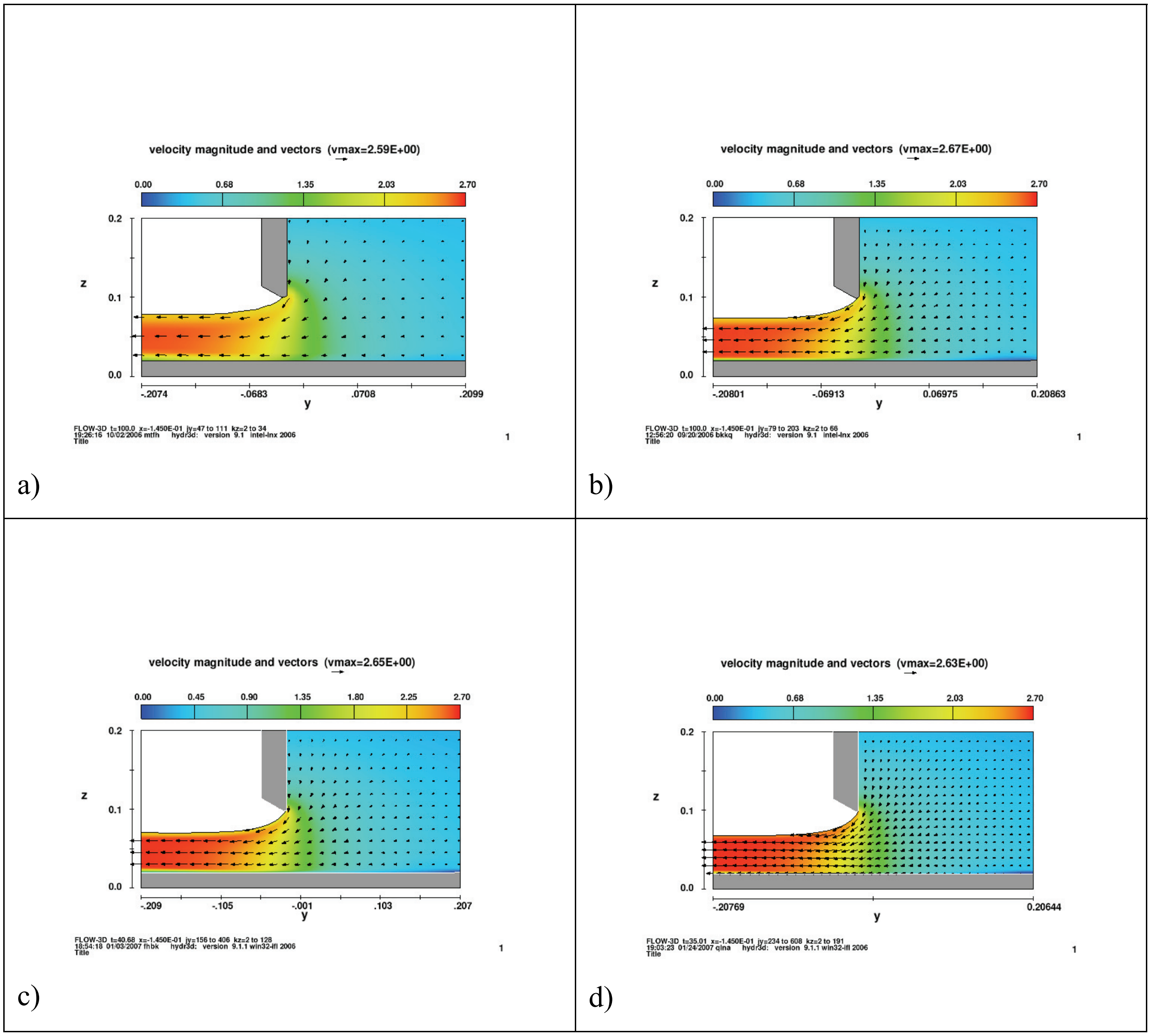

Figure B.10: Velocity Profiles for the quasi-2D 4m Gate Opening on the Diversion Structure for minimum cell sizes of a) 0.3m, b) 0.15m, c) 0.075m, d) 0.05m

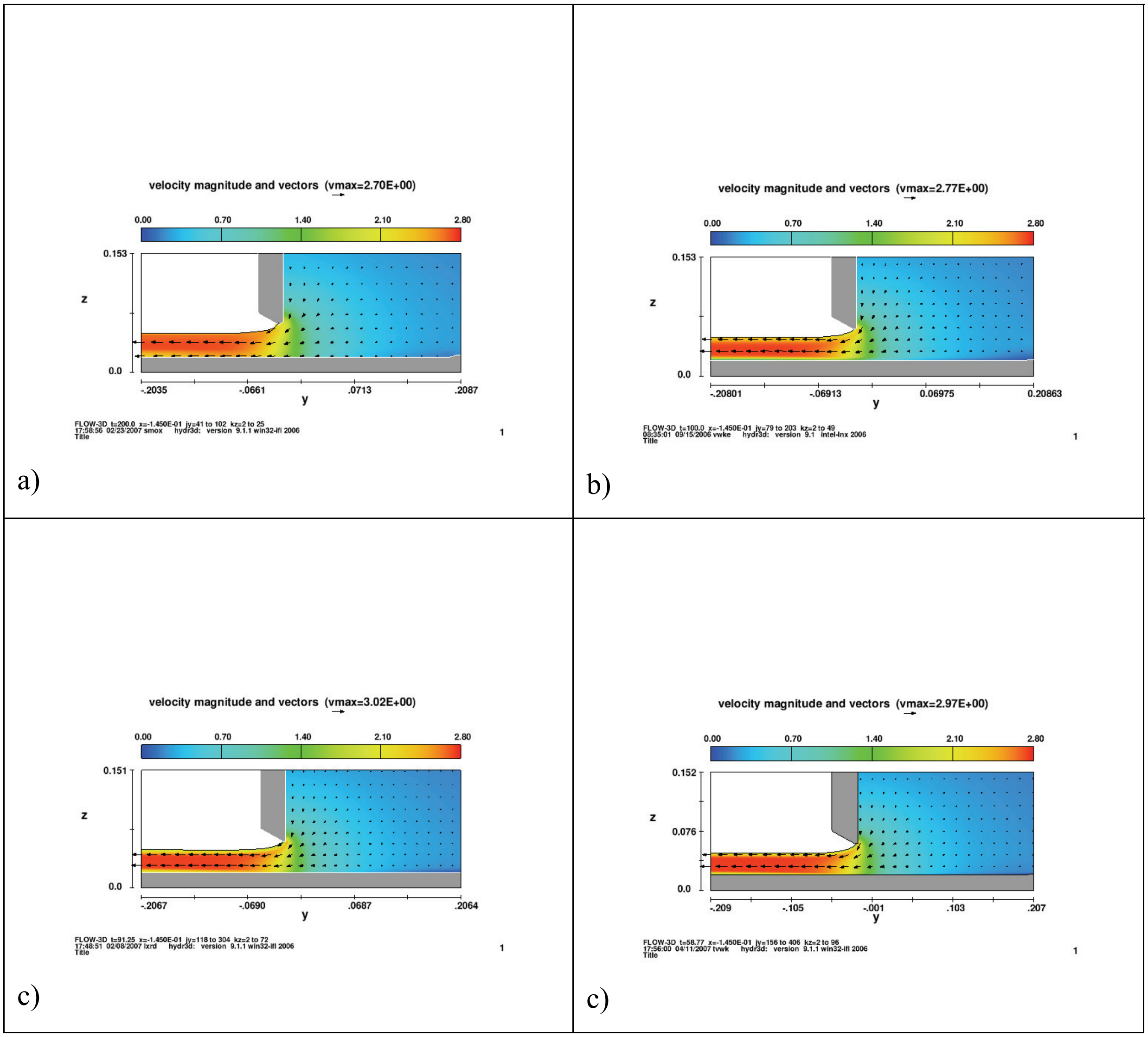

Figure B.11: Velocity Profiles for the quasi-2D 2m Gate Opening on the Diversion Structure for minimum cell sizes of a) 0.3m, b) 0.15m, c) 0.1m, d) 0.075m

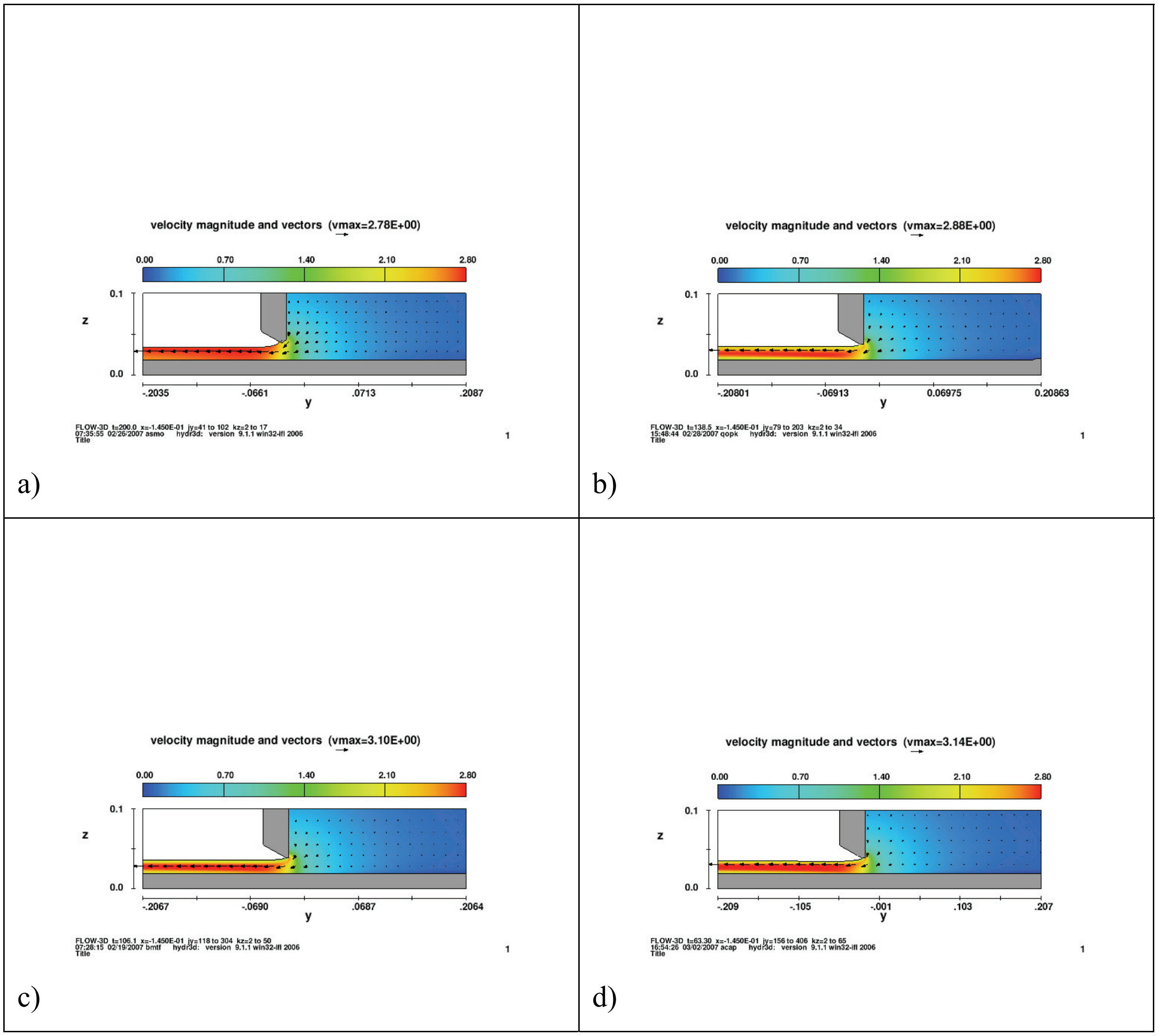

Figure B.12: Velocity Profiles for the quasi-2D 1m Gate Opening on the Diversion Structure for minimum cell sizes of a) 0.3m, b) 0.15m, c) 0.1m, d) 0.075m

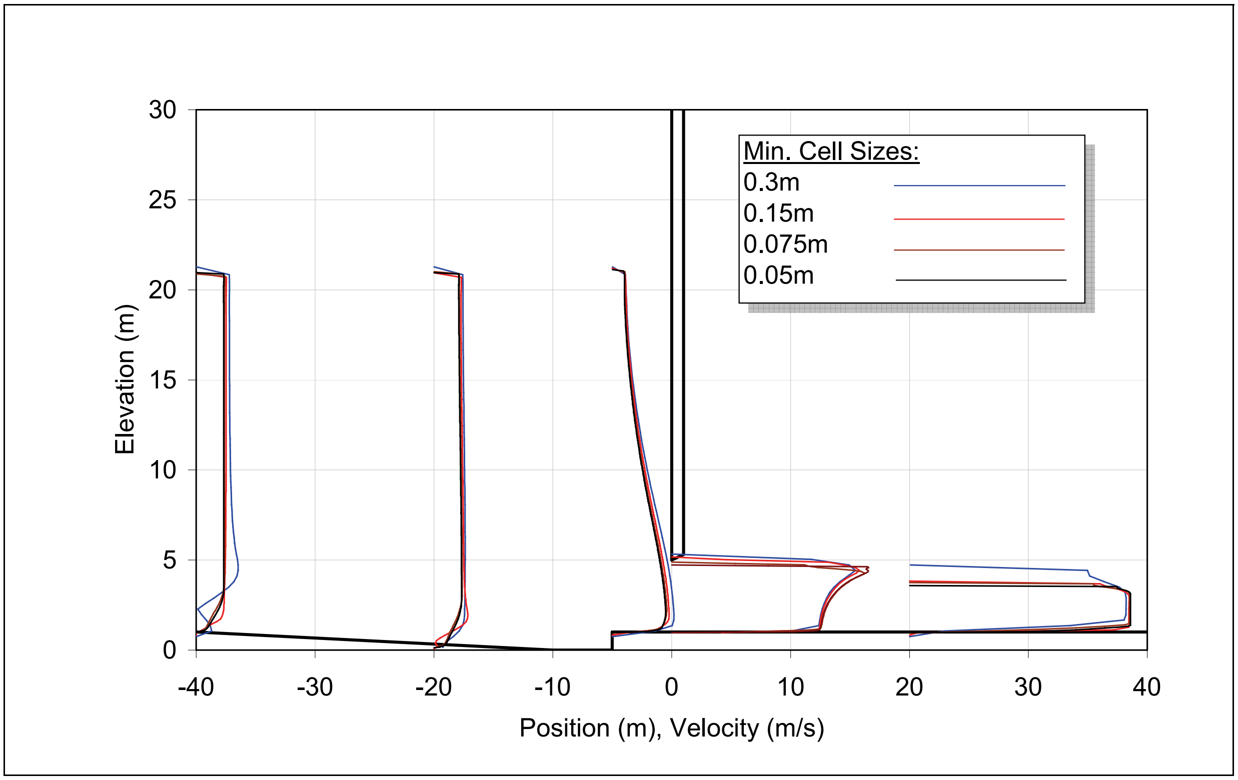

Figure B.13: Velocity Profiles for the quasi-2D 4m Gate Opening on the Diversion Structure along the Channel

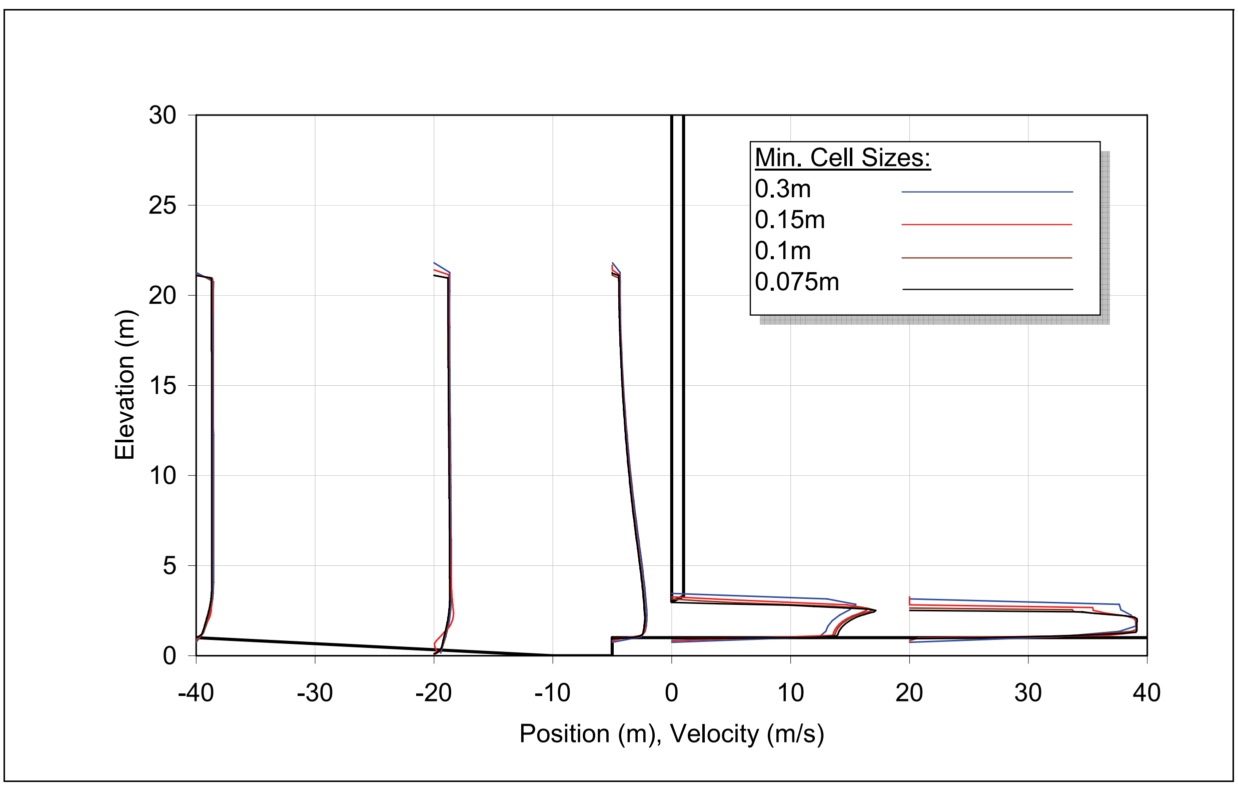

Figure B.14: Velocity Profiles for the quasi-2D 2m Gate Opening on the Diversion Structure along the Channel

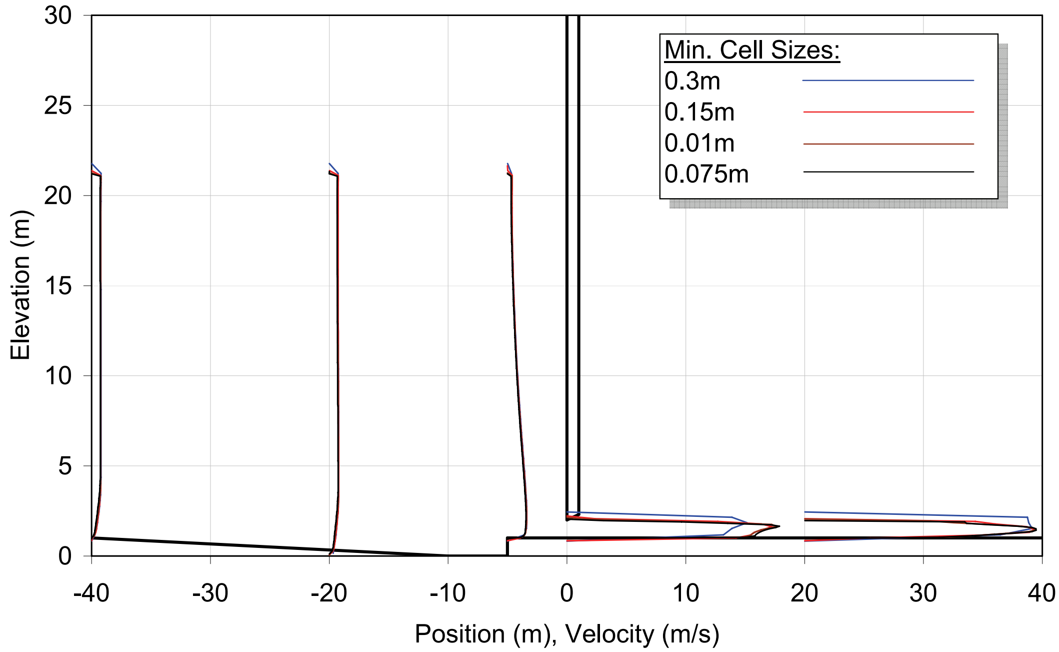

Figure B.15: Velocity Profiles for the quasi-2D 1m Gate Opening on the Diversion Structure along the Channel

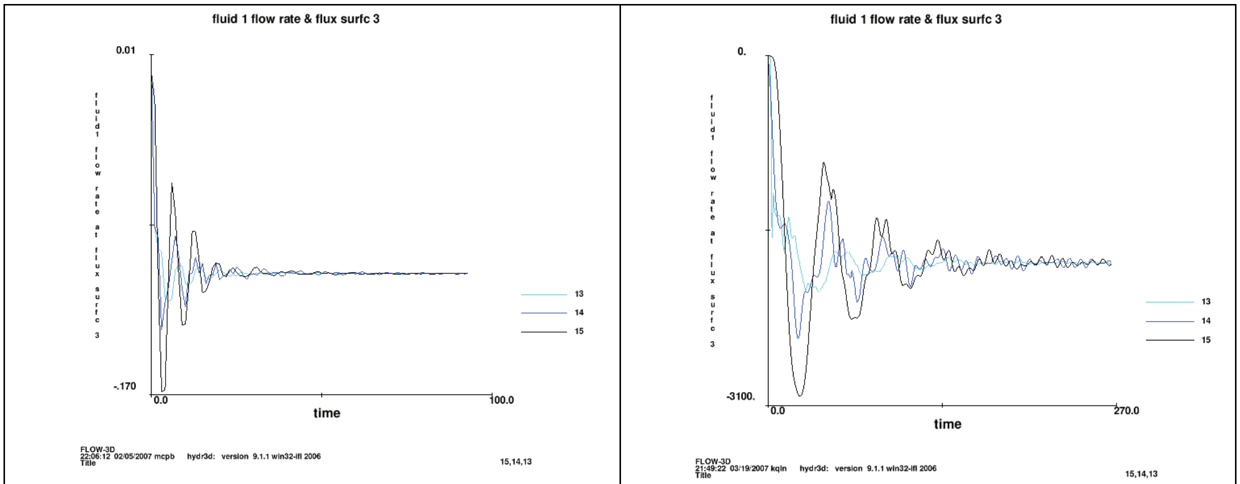

Scaled Discharge Curve | Full-Sized Discharge Curve

Figure B.16: Comparison of Scaled and Full-Sized Discharges for the Fully Open Case

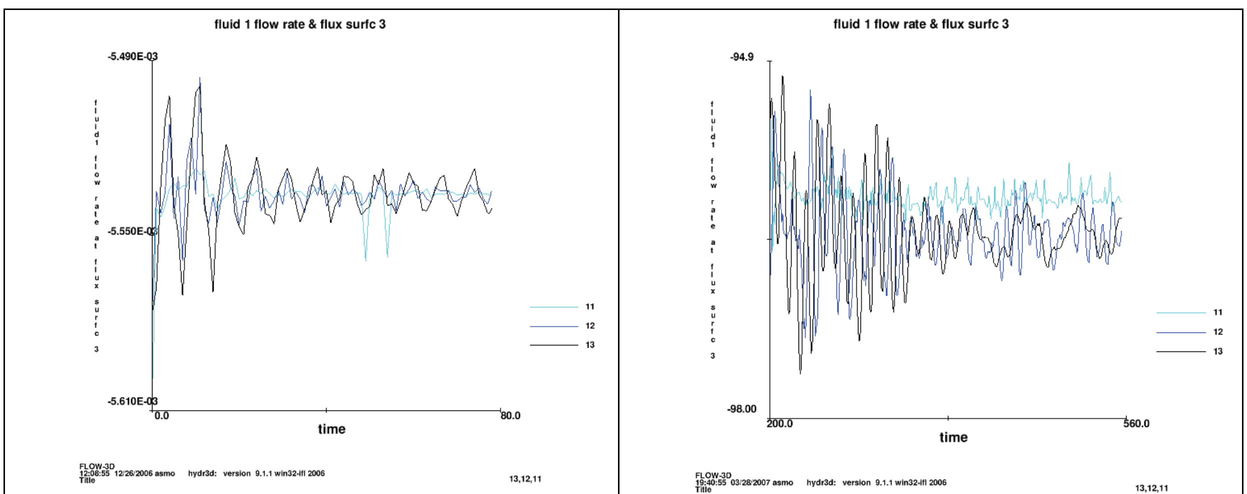

Scaled Discharge Curve | Full-Sized Discharge Curve

Figure B.17: Comparison of Scaled and Full-Sized Discharges for the 6m Gate Opening

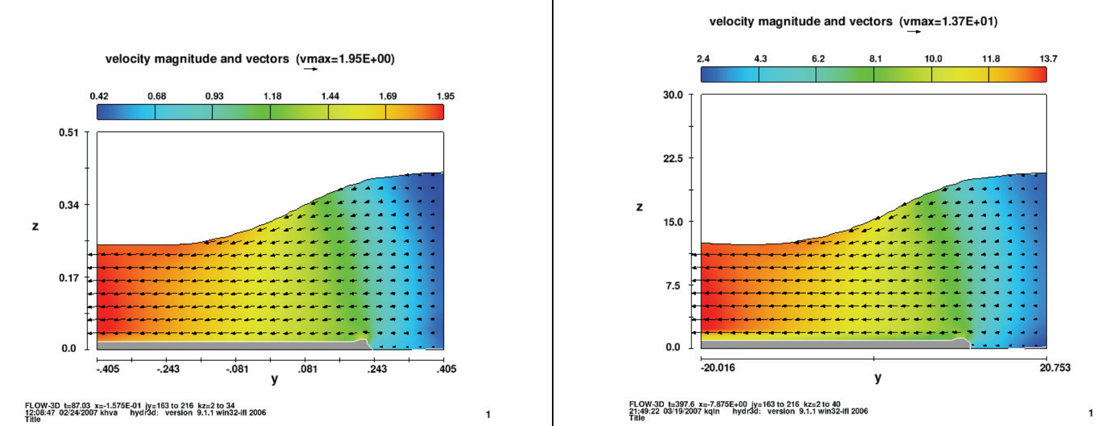

Scaled Velocity Fields

Full-Sized Velocity Fields

Figure B.18: Comparison of Scaled and Full-Sized Velocity Fields for the Fully Open Case

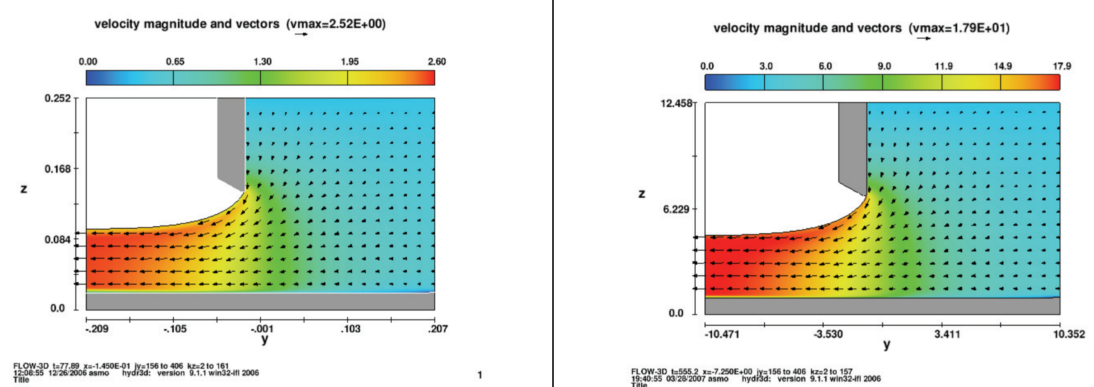

Scaled Velocity Fields

Full-Sized Velocity Fields

Figure B.19: Comparison of Scaled and Full-Sized Velocity Fields for the 6m Gate Opening

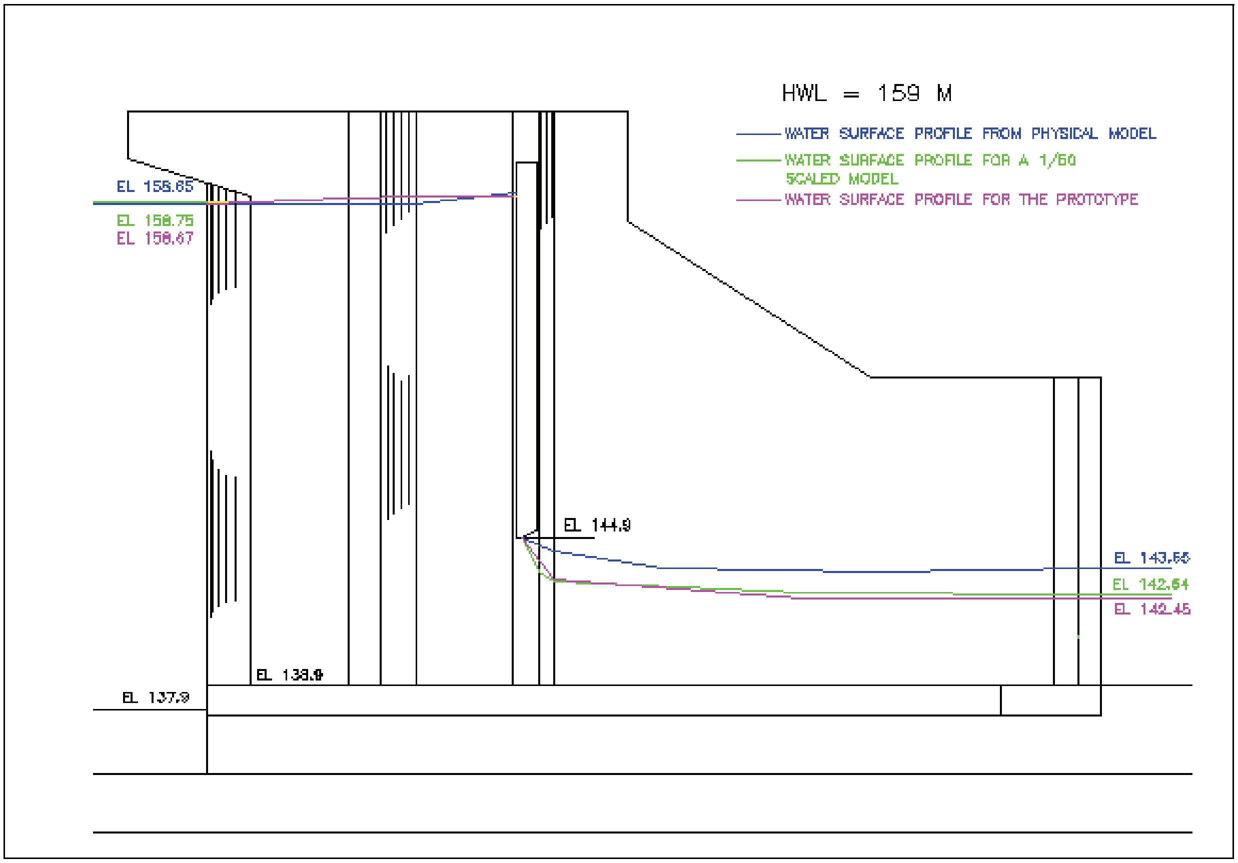

Figure B.20: Comparison of Water Surface Profiles for Scaled and Full-Sized 6m Gate Opening Diversion Cases

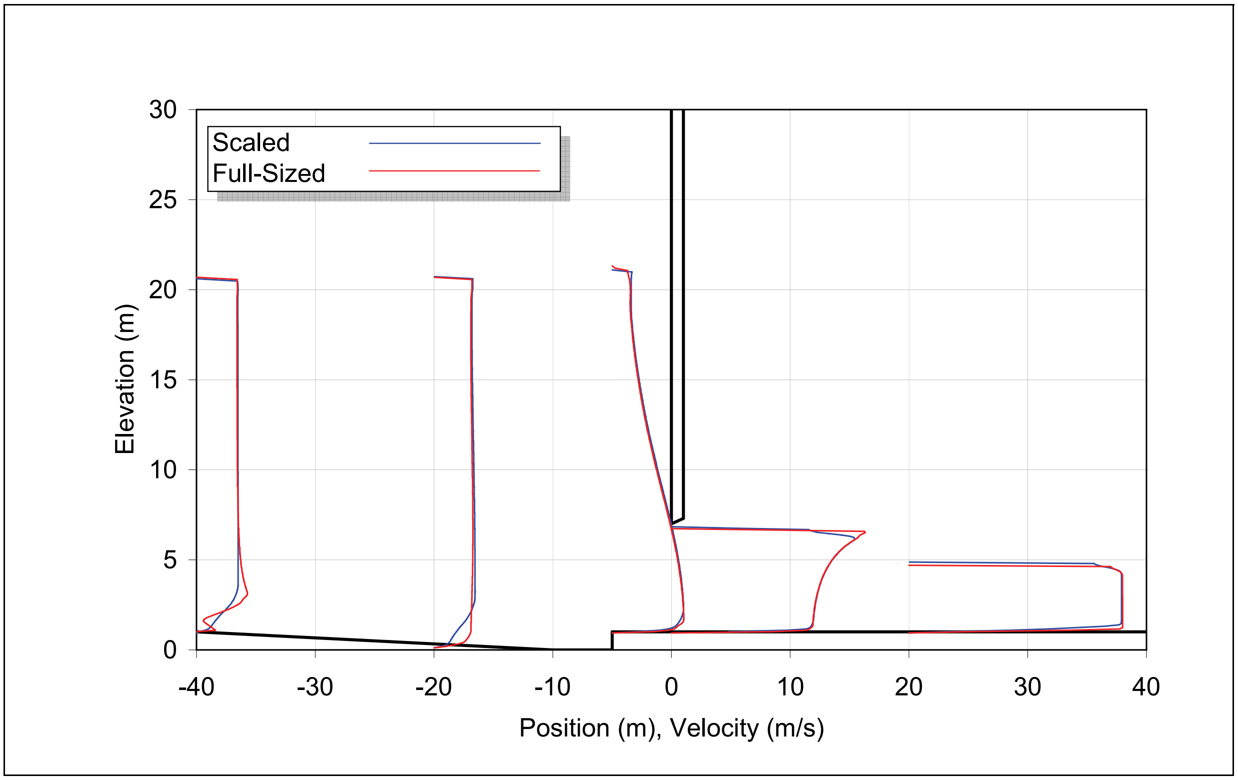

Figure B.21: Comparison of Velocity Profiles for the Scaled and Full-Sized 6m Gate Opening on the Diversion Structure

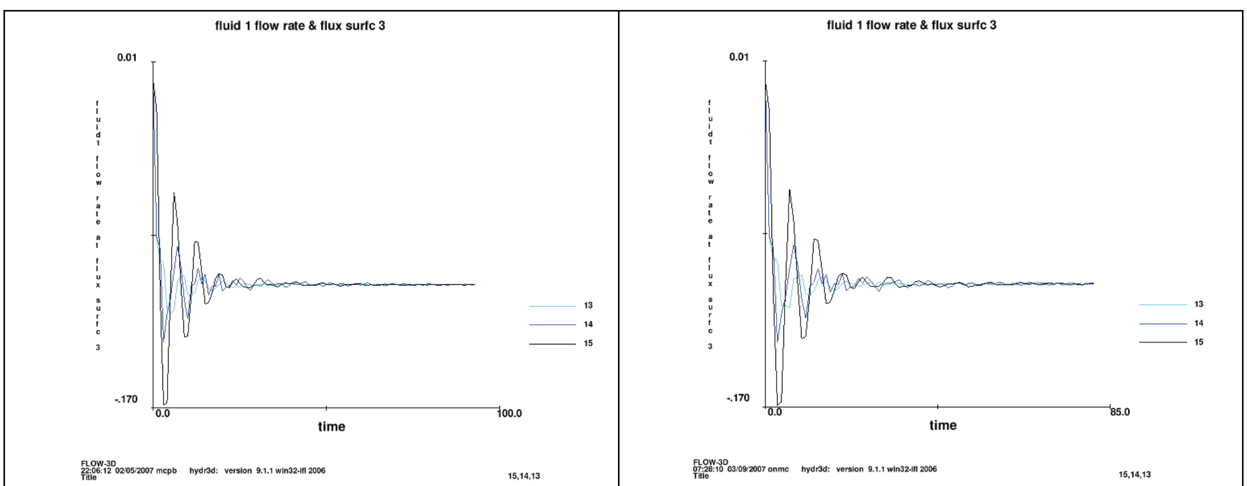

K-ε Closure Model

RNG Closure Model

Figure B.22: Comparison of K-ε and RNG Discharges for the Fully Open Case

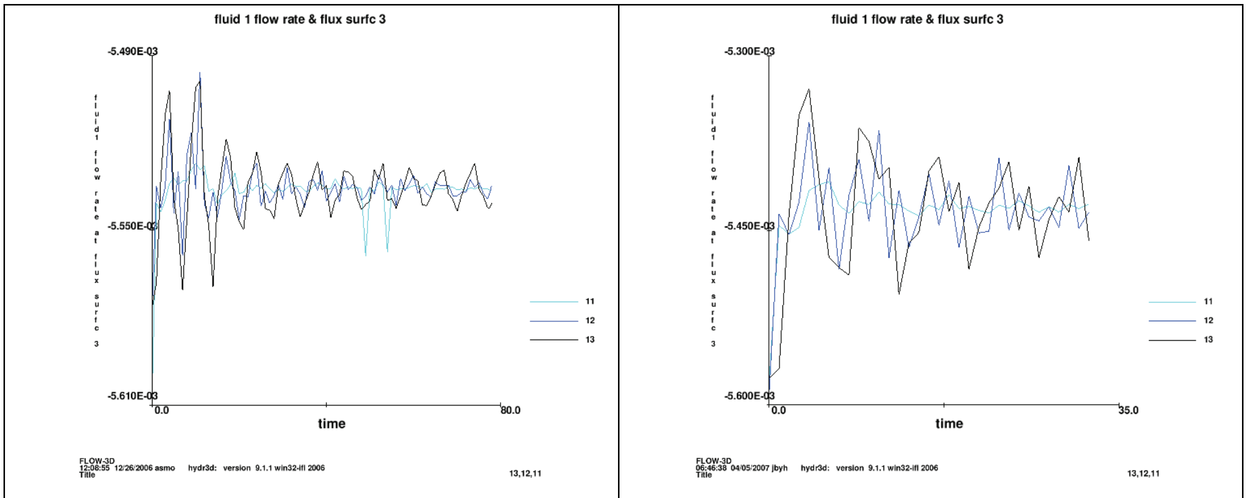

K-ε Closure Model RNG Closure Model*

Figure B.23: Comparison of K-ε and RNG Discharges for the 6m Gate Opening

*simulation was restarted due to power failure and therefore, the x axis does not reflect the full amount of time of the simulation

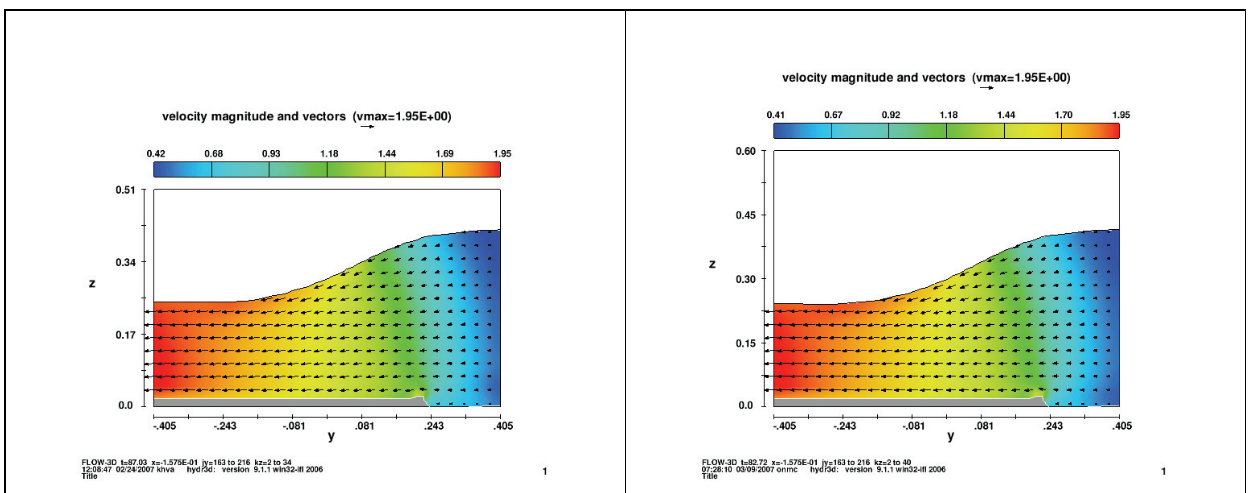

K-ε Closure Model RNG Closure Model

Figure B.24: Comparison of K-ε and RNG Velocity Fields for the Fully Open Case

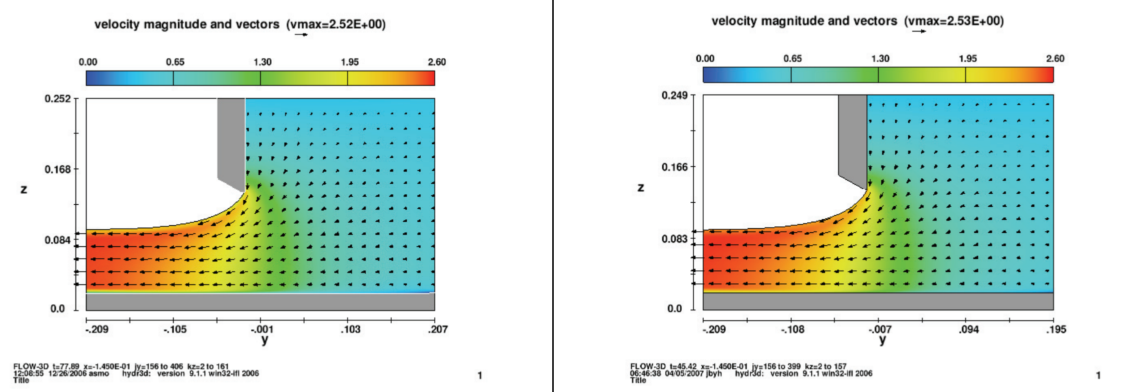

K-ε Closure Model | RNG Closure Model

Figure B.25: Comparison of K-ε and RNG Velocity Fields for the 6m Gate Opening

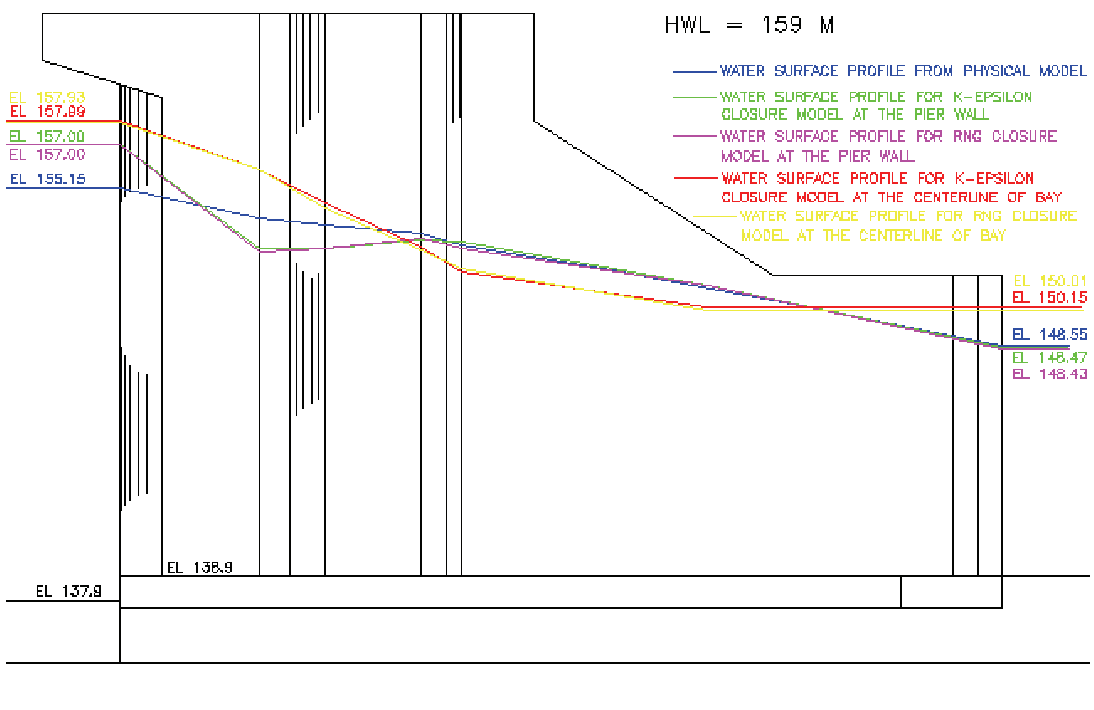

Figure B.26: Comparison of Water Surface Profiles for the K-ε and RNG Models for the 3D Fully Open Diversion Cases

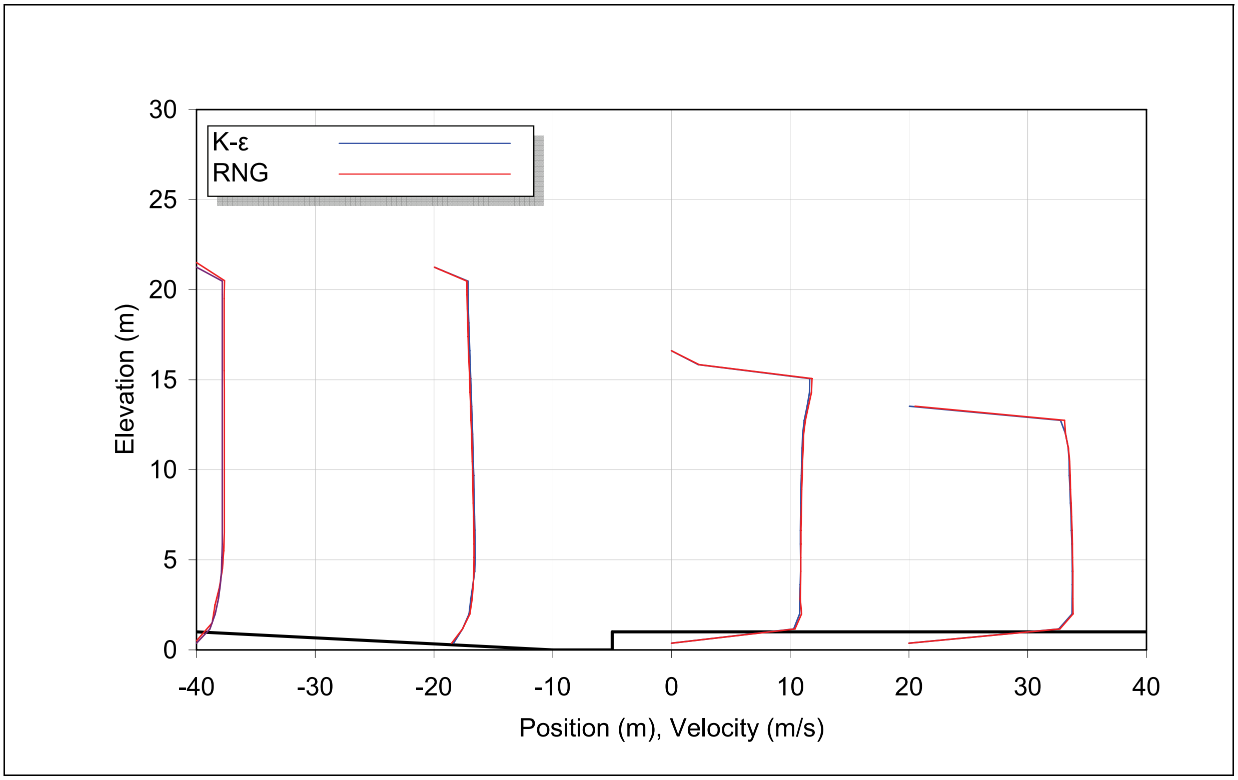

Figure B.27: Comparison of Velocity Profiles for K-ε and RNG Models for the Fully Open Case on the Diversion Structure

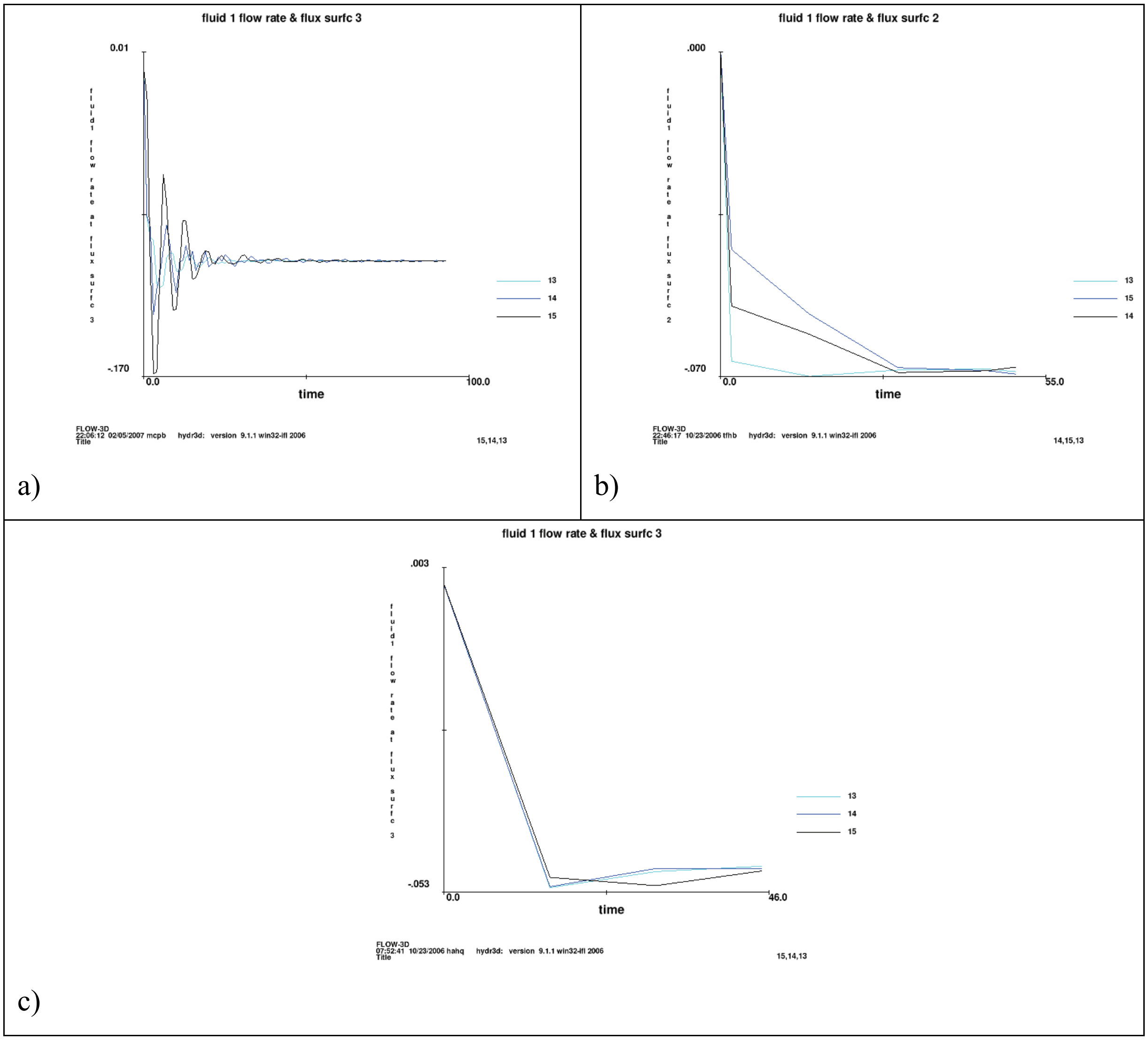

Figure B.28: Discharge vs. Time Curves for the 3D Fully Open Case on the Diversion Structure Water Levels at HWL-C of a) 159m, b) 154m, c) 151m

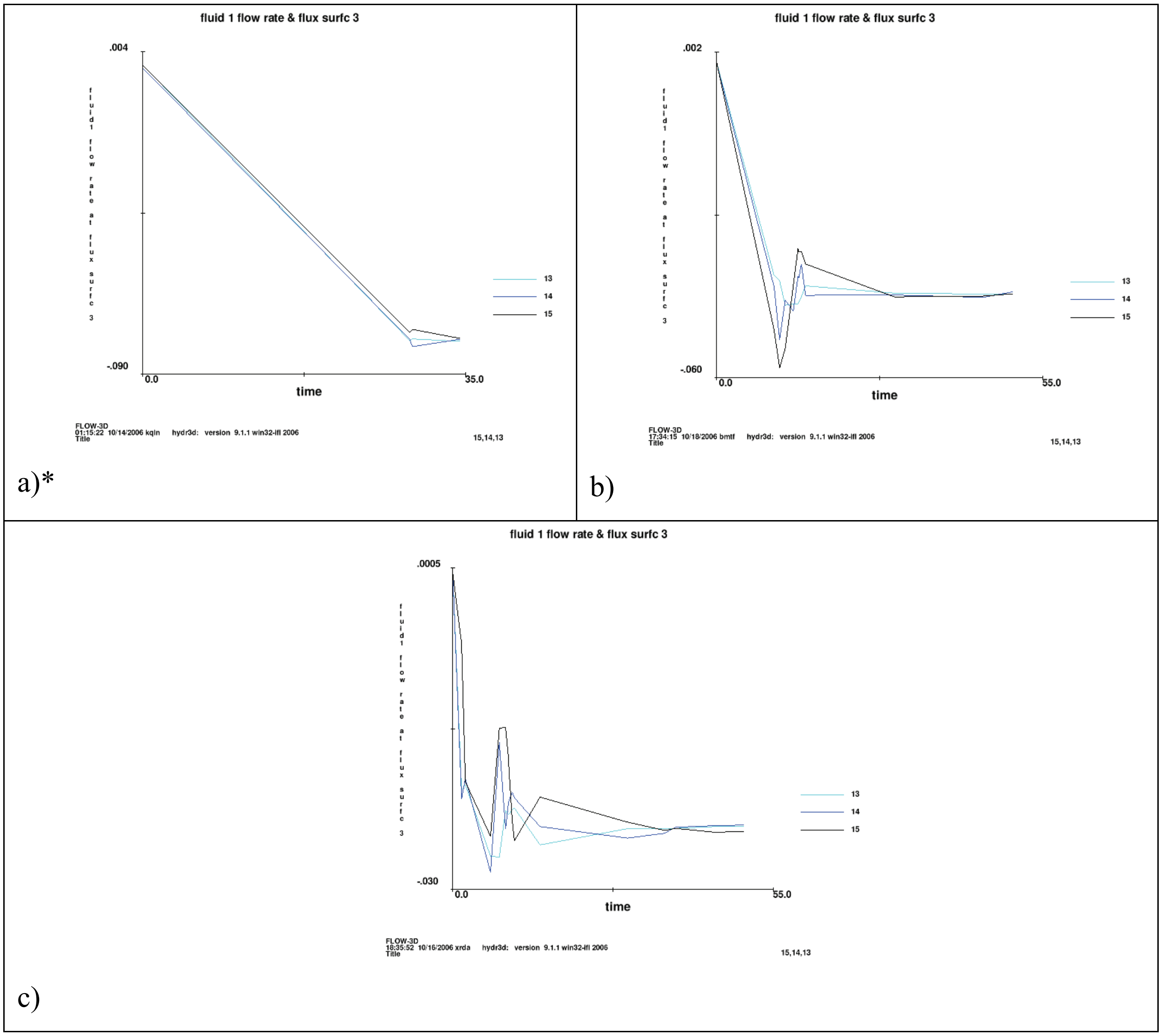

Figure B.29: Discharge vs. Time Curves for the 3D Fully Open Case on the Rollway Structure Water Levels at HWL-C of a) 159m, b) 154m, c) 151m

*simulation was restarted due to power failure and therefore, the x axis does not reflect the full amount of time of the simulation

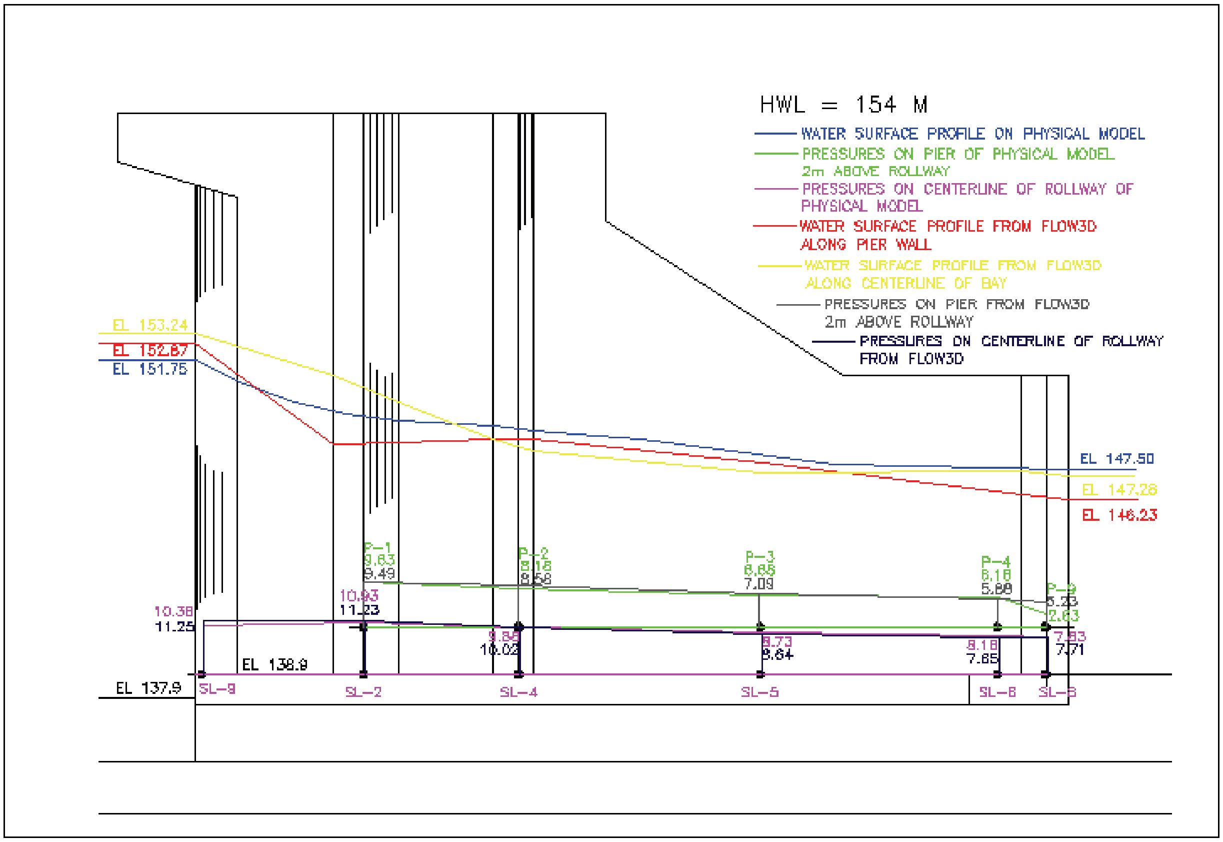

Figure B.30: Comparison of Water Surfaces and Pressures of the Physical Model and the Numerical Model for an Upstream Water Level of 154m on the Diversion Structure

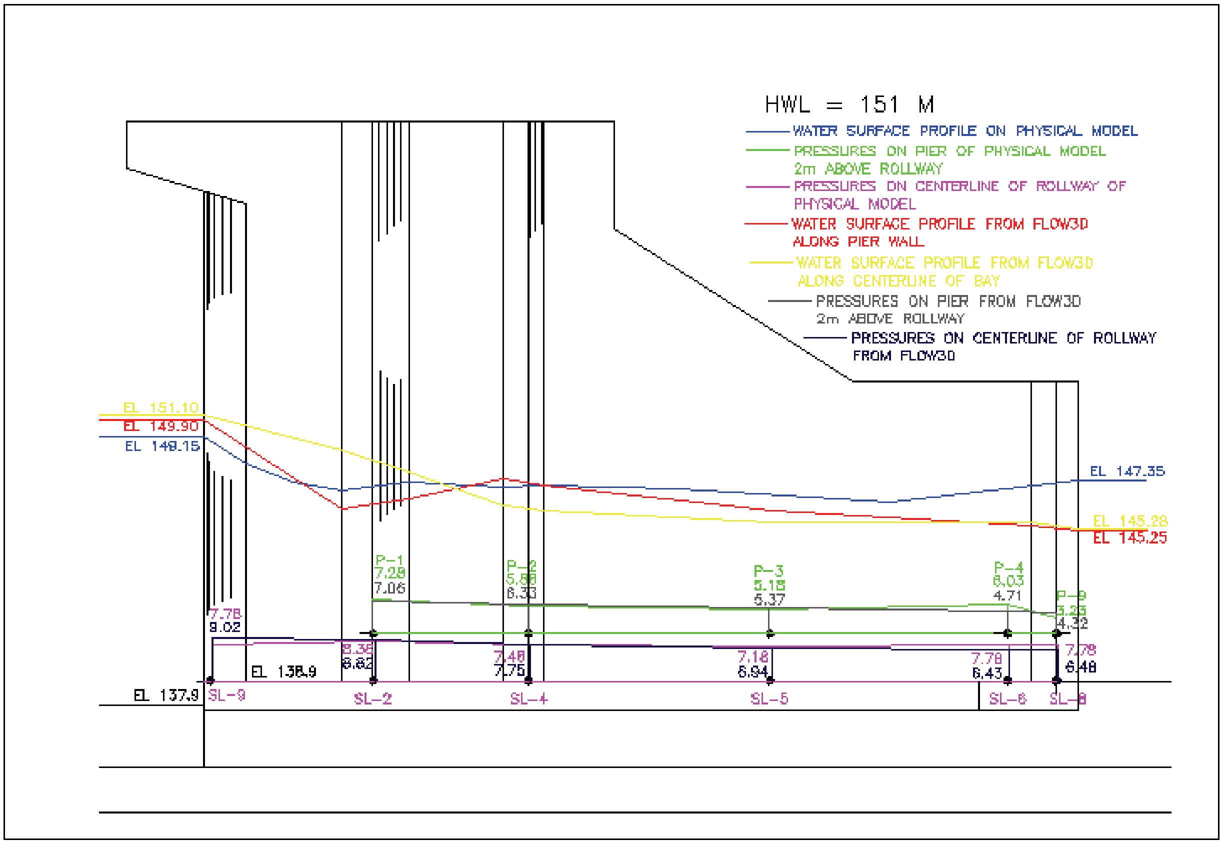

Figure B.31: Comparison of Water Surfaces and Pressures of the Physical Model and the Numerical Model for an Upstream Water Level of 151m on the Diversion Structure

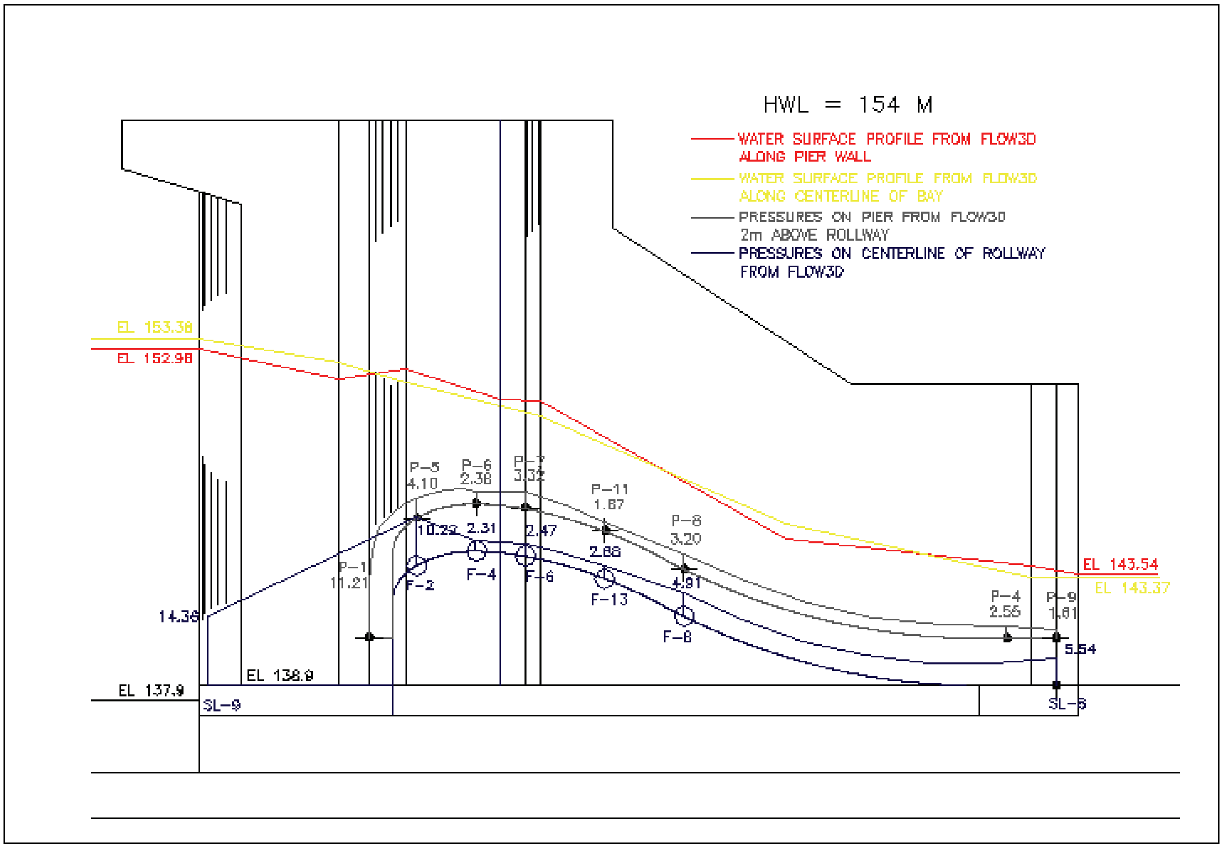

Figure B.32: Water Surfaces and Pressures from the Numerical Model for an Upstream Water Level of 154m on the Rollway Structure

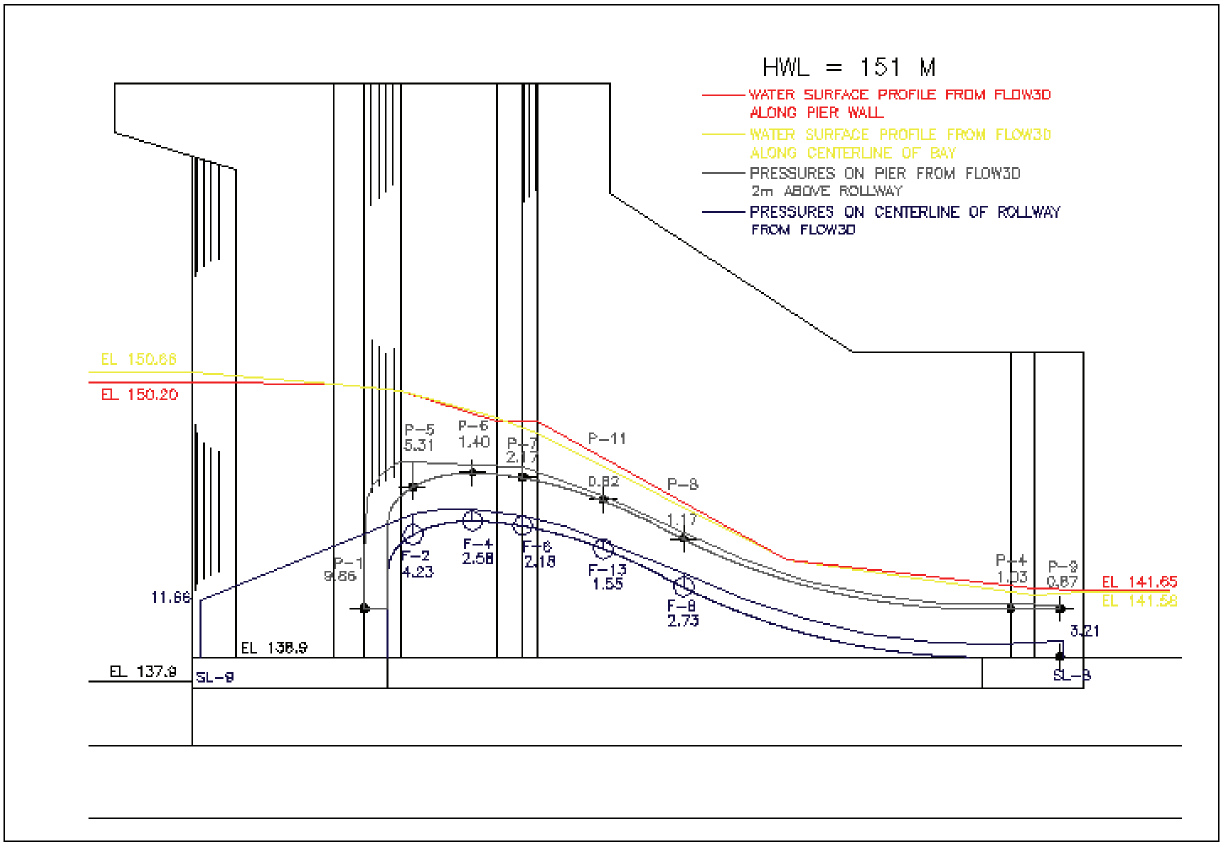

Figure B.33: Water Surfaces and Pressures from the Numerical Model for an Upstream Water Level of 151m on the Rollway Structure